Gerrit Jan Jager

Magnetic Resonance in Prostate Cancer – Clinical Potentials

Magnetic Resonance in Prostate Cancer – Clinical Potentials

Magnetic Resonance in Prostate Cancer – Clinical Potentials

een wetenschappelijke proeve op het gebied van de Medische Wetenschappen

PROEFSCHRIFT

ter verkrijging van de graad
van doctor aan de Katholieke
Universiteit Nijmegen,
volgens besluit van het College van Decanen in het openbaar te verdedigen op woensdag 11 december 1996 des namiddags om 1.30 uur precies

door

Gerrit Jan Jager

geboren 13 november 1954 te Heerlen

Promotor:	Prof. Dr. J.H.J. Ruijs
Co-promotores:	Dr. J.O. Barentsz Dr. G.O.N. Oosterhof
Manuscript commissie:	Prof. Dr. D. J. Ruiter Prof. Dr. P. de Mulder Prof. Dr. R.A. Janknegt (UM)

Financial support by
– Stichting van het Laar
– Stichting Radiologisch Onderzoek Nijmegen (Rad-ON)
– Stichting Urologie 71
– Firma Schering, Berlijn
is greatfully acknowledged

Contents

1 Introduction and Outline of the Thesis

Prostate cancer represents an important health problem in most western countries. In the Netherlands, incidence and mortality of prostate cancer are exceeded only by those of lung cancer. In 1989, 4,112 incident cases and 2,079 deaths from cancer of the prostate were recorded in a male population of 7.5 million. [1,2]. In most western countries the incidence increases with increasing age of the population, and doctors but especially patients awareness of the disease. In the USA, prostate cancer incidence rate increased by 6.4% per year between 1983 and 1989 [3]. The number of patients with occult prostate cancer exceeds by far the number of patients with clinically apparent tumors. Occult tumors (latent, clinically silent cancers discovered at autopsy) occur in up to 40% of patients in the eight decade of life whereas the incidence of clinically significant tumors is 0,04% at the age of 50 years rising to 1,4% at the age of 80 years [4].

Prostate cancer may be cured if detected at an early stage. This entails that the tumor should not extend beyond the capsule of the prostate and that there are no distant metastases. More sensitive diagnostic tools such as prostate-specific antigen (PSA) and transrectal ultrasound (TRUS) combined with ultrasound guided biopsies have led to an increased number of cancers detected at an early stage. However, because prostate cancer is often a slowly-growing, indolent tumor a number of patients will not require treatment. Therefore Whitmore's question "Is cure possible for whom it is neccessary and is cure neccessary for whom it is possible?" is still relevant [5]. This thesis deals to a large extent with the question of whether magnetic resonance (MR) imaging is capable of selecting the patients for whom cure is possible?

The extent of prostate cancer is assessed preoperatively by clinical staging, the definitive staging is being achieved by histopathologic examination. In **chapter 2**, the objective, value and controversies of clinical and pathological local staging are discussed. The pathological stage is not the only predictor of outcome in a patient with prostate cancer. Attention is payed to other prognostic factors such as tumor volume, histologic grade, and neo-vascularity.

MR is an important modality for evaluating prostate cancer [6]. With the introduction of an endorectal surface coil (ERC) the prostate can be imaged with a higher resolution and an increased signal-to-noise ratio [7]. In **chapter 3** the results of local staging in 34 patients are described. Furthermore we evaluated the potential of MR imaging with an ERC technique in the assessment of tumor volume. One of the pitfalls of MR imaging with an ERC is discussed in an **inter-**

lude, a report of a case of senile amyloidosis of the seminal vesicles mimicking seminal vesicle invasion on ERC-MR images.

When lymph node metastases occur, the patient is no longer considered a candidate for curative surgical treatment. **Chapter 4** reports the results of a 3-dimensional (3D) MR imaging technique in the evaluation of pelvic lymph nodes in 134 patients with prostate or bladder cancer. Lymph node metastases may become evident by enlargment of the node. However, a considerable number of lymph node metastases occur in non-enlarged lymph nodes. These are generally detected during operation on frozen section examination of the specimen. The finding of positive lymph nodes is diminishing rapidly as today, more patients are diagnosed in an early stage. Therefore some investigators suggest that there is no place for imaging in the preoperative evaluation of patients who are candidates for a radical prostatectomy. The second **interlude,** a letter to *CANCER*, contains a comment on an article in which is suggested that there is no role for imaging in nodal staging of prostate cancer. It is argued that there is a role for imaging of lymph nodes in a selected group of patients who are candidate for curative therapy. The reply of the author is included.

We postulated that with the use of newer MR techniques such as dynamic imaging and spectroscopy, more accurate information about stage, grade, tumor volume and biological potential of the tumor would become available. In **chapter 5** we evaluate the potential of a dynamic MR imaging technique following the injection of contrast material. The imaging results of 57 patients were compared with the final histopathology with respect to tumor location and capsular penetration.

With MR proton spectroscopy it became possible to obtain in vivo information about the presence of certain metabolites (citrate, choline, creatine) in the prostate. **Chapter 6** extensively reports the results of this technique in healthy volunteers. In **chapter 7** the results of MR proton spectroscopy in patients with benign prostatic hyperplasia (BPH) and prostate cancer are reported.

Chapter 8 is a concise discussion about the current role of MR in patients with prostate cancer and contains recommendations for future studies.

In **Chapter 9** the summary and conclusions are presented.

References

1. Gulden van der JWJ, Kiemeney LALM., Verbeek ALM, Straatman H. Mortality trend from prostate cancer in the Netherlands (1950-1989). *Prostate* **1994**;24:33-38
2. CBS . *Overledenen naar doodsoorzaak, leeftijd en geslacht in het jaar 1989.* Voorburg:CBS, **1990**
3. Lu-Yao GL, Greenberg ER. Changes in prostate cancer incidence and treatment in USA. *Lancet* **1994**;343:251-254
4. Barry MJ, Flemming C, Coley CM, Wasson JH, Fahs MC, Oesterling JE. Should medicare provide reimbursement for prostate-specific antigen testing for early detection of prostate cancer? Part I: framing the debate. *Urology* **1995**;46:2-13
5. Rosen MA. Impact of prostate-specific antigen screening on the natural history of prostate cancer. *Urology* **1995**;46:757-768
6. Schiebler ML, Schnall MD, Pollack HM, et al. Current role of MR imaging in the staging of adenocarcinoma of the prostate. *Radiology* **1993**;189:339-352
7. Schnall MD, Imai Y, Tomaszewski JE, Pollack HM, Lenkinski RE, Kressel HY. Prostate cancer: local staging with endorectal surface coil MR imaging. *Radiology* **1991**;178:797-802

Part I
Staging of Prostate Cancer

2 Primary Staging of Prostate Cancer

G. Jager[1], J. Barentsz[1], E. Ruijter[2], J. de la Rosette[2], G. Oosterhof[2]

Departments of [1]Radiology, [2]Urology and [3]Pathology, University Hospital Nijmegen, The Netherlands

Abstract

Staging prostate cancer is a systemic classification of the extent of disease based on clinical and pathological criteria. Despite the general acceptation of the TNM staging system, a lot of controversies and uncertainty, with respect to staging, still exist. This paper gives an overview of different staging modalities and emphasizes the need for incorporation of prognostic factors, such as tumor grade and tumor volume, in the staging system.

Key Words; prostate, prostate neoplasm, prostate cancer staging, staging controversies

Introduction

Prostate cancer is the most commonly diagnosed noncutaneous cancer in men and the second leading cause of cancer related deaths. The age-specific mortality rate for prostate cancer has increased steadily during the last 30 years and with the availibility of highly sensitive techniques to detect serum prostate specific antigen (PSA) the incidence has increased dramatically during the last 5 years [1].

The best treatment for localized prostate cancer is still under debate [2-6]. The mainstay for prostate cancer control is radical surgery in patients with organ-confined disease [7]. Alternative treatments for localized disease are (curative) radiotherapy [8], cryosurgery [9,10] and deferred treatment (watchfull waiting) [3,11]. For tumor that extends beyond the pseudocapsule or in cases with metastases "hormonal ablation" is a treatment option [2].

Ideally, clinical staging stratifies patients into comparable groups for definitive therapy and allows comparison of the effectiveness of different therapies, whereas pathological staging is important to predict prognosis and the need for additional therapy.

In 1992, the American Joint Committee on Cancer (AJCC), in collaboration with the International Union Against Cancer (IUCC) adapted a revision of the TNM staging system (table 1) [12]. The revision permitted transition from the classical Whitmore ABCD system to the TNM classification: for example stage A becomes T1, stage B becomes T2 and stage C becomes T3.

Table 1. TNM classification: Primary tumor (T) 1992 revision [12]

TX Primary tumor cannot be assessed
T0 No evidence of primary tumor
T1 Clinically apparent tumor, not palpable nor visible by imaging
– T1a Tumor is incidental histologic finding in 5% or less of tissue resected
– T1b Tumor is incidental finding in more than 5%
– T1c Tumor identified by needle biopsy (due to elevated serum PSA)
T2 Tumor palpable or visible by imaging confined to the prostate
– T2a Tumor involves half of a lobe or less
– T2b Tumor involves more than half of a lobe but not both lobes
– T2c Tumor involves both lobes
T3 Tumor extends through the prostatic capsule
– T3a Unilateral extracapsular extension
– T3b Bilateral extracapsular extension
– T3c Tumor invades seminal vesicles
T4 Tumor is fixed or invades adjacent structures other than seminal vesicles
– T4a Tumor invades bladder neck and/or external sphincter and/or rectum
– T4b Tumor invades levator muscles and/or is fixed to pelvic wall

Other changes in 1992 included the definition of a T1c subcatagory to describe prostate cancer discovered by biopsy prompted by an elevated prostate specific antigen (PSA) level, to allow T classification by imaging and to group disease with capsular invasion without penetration from the pT3 category in the 1987 edition, into the pT2 category.

Anatomy

The prostate can be divided into four glandular zones: the peripheral zone (PZ), central zone (CZ), transition zone (TZ) and periurethral zone. Most of the peripheral glandular units of the prostate do not reach the outer margin of the prostate. They are separated from the periprostatic connective tissue by a 2- to 3-mm band of stromal tissue of concentrally placed fibromuscular tissue, the so-called prostatic capsule. This is not a capsule in the strict sense, but an inseparable component of the prostatic tissue. At the apex the capsule is no longer present facilitating extra-capsular tumor growth [13].

Seventy percent of tumors arise in the PZ. Tumors arising in the PZ can be seen by Transrectal Ultrasound (TRUS) and Magnetic Resonance (MR) imaging [14]. About 10% of the cancers arise in the CZ, and approximately 20% arise in the TZ. The TZ is the site of origin of benign prostatic hyperplasia (BPH) and therefore often comprises a much larger portion of the gland in older men [15]. It is often difficult to distuinguish BPH and cancers in the TZ by MRI and TRUS [16].

Primary staging

The goal of primary staging is to determine the local extent of disease, the T category. In general practice it is important to determine which patients are candidate for curative therapy on account of locally confined disease.

Digital rectal examination (DRE)

Historically, DRE plays a central role in local staging. Although the findings of DRE are so wide-spread used there are little data available on the reliability of DRE in clinical staging [17]. There are no data of intra- or inter observer variability. Data accumulated from carefully examined prostatectomy specimens revealed that DRE underestimated the local extent of cancer in 40-60% of cases [18,19]. Most of the understaging is based on microscopic penetration of the capsule or invasion in the seminal vesicles.

Prostate Specific Antigen (PSA)

PSA is the most accurate marker to screen for prostate cancer but has limited accuracy in staging because there is a substantial overlap in PSA concentrations and pathologic stages. Nevertheless the combination of serum PSA concentration and other variables like tumor grade, volume and clinical stage, significantly enhance the predictive value of serum PSA for the pathological stage [20].

TRUS

TRUS has become essential for the diagnosis of disease in a short period of time, although for staging TRUS is not generally accepted. TRUS has the advantage of allowing visualization of cancers as a hypoechoic lesion in the PZ in many cases (fig.1). Capsular penetration is diagnosed by local contour deformity and/or interruption of the periprostatic fat echos [21] (fig. 2).

There is considerable inter and intra observer variability in the assignment of clinical stage. Detection of microscopic extension of prostate cancer is beyond the capabilities of TRUS [22]. Despite the widespread use, the role of TRUS in staging prostate cancer had not yet been established [17]. In the study of Rifkin et al. [21] the overall accuracy was 58%. Correct staging was achieved in 46% of

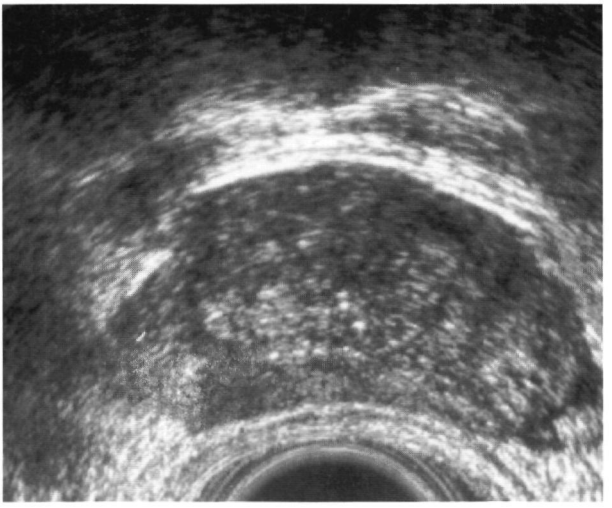

Figure 1. Trans rectal ultrasonography of a T2 carcinoma. The carcinoma is visualised as a hypoechoic lesion in the periperal zone (arrows).

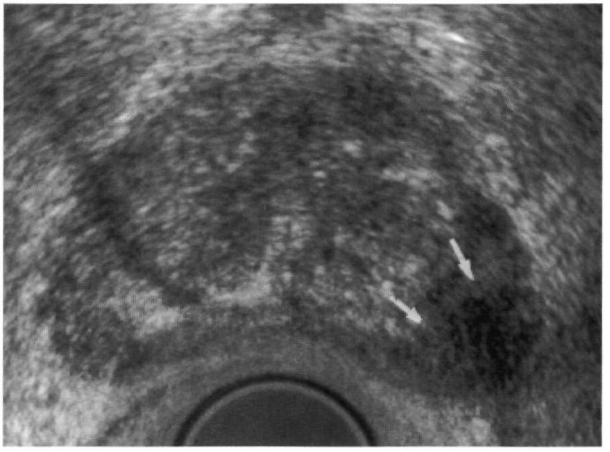

Figure 2. Trans rectal ultrasonography shows a T3 tumor on the left side (arrows). Capsular penetration is demonstrated as a local contour deformity (small arrows).

localized and 66% of advanced cancers. The advantage of TRUS compared to MR imaging, is that it allows directed biopsies of suspected lesions and of the seminal vesicles, thus improving staging [23].

Computed Tomography (CT)

CT does not allow direct visualization of prostate cancer and is considered of little value in local staging [24]. The role of CT is limited to nodal staging [25].

MR Imaging

MR imaging provides the best depiction of the anatomy of the prostate and seminal vesicles. The internal architecture is clearly visible on T2-weighted images. Prostate cancer is usually visible as a low signal intensity lesion in a bright peripheral zone. The capsule is visible as a low signal intensity rim (fig. 3).

Capsular perforation is most often visible as a disruption of the prostatic capsule and infiltration of the periprostatic fat. Seminal vesicle invasion is visible as an abnormal low signal intensity within the lumen of the seminal vesicle (fig. 4).

MR imaging using traditional body coils (fig. 5) has been disappointing in staging of prostate cancer and is not superior to TRUS. The reported accuracy was 69% [21]. The accuracy of MR imaging with an endorectal coil was initially reported 82% [26]. However, more recent data suggest a lower accuracy level, almost equal to the body coil technique [27].

Further evaluation of MR imaging is obviated because of the continuing development of fast imaging sequences and new coils. A recent study of MR imaging with an integrated endorectal pelvic phased-array coil [28] reported an accuracy rate of 76%.

Pathologic staging

Pathologic staging is the best prognostic marker to date and far more accurate than clinical staging. It should be noted however, that the pathologic stage may

Figure 3. Endorectal coil MR image of the prostate. Transaxial T2-weighted image demonstrating prostate cancer as a low signal intensity lesion in the bright peripheral zone (small arrow). The capsule is visible as a low signal intensity rim. Note the presence of BPH in the central zone (large arrow). BPH has signal intensity almost equal compared to cancer.

Figure 4. Coronal T2-weighted image of the prostate obtained with an endo-rectal coil. Large T3 tumor on the left side. Note capsular perforation and abnormal low signal intensity within the lumen of the seminal vesicle (arrow) representing tumor invasion of the seminal vesicles.

depend on the way the radical prostatectomy specimen is examined. For example, whole-mount sectioning increases the number of capsular penetration sites compared to random sectioning [29,30].

Secondly, Epstein et al. [31] reported that when urologists review pathology reports, these may be misunderstood in a number of cases. This is due to the amount of often imprecise terms used to describe involvement of the capsule, such as invasion, extension into, penetration, permeation, transgression and the use of adjectives such as focal, microscopic, minimal and gros perforation.

Figure 5. Transaxial T2-weighted MR image obtained with a body coil shows a low signal intense area in the peripheral zone (arrow). The lesion was found at radical prostatectomy to represent a T2 prostate cancer. Note that due to the lower resolution, the capsule is less easy to define than on endo-rectal coil images.

Discussion

Increasing costs of healthcare have caused a critical view on staging of prostate cancer. The number of patients with localized cancer is rapidly increasing causing an enormous increase of costs when all staging modalities are performed. The way to assess the clinical status varies from institution to institution. PSA, grade and DRE may be used to tailor the diagnostic work-up in patients with prostate cancer. The additional value of MR imaging, although considered the best imaging modality in the primary staging of prostate cancer, is often limited. A recent study demonstrated that MR imaging for local staging is valuable for the subgroup of patients with a PSA between 10-20 ng/ and Gleasons score of 5 to 7 [32].

Despite the widespread acceptance of the 1992 AJCC/UICC TNM staging classification, areas of controversy and uncertainty exist. The role that imaging should play is still debatable. For example what should be the clinical stage of a patient with one palpable node (T2a), that TRUS can not define while sextant bipsies reveal bilateral disease (uT1c) and finally MR imaging demonstrates one lesion contralateral to the index lesion with evidence of capsular penetration (mT3a). Because there is such wide divergence in the medical community on the reliability of prostatic imaging, there will be inconsistency in staging. Some urologists disregard imaging findings to a large extend and rely only on DRE to assign a clinical T stage [33].

Prognostic factors

Another area of uncertainty is that the natural history of disease or response to therapy of a patient cannot be predicted by stage alone. Patients with the same clinical or pathological stage may not have the same clinical outcome and reversed, patient with different pathological stage may have the same prognosis. E.g. the prognosis of a patient with prostate cancer is not affected by focal capsular penetration (pT3) and comparable to a patient with a pT2 tumor [31].

Pathological stage is the single most powerfull prognostic variable [7], but also other factors such as grade, tumor volume [34], and other molecular, tumor-cell specific markers such as DNA ploidy [35], nuclear morphometry [36], PSA level [37] and neovascularisation [38] strongly influence prognosis and therefore should be included into the staging algorithme [6]. Unfortunately the TNM system is not well designed to accomodate additional variables.

Tumor volume

It is stated that if tumor volume is smaller than 4cc metatasis are unlikely whereas with a tumor volume of more than 12cc metastases are highly likeky [39]. DRE, TRUS and MR images with standard body coil and conventional SE techniques have not been accurate in preoperatively estimating tumor volume [40-46]. FSE MR images obtained with a phased-array coil showed a better estimation of tumor volume [47]. Initial experience with dynamic T1-weighted single slice technique following intravenous contrast with a high time resolution (1 image/sec) suggest that a better delineation of prostate cancer volume may be possible [48].

Gleason grade

No imaging method provides information on Gleason grade. Biopsies can provide information about tumor grade, however because prostate cancer is a heterogeneous tumor, grade is even difficult to assess with multiple biopsies.

In vivo proton MR spectroscopy demonstrates a relation between the citrate level and grade. Low citrate concentration correlates well with poorly differentiated tumors [49].

Neovascularity

There is an increased density of capillairies in prostatic carcinoma compared to benign prostatic tissue. The number of microvessels is related to the prognosis [38]. To date it is not clear whether imaging can demonstrate the neovascularity. Color doppler US can show flow in larger vessels but not in capillairies. This technique may be usefull to increase the specificity of TRUS in detecting prostate cancer [50].

With late postcontrast MR imaging no differentiation between prostate cancer and normal glandular tissue can be demonstrated, but with dynamic MR imaging using a fast imaging technique, differentiation may be possible due to early and rapid enhancement of prostate cancer [48]. The relation of this enhancement pattern and microvessel density is still under investigation.

Conclusion

Allthough the revised TNM staging system allows imaging results to play a role in the description of a local lesion they play still a limited role

No preoperative primary staging methods however, will accurately predict pathologic stage nor clinical outcome Therefore, staging classification needs to be flexible to incorporate other prognostic factors

Further evaluation of the preoperative assessment of stage and prognostic factors with new techniques like dynamic MR imaging and MR spectroscopy is needed

References

1 Borings CC, Squires TS, Tong T Cancer statistics, 1993 *CA Cancer J Clin* **1993** 43 7-26
2 Catalona WJ Management of cancer of the prostate *N Engl J Med* **1994**,331 996-1004
3 Flemming C, Wasson JH, Albertsen PC, Barry MJ, Wennberg JH A decision analysis of alternative treatment strategies for clinically localized prostate cancer *JAMA* **1994**, 269 2650-2658
4 Chodak GW, Thisted RA, Gerber GS, et al Results of conservative management of clinically localized prostate cancer *N Engl J Med* **1994**,330 242 248
5 Wasson JH, Cushman CC, Bruskewitz RC, Littenberg B, Mulley AG, Wennberg JE A structured literature review of treatment for localized prostate cancer *Arch Fam Med* **1993**, 2 487-493
6 Denis LJ, Murphy GP, Schroeder FH Report of the consensus workshop on screening and global strategy for prostate cancer *Cancer* **1995**,75 1187-1207
7 Catalona WJ Surgical management of prostate cancer contemporary results with anatomic radical prostatectomy *Cancer* **1995** 75 1903-1908
8 Epstein BE, Hanks GE Prostate cancer evaluation and radiotherapeutic managment *CA Cancer J Clin* **1992**,42 233-240
9 Schmidt JD Clinical diagnosis of prostate cancer *Cancer* **1992**,70 221 224
10 Steinfield AD Questions regarding the treatment of localized prostate cancer *Radiology* **1992**,184 593-598
11 Johansson J E Watchfull waiting for early stage prostate cancer *Urology* **1994**,43 138-142
12 Schroeder FH, Hermanek P, Denis I , Fair WR, Gospodarowicz MK, Pavone-Macaluso M The TNM classification of prostate cancer *Prostate* **1992**,4(Suppl) 129-138
13 Ayala GA, Ro JY, Babaian R, Troncoso P, Grignon DJ The prostatic capsule does it exist? *Am J Surg Pathol* **1989**,13 21-27
14 Carrol CL, Sommer FG, McNeal JE, Stamey TA The abnormal prostate MR imaging at 1 5 T with histopathologic correlation *Radiology* **1987**,163 521-525
15 McNeal JE Normal anatomy of the prostate and changes in benign prostatic hypertrophy and carcinoma *Sem in US,CT,and MR* **1988** 9 329-334
16 Ling D, Lee JK, Heiken JP, Balfe DM, Glazer HS, McClennan BL Prostatic carinoma and benign prostatic hyperplasia Inability of MR imaging to distinguish between the two diseases *Radiology* **1986**,158 103-107
17 Montie JE Staging of prostate cancer *Cancer* **1995** 75 1814-1818
18 Voges GE, McNeal JE, Redwine E, Freiha FS, Stamey TA Morphologic analysis of surgical margins with positive findings in prostatectomy for adenocarcinoma of the prostate *Cancer* **1992** 69 520-526
19 Epstein JI, Pizov G, Walsh PC Correlation of pathologic findings with progression after radical retropubic prostatectomy *Cancer* **1993**,71 3582 3593

20 Kleer E, Oesterling JE PSA and staging of localized prostate cancer *Urol Clin North Am* **1993**,20 695-704
21 Rifkin MD, Zerhouni EA, Gatsonis CA, et al Comparison of magnetic resonance imaging and ultrasonography in staging early prostate cancer Results of a multi-institutional cooperative trial *N Engl J Med* **1990**,323 621-626
22 Scardino PT, Shinohara K, Wheeler TM, Carter SS Staging of prostate cancer Value of ultrasonography *Urol Clin North Am* **1989**,16 713
23 Olson MC, Poniak HV, Fisher SG, et al Directed and random biopsies of the prostate indication based on combined results oftransrectal sonography and Prostate-Specific Antigen density determination *AJR* **1994**,163 1407-1411
24 Platt JF, Bree RL, Schwab RE The accuracy of CT in the staging of carinoma of the prostate *AJR* **1987**,149 315-318
25 Oyen RH, Van Poppel HP, Ameye FE, Van de Voorde WA, Baert AL, Baert LV Lymph node staging of localized prostatic carcinoma with CT and CT-guided fine-needle aspiration biopsy prospective study of 285 patients *Radiology* **1994**,190 315-322
26 Schnall MD, Imai Y, Tomaszewski JE, Pollack HM, Lenkinski RE, Kressel HY Prostate cancer local staging with endorectal surface coil MR imaging *Radiology* **1991**,178 797-802
27 Tempany CMC, Zhou X, Zerhouni EA, et al Staging of prostate cancer results of radiology diagnostic oncology group project comparison of three MR imaging techniques *Radiology* **1994**,192 47-54
28 Hricak H, White S, Vigneron DB, et al Carcinoma of the prostate gland MR imaging with pelvic phased-array coils versus integrated endorectal-pelvic phased-array coils *Radiology* **1994**,193 703-709
29 McNeal JE, Villers A, Redwine E, Freiha FS, Stamey TA Capsular penetration in prostate cancer Significance for natural history and treatment *Am J Surg Pathol* **1990**,14 240-247
30 Epstein JI Evaluation of radical prostatectomy capsular margins of resection the significance of margins designated as negative, closely approaching, and positive *Am J Surg Pathol* **1990**,14 626-632
31 Epstein JI, Carmichael MJ, Pizov MJ, Walsh PC Influence of capsular penetration on progression following radical prostatectomy A study of 196 cases with long-term follow up *J Urol* **1993**,150 135-141
32 d'Amico AV, Whittington R, Schnall MD, et al The impact of the inclusion of endorectal coil magnetic resonance imaging in a multivariate analysis to predict clinically unsuspected extraprostatic cancer *Cancer* **1995**,75 2368-2372
33 Montie JE 1994 Staging system for prostate cancer *Cancer* **1994**,74 1-3
34 Bostwick DG, Graham SD, Napalkov P, et al Staging of early prostate cancer a proposed tumor volume-based prognostic index *Urology* **1993**,41 403-411
35 Forsslund G, Esposti P-G, Nilsson B, Zeterberg A The prognostic significance of nuclear DNA content in prostatic carcinoma *Cancer* **1992**,69 1432-1439
36 Mohler JL, Figlesthaler WM, Zhang X-Z, Partin AW, Maygarden SJ Nuclear shape analysis for the assessment of local invasion and metastases in clinically localized prostate carcinoma *Cancer* **1994**,74 2996-3001
37 Oesterling JE Prostate specific antigen a critical assessment of the most usefull tumor marker for adenocarcinoma of the prostate *J Urol* **1991**,145 907-923
38 Brawer MK, Deerings RE, Brown M, Preston SD, Bigler S Predictors of pathologic stage in prostatic carcinoma The role of neovascularity *Cancer* **1994**,73 678-687
39 Stamey TA, Freiha JF, McNeal JE, Redwine E, Whittemore AS, Schmidt HP Localized prostate cancer Relationship of tumor volume to clinical significance for treatment of prostate cancer *Cancer* **1993**,suppl 71 933-938
40 Bezzi M, Kressel HY, Allen KS, et al Prostatic carcinoma staging with MR imaging at 1 5 T *Radiology* **1988**,169 339-346
41 Kahn T, Bürrig K, Schmitz-Drager B, I ewin JS, Fürst G, Modder U Prostatic carcinoma and benign prostatic hyperplasia MR imaging with histopathologic correlation *Radiology* **1989**,173 847-851
42 McSherry SA, Levy F, Schiebler ML, Keefe B, Dent GA, Mohler JL Preoperative prediction

of pathological tumor volume and stage in clinically localized prostate cancer comparison of digital rectal examination, transrectal ultrasonography and magnetic resonance imaging *J Urol* **1991**,146 85-89

43 Outwater E, Schiebler ML, Tomaszewski JE, Schnall MD, Kressel HY Mucinous carcinoma involving the prostate atypical findings at MR imaging *JMRI* **1992**,2 597-600

44 Bryan PJ, Butler HE, Nelson AD, et al Magnetic resonance imaging of the prostate *AJR* **1986**,146 543-548

45 Sesterhenn IA, Mostofi FK, Mattrey RR, Sands JP, Davis CJ,Jr , McCarthy WF Preliminary results of three-dimensional reconstruction of previously imaged prostates *Prostate* **1992**,Suppl 4 33-41

46 Sommer FG, Nghiem HV, Herfkens R, McNeal JE, Low RN Determing the volume of prostatic carcinoma value of MR imaging with an external-array coil *AJR* **1993**,161 81-86

47 Kier R, Wain S, Troiano R Fast spin-echo MR imaging of the pelvis obtained with a phased-array coil value in localizing and staging prostatic carcinoma *AJR* **1993**, 161 601-606

48 Jager GJ, Barentsz JO, de la Rosette J, Peters H, Hanselaar A, Oosterhof GON Value of dynamic subtraction turbo-FLASH MR imaging in prostate cancer *Radiology* **1994**,193(P) 316(Abstract)

49 Kurhanewicz J, Dahiya R, Macdonald JM, Chang L-H, James TI , Narayan P Citrate alterations in primary and metastatic human prostatic adenocarcinomas ^{1}H Magnetic resonance spectroscopy and biochemical study *MRM* **1992**,29 149-157

50 Kelly IMG, Lees WR Prostate cancer and the role of color doppler US *Radiology* **1993**,189 153-156

3 Local Staging of Prostate Cancer with Endorectal MR Imaging: Correlation with Histopathology

G. Jager[1], E. Ruijter[2,3], C. van de Kaa[3], J. de la Rosette[2], G. Oosterhof[2], J. Thornbury[4], J. Barentsz[1]

Departments of [1]Radiology, [2]Urology and [3]Pathology, University Hospital Nijmegen, The Netherlands; [4]Department of Radiology, University of Wisconsin-Madison, USA

Abstract

Objective

To evaluate the accuracy of MR imaging of the prostate with an endorectal surface coil in determining presence, localization, volume, and local stage of prostate carcinoma.

Subjects and Methods

MR images of 34 patients with biopsy-proven cancer were correlated retrospectively with the histologic mappings of radical prostatectomy specimens. The volume and number of tumor lesions on MR images were calculated and compared with the surgical specimens used as the gold standard. Tumor stage based on MR imaging was compared with the pathological stage according to the TNM classification. Predictive values were calculated seperately for all lesions and for the lesions correctly localized with MR.

Results

MR imaging correctly depicted the location of 67% of the tumors. Twenty percent of the lesions depicted by MR appeared to be false-positive errors. The tumors that were missed were located centrally and ventrally in the prostate. Tumor volume as shown by MR imaging was within a 25% range of the actual tumor volume in 10 cases, overestimated in 16 cases, and underestimated in eight cases. Histopathology showed capsular penetration in 12 of 34 patients (35%) and in 14 of 52 lesions (27%). Sensitivity, specificity, and positive predictive values were 43%, 84%, and 55%, respectively. Histologically, capsular penetration extended less than 1 mm into the periprostatic adipose tissue in seven patients. Sensitivity for capsular penetration less than 1 mm was 14%. Sensitivity for capsular penetration more than 1 mm was 71%. Accuracy for differentiating a pT2 from a pT3 tumor was 68%.

Conclusions

Results from this study indicate that the accuracy of the technique was not satisfactory for predicting actual tumor volume. Tumor detection and localization was more accurate in the peripheral zone than in the central zone. Accuracy was poor for detecting capsular penetration of less than 1 mm, but accuracy was

much better for penetration of more than 1 mm Because recent reports suggest that capsular penetration of less than 1 mm does not adversely affect surgical cure, MR imaging still may be practical in the selection of patients for radical prostatectomy

Introduction

The incidence of prostate cancer is still increasing The disease trails only lung cancer as the leading cause of death in men [1] Staging of prostate cancer is a systematic classification of the extent of disease based on clinical and pathologic criteria Clinical stage is used to sort patients into comparable groups for definitive therapy, whereas pathological stage is important in predicting prognosis and the need for additional therapy Curative treatment is considered possible only if the tumor is confined to the prostate gland (stage $\leq$ T2) [2] Therefore, differentiation between a T2 and a T3 tumor is of clinical importance On the other hand, several reports have stated that patients with minimal capsular penetration have a prognosis similar to that of patients whose tumors are completely confined to the prostatic capsule [3,4]

It is still not established what MR imaging technique results in the most accurate diagnosis and preoperative staging Initially, the accuracy of body coil MR imaging with conventional spin-echo sequences was promising [5] Body coil MR imaging has the advantage that pelvic bones and lymph nodes can also be evaluated during the same session However, the signal-to-noise ratio and the spatial resolution are too low to provide high-resolution images of the prostate [6]

With the recent development of an endorectal surface coil (ERC), the prostate and its surrounding structures are visualized much better [7] With fast spin-echo (FSE) techniques, T2-weighted images in three different planes are obtained in a shorter time with a higher-resolution matrix and fewer motion artifacts than images obtained with conventional spin-echo sequences [8] The results is suggested, is improved staging accuracy

Several recent studies have reported the results of MR imaging with ERC technique imaging for staging prostate cancer [7,9-16] Accuracy levels ranged from 54% to 83% In three of these studies, FSE MR images with an ERC were correlated with histopathologic mapping [12,14,16]

As an adjunct to staging, the volume of prostate cancer is also important for prognosis [17-19] When tumor volume is smaller than 4 cc, metatasis is very unlikely whereas when tumor volume exceeds 12 cc metastases is highly likely [20] MR sequences with standard body coil and conventional spin-echo techniques have not given accurate images for estimating tumor volume before surgery [5,21-25] However FSE MR images obtained with a phased-array coil showed a better job of estimating of tumor volume [8]

In our study we evaluate the diagnostic accuracy of MR imaging with FSE sequences that use an ERC to determine tumor presence, tumor volume, and the preoperative stage of prostate carcinoma In addition, we identify common pitfalls of MR interpretation and the correlation of MR images with pathology

Subjects and Methods

Patient population

The study population was 34 patients with needle biopsy-proved adenocarcinoma. We performed MR imaging that used an ERC technique and followed that with radical retropubic prostatectomy. Patients mean age was 65 years old (range, 50-73 years). When biopsies preceded MR imaging, the average time was three weeks. Patients underwent radical prostatectomy within three weeks of imaging. Patients who underwent MR imaging and then received hormonal treatment before surgery were excluded from this study. All patients had clinical T2-3 disease according to the TNM classification (Table 1) [26]. We detected no lymph-node metastases in frozen sections at laparoscopic or open lymph-node dissection that preceded the radical prostatectomy.

MR Technique

All images were obtained using a 1.5 T Siemens SP system (Siemens, Erlangen, Germany), and a Medrad® endorectal coil (Medrad, Pittsburgh, PA). We placed the coil with the patient in the lateral decubitus position and inflated the coil with 50-100 cc of air. Peristalsis was suppressed by IV administring 1 mg of glucagon. A tight band was wrapped around the patients abdomen to decrease respiratory movement.

A sagittal T1-weighted localized image was obtained to confirm coil positioning and to select locations for the axial images. Axial T-1 weighted images (420/22[TR/TE]) as well as axial, sagittal and coronal FSE T2-weighted images (2940/160[TR/TE], echo-train length of 13) were performed. All examinations

Table 1. TNM classification. Primary tumor (T) 1992 revision [26]
Number of cases, figure in parentheses is the number correctly identified by MR

TX Primary tumor cannot be assessed	
T0 No evidence of primary tumor	0 (0)
T1 Clinically apparent tumor, not palpable nor visible by imaging	
– T1a Tumor is incidental histologic finding in 5% or less of tissue resected	0 (0)
– T1b Tumor is incidental finding in more than 5%	0 (0)
– T1c Tumor identified by needle biopsy (due to elevated serum PSA)	0 (0)
T2 Tumor palpable or visible by imaging confined to the prostate	
– T2a Tumor involves half of a lobe or less	2 (0)
– T2b Tumor involves more than half of a lobe but not both lobes	0 (0)
– T2c Tumor involves both lobes	20 (11)
T3 Tumor extends through the prostatic capsule	
– T3a Unilateral extracapsular extension	3 (0)
– T3b Bilateral extracapsular extension	3 (2)
– T3c Tumor invades seminal vesicles	6 (3)
T4 Tumor is fixed or invades adjacent structures other than seminal vesicles	0 (0)
– T4a Tumor invades bladder neck and/or external sphincter and/or rectum	
– T4b Tumor invades levator muscles and/or is fixed to pelvic wall	

Correct local staging by MR imaging as confirmed by histo-pathological examination according to TNM: 16/34 = 47%

were performed using a 4- or 5- mm slice thickness with a 1- or 2- mm gap, 26 cm field of view, and a 512 x 216 matrix. An equalizing processing after application and a filter algorithm to compensate for near-field effect were also used. We also changed the phase encoding gradient to decrease motion artifacts over the prostate. An examination usually lasted 30 to 45 minutes.

MR imaging examination

The MR images were retrospectively interpreted by a single reader (G.J.) who had been interpreting MR examinations for prostate cancer and correlating the results with clinical and pathologic outcome for more than two years. The reader had no knowledge of the clinical findings, the PSA level, or the results of histopathologic examination or transrectal sonography. Image quality was recorded with special regard to motion artifacts. An image was considered to be of poor quality when the delineation of the anatomic structures was degraded by motion artifacts. Good quality meant that these artifacts did not significantly degrade delineation of structures.

On T2-weighted images, an area in the peripheral zone with a low signal intensity when compared with the adjacent peripheral zone was considered to be a malignancy. Low signal-intensity areas in the central zone were not interpreted as malignancy [27]. If a low signal intensity showed high signal on the corresponding T1-weighted image, the area was considered to be a hematoma.

Tumors separated by more than 1 cm, without connection to another tumor in an adjacent section were interpreted as separate tumor lesions. Tumor volume was calculated by the sum of tumor areas multiplied by slice thickness, including gaps between slices.

We used the following criteria to define capsular perforation: disruption of the prostatic capsule, infiltration of the periprostatic fat, low-signal-intensity stranding, and involvement of the neurovascular bundle. A bulge in the contour or capsular thickening was not interpreted as capsular perforation [9,12]. Abnormally low signal intensity within the lumen of the seminal vesicle or focal thickening of the seminal wall was interpreted as seminal vesicle invasion [9]. Final staging was recorded according to the TNM classification (Table 1) [26].

Pathologic examination

The prostatectomy specimens were in toto fixed overnight in a solution of 4% neutral buffered formalin. Step-sections were made at 4 mm intervals in a plane parallel to the base of the prostate, which corresponded to the slices used on MR imaging. After separating the step-sections into right and left halves, all sections were routinely embedded in paraffin. Tissue sections of 5 μm were prepared and stained with hematoxylin and eosin. Regions representing cancer were outlined on the glass cover and retraced onto a diagram of the axial histologic sections that extended from the base to the apex of the prostate. To estimate tumor volume, the sum of the cancer areas on all sections was multiplied by 4 mm (slice thickness). The volume was then multiplied by a factor 1.1 to correct for tissue

shrinkage due to fixation. Length and depth of penetration through the capsule and involvement of each seminal vesicle was recorded. Definitive staging was performed with the TNM classification [26].

Data Analysis

Analysis of the correlation of MR findings and histopathology were performed by a radiologist (G.J.) and a pathologist (E.R). The MR images were correlated with tumor maps that were based on the histopathologic sections. Tumor localization, number of tumors, tumor volume, status of the prostate capsule, involvement of each seminal vesicle, and definitive stage were evaluated.

To offset the bias of incorrectly identified lesions (false positives), we analyzed matched lesions (true positives). A tumor location was considered to match if the tumor was present in the same craniocaudal third of the prostate (proximal, mid, or distal) and the tumor was localized in the same quadrant, regardless of the size of the lesion. Penetration through the capsule was compared for each tumor lesion.

Results

The endorectal coil was well-tolerated by all patients. In 28 patients, images obtained with the ERC provided detailed visualization of the prostate, prostatic capsule, and periprostatic structures, including the seminal vesicles. In six patients, image quality was poor due to motion artifacts caused by bowel motion (N=5) or due to upwards migration of the endorectal coil (N=1). Minor image degradation resulted from biopsy hematoma, high signal intensity close to the ERC (near-field effect), and shallow penetration depth of the ERC, however, image quality remained good.

Pitfalls in correlating MR images with histopathologic findings

The correlation between MR images and tumor maps based on histopathology was difficult in almost all patients. The most caudal section of MR images was 0.5–1.5 cm lower than the section representing the apex in the prostatectomy specimen. Also, the angle by which the sections were cut was never exactly the same for either technique (difference 5°–15°). Furthermore, the shape of the prostate changed after fixation. Also making correlation difficult was the fact that the prostate tumors were markedly irregular and often demonstrated fingerlike projections with ill-defined margins that did not display on MR images of 4 or 5 mm (while the histologic sections are only 4 μm thick). We tried to overcome these problems by using tumor maps, which gave a good three-dimensional picture of the prostate. We also employed our definition of a matched lesion.

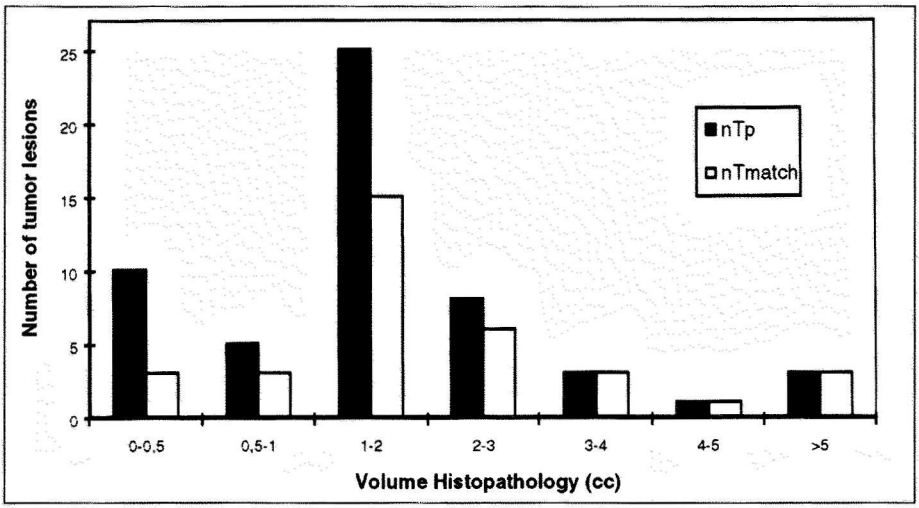

Fig. 1. Bar graph shows the distribution of lesions determined with histopathology (*solid bar*) ranged in order of the actual tumor volume and the degree of match lesions (*open bar*), tumors less than 2cc easily remain undetected with MRI.

Number and localization of tumor lesions

A total of 44 separate tumor lesions were visualized with MR imaging and 52 were found on histopathologic examination of 34 patients (mean number of tumors, 1.5; range 1-3). Thirty-four tumors were defined matched lesions (Fig. 1). In 10 false-positive lesions identified by MR imaging, histopathology showed adjacent cystic changes in six cases. In four other false-positive lesions identified by MR imaging, histopathology failed to show an explanation for the low signal intensity.

MR imaging correctly depicted the location of 67% of the tumors. Twenty-two percent of the lesions depicted by MR appeared to be false-positive errors. Fourteen of the 18 tumors that were missed were located in the central or ventral part of the prostate.

Tumor volume

The accuracy of MR imaging in predicting tumor volume is presented in Figure 2.

The mean volume of 44 tumor lesions captured on imaging with ERC was 2.3 cc (range, 0.25-11.6 cc). The mean volume of 52 histopathologically detected lesions was 1.5 cc (range, 0.4-7.2 cc). When we compared only matched lesions, the mean volume was 2.6 cc by MR imaging with ERC and 1.8 cc by histopathology. In seven matched lesions, the tumor volume estimated by MR imaging fell within a 25% range of the actual volume. In 19 other cases, MR imaging overestimated the actual tumor volume by more than 25% (Fig. 3) and in eight other cases, the underestimation by MR imaging exceeded 25%. In the latter group, 50% of the lesions were located in the central or ventral part of the prostate.

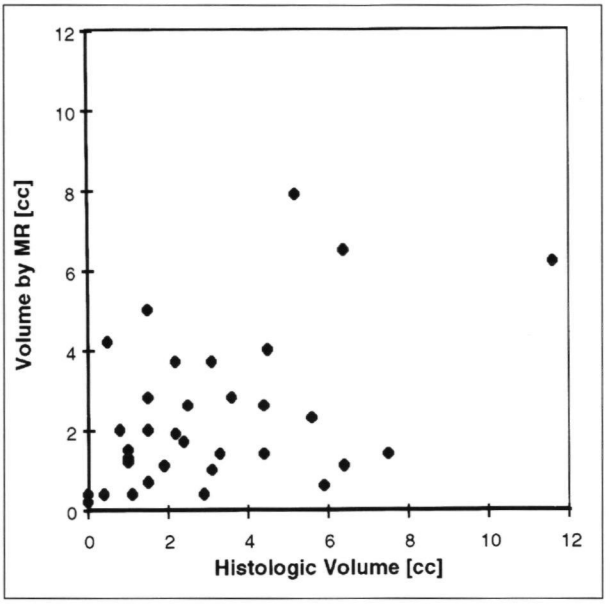

Fig. 2. Scatterplot shows poor correlation between volume determined by MR imaging and the actual tumor volume.

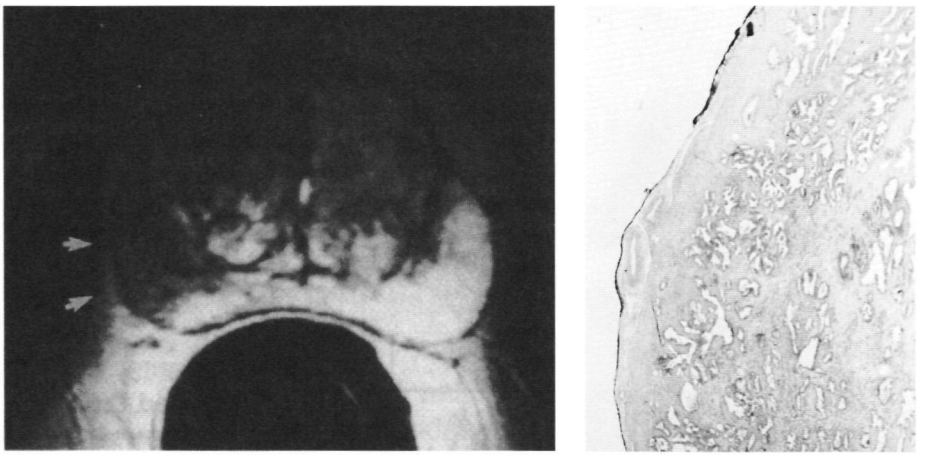

Fig. 3. Overestimating of tumor volume and underestimating of number of tumors in a 62-year-old man. **A**, Axial fast-spin-echo T2-weighted image shows zone of decreased intensity on right (*arrows*), interpreted as carcinoma. The estimated volume was 3.3 cc. At pathologic examination there was almost symetrical bilateral tumor location. The calculated tumor volume both right and left was 0.7cc. **B**, Photograph of histopathologic section shows Adenocarcinoma diffusely growing between benign glands.

Capsular penetration

In 11 of 44 (25%) lesions identified by MR imaging, evidence of capsular penetration was stated. In 14 of 52 (27%) lesions detected by histopathology, capsular penetration was present. False-positive capsular penetration was present in four matched and in one false-positive lesion. Three cases of false-positive

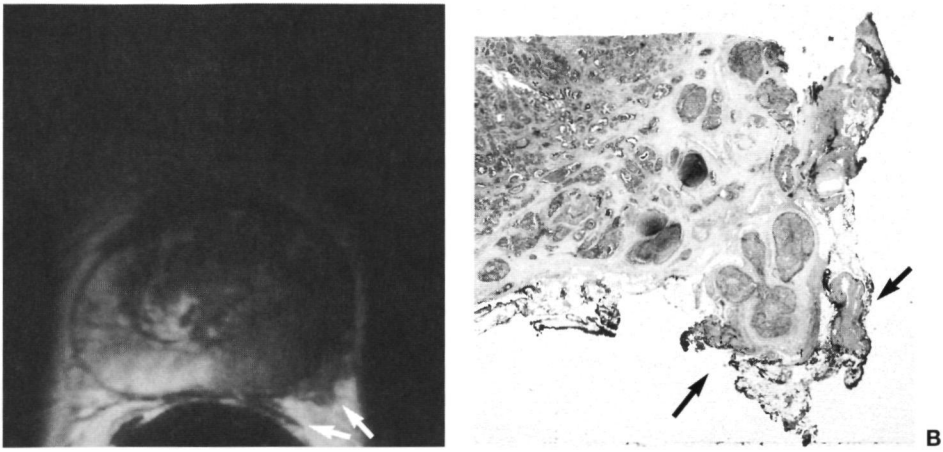

Fig 4. Good correlation between MR imaging and pathology in a 57-year-old patient. **A**, Axial T2-weighted fastspin-echo image shows gross extracapsular tumoral involvement of the extraprostatic tissue (*arrows*). **B**, The photograph of pathologic specimen shows close match for the status of the capsule and tumor volume (*arrows*).

Table 2. Results of MR imaging for capsular penetration with all histologic lesions

	Histopathology		
MR Findings	Present	Absent	Total
Present	6	5	11
Absent	8	33	41
Total	14	38	52

Note: Sensitivity = 42%, specificity = 87%, accuracy = 75%, positive predictive value = 55%.

Table 3. Results of MR imaging for capsular penetration with matched lesions

	Histopathology		
MR Findings	Present	Absent	Total
Present	6	4	10
Absent	5	19	24
Total	11	23	34

Note: Sensitivity = 55%, specificity = 85%, accuracy = 74%, positive predictive value = 60%.

capsular penetration occured in MR examinations with poor image quality due to motion artifacts.

Histologically, seven patients had capsular penetration with a width of more than 5 mm; MR imaging correctly identified the capsular penetration in four of them. Seven patients had capsular penetration with a width less than 5 mm; MR imaging correctly identified two of them. Histologically, capsular penetration extended less than 1 mm into the periprostatic adipose tissue in seven lesions, 1–3 mm, in six; and more than 3mm, in 1 patient (Fig. 4). Sensitivity of MR for depicting capsular penetration into the periprostatic tissue was respectively 14% when that penetration was less than 1 mm, 67% when 1–3 mm, and 100%. when more than 3 mm (Fig. 5).

The capsular bulge sign was not used because it may lead to false-positive findings [9]. Capsular bulge was found in four cases, once in a true-positive T2 tumor, once in a false-negative T3 tumor and twice in (for other reason) true-positive T3 tumors. Thus this criterium would not change the overall accuracy for capsular penetration.

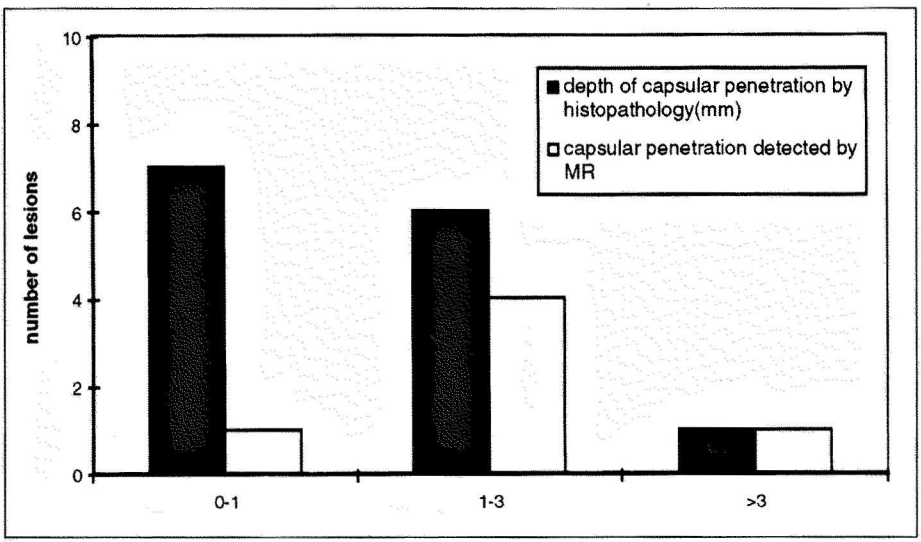

Fig 5. Bar graphs shows the relation of detecting capsular penetration with MR imaging (*open bar*), to the depth of tumor invasion (mm) on histopathology (*solid bar*). Sensitivity was 14%, 70% and 100%. for capsular penetration of less than 1 mm, between 1 and 3 mm, and more than 3mm, respectively.

Table 4. Results of MR imaging for seminal vesicle invasion

	Histopathology		
MRI	Present	Absent	Total
Present	4	7	11
Absent	7	51	57
Total	11	57	68

Note: Sensitivity = 36%, specificity = 88%, accuracy = 79%, positive predictive value = 36%.

Table 5. Results of MR imaging for seminal vesicle invasion for each patient

	Histopathology		
MR Findings	Present	Absent	Total
Present	3	5	8
Absent	6	20	26
Total	9	25	34

Note: Sensitivity = 33%, specificity = 80%, accuracy = 68%, positive predictive value = 38%.

Five patients had also positive surgical margins. However, because the surgeon incised the capsule, capsular penetration could not be evaluated in those sections. (Overall figures are given in Tables 2 and 3).

Invasion of seminal vesicles

All 68 seminal vesicles were visualized. MR imaging showed tumor invasion in 11 seminal vesicles of eight patients, of which four lesions were confirmed on histopathology. In 51 out of 57 seminal vesicles, invasion was correctly excluded with MR imaging. The sensitivity was 36% (4/11). The specificity was 88% (51/57). The positive predictive value was 36% (4/11). The results are presented in Table 4 and 5. The seven false-positive seminal vesicles showed no abnormalities in the corresponding histopathologic sections. In particular, fibrosis, inflammatory

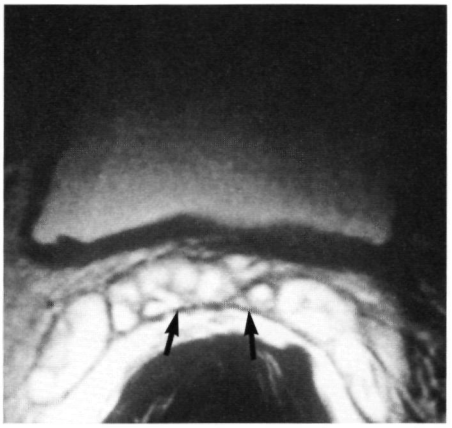

Fig 6. Axial T2-weighted fastspin-echo image of a 67-year-old patient shows thickening of the wall of the seminal vesicles (*arrows*). Seminal vesicle invasion was confirmed at pathologic examination.

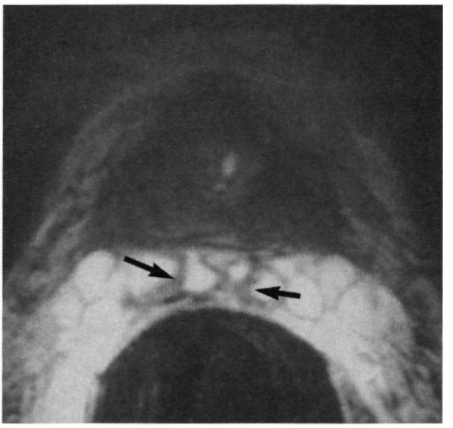

Fig 7. Axial T2-weighted fastspin-echo image of a 63-year-old patient shows more pronounced tubular thickening (*arrows*) is demonstrated in this patient, but seminal vesicle invasion was not present at pathologic examination.

Table 6. Results of detecting extra prostatic disease (T3)

	Histopathology		
MR Findings	p ≤ T2	p ≥ T3	Total
m ≤ T2	15	4	19
m ≥ T3	7	8	15
Total	22	12	34

Note: Sensitivity T3 = 67%, specificity T3 = 68%, accuray = 68%, negative predicting value T3 = 79%, positive predicting value T3 = 53%.

infiltrate, amyloid depositions and blood were excluded. Eight vesicles showed focal thickening of the tubular wall. Only four of them were true positive (Figs. 6 and 7).

Staging prostate cancer

For all patients, we evaluated final staging of prostate cancer by comparing MR images with pathologic appearances (Table 1). With the TNM classification, staging was correct in 15 out of 34 (34%) patients. When staging was limited to depict locally advanced disease, (≥ T3, formerly Jewitt stage C) sensitivity, specificity, accuracy and positive predictive values of MR staging were 67%, 68%, 68%, and 53%, respectively (Table 6).

One patient who had stage pT3b (bilateral capsular penetration) disease was staged with MR imaging as mT3c without capsular perforation. Another patient was correctly staged as mT3 because of a false-positive and a false-negative lesion; thus staging by MR imaging in these patients was correct for an incorrect reason.

Discussion

Motion artifacts were the primary cause of low-quality images in five examinations (14%). Also, of these five cases, three had false-positive capsular penetration. Little is reported in the literature about significant motion artifacts and the use of ERC. However, with FSE imaging and a pelvic phased-array multicoil, one study reported significant motion artifacts in up to 45% of examinations when glucagon was not used versus 7% with glucagon [8].

Number and localization

In our study, we achieved good correlation between number and localization of tumors. The positive predictive value and sensitivity level was relatively high, comparable to that of other studies [12, 14, 25, 28]. We confirmed that tumors located ventrally and centrally on histopathologic examination are pitfalls for false-negative tumors. Carter et al. [28] found a sensitivity of 15% in detecting anterior tumors, a percentage considerably lower than they achieved in detecting posterior tumors (85%). Outwater et al. [12] did not identify any of 29 central gland tumors, and 41 of 56 (73%) of peripheral tumors on MR imaging that used an ERC technique.

Causes for false-positive findings that are reported in the literature include hyperplasia, prostatitis, postbiopsy hemorrahge with blood in the extracellular methaemaglobin state, and areas of cystic change [25]. Cystic change increases the signal intensity of the peripheral zone, resulting in a relatively low signal intensity compared with adjacent areas of normal prostate which may be confused with malignant lesions. We found histologic evidence of hematoma nor other pathologic changes in areas defined as haematoma on T1-weighted images. These findings concur with a study in which 27 false-positive lesions that corresponded with areas of hemorrhage on T1-weighted images did not show any pathologic substrate, especially no evidence of hemorrhage [14]. Also the pathologist, cited by Tempany et al., stated that the effects of hemorrhage and biopsy are difficult to quantify and cannot always be identified at pathologic analysis [16].

Tumor volume

Tumor volume is a known predictor of pathologic stage [17]. With a tumor volume larger than 12 cc, extraprostatic spread of disease has likely occurred, whereas tumors smaller than 4 cc are usually locally confined [20]. Tumor volume is reported to correlate more closely with progression than with capsular penetration [19].

We found a poor correlation between tumor volumes calculated from MR images and those found at pathologic examination. Although pathologic examination frequently showed tumor extension into the central and ventral part of the prostate, MR images overestimated mean volume in all lesions and in matched lesions. We could not identify any reasons for this overestimate of tumor volume by MR imaging.

Studies performed with MR imaging using body coils reported a poor correlation between tumor volume as depicted on MR imaging and the volume calculated from the pathologic specimen [5, 21, 22, 24]. No studies in the literature used an ERC, although one study was performed with an external array coil and FSE technique [25]. This study reported a significant correlation between tumor volume calculated with MR images and that of the pathological specimen ($R=0.81$, $P<0.001$), but their accuracy was not enough to be helpful in making clinical decisions.

To meet the problems of low predictive values for detecting tumors and estimating their volumes, studies have been performed that evaluated IV contrast medium enhanced T1-weighted images [11,29]. However improvement over T2-weighted FSE images was not observed. Nonetheless, the report of one study that used dynamic, single-slice T1-weighted technique after IV contrast medium with a high-time resolution (one image/sec) suggests that a better delineation of prostate cancer detection, volume, and staging may be possible with MR imaging [30].

Capsular penetration

Accuracy for capsular penetration in our study was low for matched lesions (55%) because capsular penetration was less than 3 mm in all but one case. On matched lesions we found no relation between the width or length of the capsule at pathologic examination and the staging accuracy with MR imaging. Five patients with positive surgical margins due to incission by the surgeon through the capsule were classified as T2 because penetration through the prostatic capsule could not be confirmed. Of these five, MR classification was T2 in three and T3 in two cases.

In a recent overview, Schriebler et al. stated that body coil MR imaging proves unsatisfactory at detecting capsular penetration due to the limited spatial resolution of the imaging technique [31]. MR imaging that uses ERC technique is reported to provide a more reliable identification of the prostatic capsule [15]. Detection of capsular penetration with MR imaging with ERC technique had a sensitivity of 67% compared with body coil MR imaging that had a sensitivity of 44% in the same patient cohort. However results of recent studies of MR imaging with ERC technique showed limited accuracy for detecting capsular penetration [9, 12, 14, 16]. For example, Tempany et al. reported accuracy rates of MR imaging with ERC technique for detecting capsular penetration from different institutions ranged from 33% to 54%, less accurate compared to conventional body-coil MR imaging [16].

These conflicting findings may result from the lack of highly specific and sensitive diagnostic criteria for capsular penetration. One study has evaluated six different diagnostic criteria for capsular penetration [12]. The positive predictive value of each individual sign ranged from a minimum of 4% for capsular thickening to a maximum of 34% for extracapsular tumor.

It should be noted that focal penetration probably has a prognosis comparable to T2 tumors [3]. Therefore, only identification of deeper penetration may be of clinical importance [32].

Seminal vesicle invasion

The accuracy for detecting seminal vesicle involvement in our series agreed with that in other series. A high specificity (85%-97%) and a low sensitivity (21%-63%) [9, 14, 16] were reported. In our study, the figures were 82% and 50%, respectively. Although we could not explain the false-positive findings in the histopathology, low signal intensity of the seminal vesicles on T2-weighted images can be caused by amyloid deposits [33], or seminal vesicles that contains stones or blood [31]. Focal tubular thickening proved unreliable in predicting seminal vesicle involvement in our series.

Overall staging

In our study, staging according to the TNM classification was correct in 47% of the patients. Accuracy for differentiating a T2 from a T3 tumor was 68%. Except for Hricak et al. [14] other studies restricted staging to differentiating T2 from T3. The first series on imaging with an ERC reported a 82% accuracy rate which was a 16% improvement over body coil staging with the same cohort of patients [15]. Recent series reported an overall accuracy of 54%-68% for MR imaging that used an ERC [9,12,14,16]. It must be noted that the accuracy in prospective studies (51%) is considerable lower than in retrospective studies (67%) [14, 34].

The patient group in our study was limited to the patients who underwent radical prostatectomy. It should be emphasized that we also perform MR imaging on the prostates of patients who did not underwent radical prostatectomy for reasons of positive lymph nodes, or because of the overall staging results. The accuracy rate might well be different if this group was also included

Difficulties in evaluating the literature

The continuous, rapid technical development of image sequences and coil design like pelvic phased-array and integrated endorectal pelvic phased-array coils [35] can produce a wide divergence of image quality. Imaging with the combination of an ERC and a phased-array multicoil is now advocated as the most powerfull imaging tool.

In addition, a broad spectrum of diagnostic signs (often indirect) and differently defined criteria for capsular penetration make meta-analysis of the literature difficult. For example, authors of one report changed image sequences, surface coils, and diagnostic criteria during the study [14]. Also, not all reports are blinded in the same way. Accuracy levels may be pushed higher when clinical data (PSA, prior histories of prostatitis, and locations of the positive biopsy findings) are integrated with interpretation of the images as recommended by Schiebler et al. [31]. Furthermore it is often difficult to assess the extent that information gained from MR imaging was used in patient management (verification bias) [36,37]. In our institution, the prevalence of T3 tumors at operation has decreased from 63% in the study by Jager et al. [10] to 35% in this study. Because prostate cancer often leads to surgery at an early stage [38], correction for verification bias remains impossible. For these reasons, comparison of our presented figures to those of other studies is very difficult.

Conclusion

Although MR imaging using an ERC with FSE was not highly accurate in predicting definitive tumor volume or definitive stage, the technique may prove helpful when selecting patients for definitive therapy because small capsular penetration of less than 1 mm often not detected by MR-imaging, does not rule out radical prostatectomy Follow-up studies are neccessary to evaluate the effect of understaging minimal capsular penetration

In our series, overstaging occurred frequently in cases with low quality image due, at least in a part, to motion artifacts

Because tumor volume is likely to be more important than focal capsular penetration, the accuracy of assessing tumor volume must improve Dynamic, single-slice T1-weighted technique that uses an IV contrast medium with high-time resolution (1 image/sec) shows promise of improved accuracy [30]

Because the value of MR imaging is not yet established and because the results of studies are difficult to compare, we conclude that those who perform MR imaging in cases of prostatic cancer should determine their own standard of accuracy by carefully comparing their imaging results with histopathologic findings

Acknowledgments

The authors like to thank Prof Dr D J Ruiter and Dr J A Schalken for helpful comments

References

1 Borings CC, Squires TS, Tong T Cancer statistics, 1993 *CA Cancer J Clin* **1993**,43 7-26
2 Steinfield AD Questions regarding the treatment of localized prostate cancer *Radiology* **1992**,184 593-598
3 Epstein JI, Carmichael MJ, Pizov MJ, Walsh PC Influence of capsular penetration on progression following radical prostatectomy A study of 196 cases with long-term followup *J Urol* **1993**,150 135-141
4 Epstein JI, Pizov G, Walsh PC Correlation of pathologic findings with progression after radical retropubic prostatectomy *Cancer* **1993**,71 3582 3593
5 Bezzi M, Kressel HY, Allen KS, et al Prostatic carcinoma staging with MR imaging at 1 5 T *Radiology* **1988**,169 339-346
6 Rifkin MD, Zerhouni EA, Gatsonis CA, et al Comparison of magnetic resonance imaging and ultrasonography in staging early prostate cancer Results of a multi-institutional cooperative trial *N Engl J Med* **1990**,323 621-626
7 Schnall MD, Lenkinski RE, Pollack HM, Imai Y, Kressel HY Prostate MR Imaging with an endorectal surface coil *Radiology* **1989**,172 570-574
8 Kier R, Wain S, Troiano R Fast spin-echo MR imaging of the pelvis obtained with a phased-array coil value in localizing and staging prostatic carcinoma *AJR* **1993**,161 601 606
9 Chelsky MJ, Schnall MD, Seidmon EJ, Pollack HM Use of endorectal surface coil magnetic resonance imaging for local staging of prostate cancer *J Urol* **1993** 150 391-395
10 Jager GJ, Barentsz JO, Rosette de la JJMCH, Rosenbusch G Preliminary results of endorectal surface coil magnetic resonance imaging for local staging of prostate cancer *Radiologe* **1994**,34 129 133

11 Mirowitz SA. Seminal Vesicles biopsy related hemorrhage simulating tumor invasion at endorectal MR imaging *Radiology* **1992**,185 373-376
12 Outwater E, Petersen RO, Siegelman FS, Gomella LG, Chernesky CE, Mitchell DG Prostate carcinoma assessment of diagnostic criteria for capsular penetration on endorectal coil MR images *Radiology* **1994**,193 333-339
13 Parivar F, Rajanayagam V, Waluch V, Eto RT, Jones LW, Ross BD Endorectal surface coil MR Imaging of prostatic carcinoma with the inversion-recovery sequence *JMRI* **1991**,1 657-664
14 Quinn SF, Franzini DA, Demlow TA, et al MR imaging of prostate cancer with an endorectal surface coil technique correlation with whole-mount specimens *Radiology* **1994**, 190 323-327
15 Schnall MD, Imai Y, Tomaszewski JE, Pollack HM, Lenkinski RE, Kressel HY Prostate cancer local staging with endorectal surface coil MR imaging *Radiology* **1991**,178 797-802
16 Tempany CMC, Zhou X, Zerhouni EA, et al Staging of prostate cancer results of Radiology Diagnostic Oncology Group project comparison of three MR imaging techniques *Radiology* **1994**,192 47-54
17 Bostwick DG, Graham SD, Napalkov P, et al Staging of early prostate cancer a proposed tumor volume-based prognostic index *Urology* **1993**,41 403-411
18 Stamey TA, Freiha JF, McNeal JE, Redwine E, Whittemore AS, Schmidt HP Localized prostate cancer Relationship of tumor volume to clinical significance for treatment of prostate cancer *Cancer* **1993**,suppl 71 933-938
19 McNeal JE, Villers A, Redwine E, Freiha FS, Stamey TA Capsular penetration in prostate cancer Significance for natural history and treatment *Am J Surg Pathol* **1990**,14 240-247
20 McNeal JE Cancer volume and site of origin of adenocarcinoma of the prostate relationship to local and distant spread *Hum Pathol* **1992**,23 258-266
21 Kahn T, Bürrig K, Schmitz-Drager B, Lewin JS, Fürst G, Modder U Prostatic carcinoma and benign prostatic hyperplasia MR imaging with histopathologic correlation *Radiology* **1989**,173 847-851
22 McSherry SA, Levy F, Schiebler MI , Keefe B, Dent GA, Mohler JL Preoperative prediction of pathological tumor volume and stage in clinically localized prostate cancer comparison of digital rectal examination, transrectal ultrasonography and magnetic resonance imaging *J Urol* **1991**,146 85-89
23 Outwater E, Schiebler ML, Tomaszewski JE, Schnall MD, Kressel HY Mucinous carcinoma involving the prostate atypical findings at MR imaging *JMRI* **1992**,2 597-600
24 Quint I E, Van Erp JS, Bland PH, et al Prostate cancer correlation of MR images with tissue optical density at pathologic examination *Radiology* **1991**,179 837-842
25 Sommer FG, Nghiem HV, Herfkens R, McNeal JE, Low RN Determing the volume of prostatic carcinoma value of MR imaging with an external-array coil *AJR* **1993**,161 81-86
26 Schroeder FH, Hermanek P, Denis I , Fair WR, Gospodarowicz MK, Pavone-Macaluso M The TNM classification of prostate cancer *Prostate* **1992**,4(Suppl) 129-138
27 Schiebler ML, Tomaszewski JE, Bezzi M, et al Prostatic carcinoma and benign prostatic hyperplasia correlation of high-resolution MR and histopathologic findings *Radiology* **1989**,172 131-137
28 Carter HB, Brem RF, Tempany CMC, et al Nonpalpable prostate cancer detection with MR imaging *Radiology* **1991**,178 523-525
29 Sommer FG, Nghiem HV, Herfkens R, McNeal JE Gadolinium-enhanced MRI of the abnormal prostate *Magn Reson Imaging* **1993**,11 941-948
30 Jager GJ, Barentsz JO, de la Rosette JJMCH, Peters H, Hanselaar A, Oosterhof GON Value of dynamic subtraction turbo-FLASH MR imaging in prostate cancer *Radiology* **1994**, 193(P) 316(Abstract)
31 Schiebler MI , Schnall MD, Pollack HM, et al Current role of MR imaging in the staging of adenocarcinoma of the prostate *Radiology* **1993**,189 339-352
32 Langlotz CP, Schnall MD, Malkowicz JB, Tomaszewski JE Prediction of subsequent prostate carcinoma recurence with preoperative staging with MR imaging Results of 3-year follow-up *Radiology* **1994**,193(P) 316(Abstract)
33 Ramchandani P, Schnall MD, LiVolsi VA, Tomaszewski JE, Pollack HM Senile amyloidosis

of the seminal vesicles mimicking metastatic spread of prostatic carcinoma on MR images *AJR* **1993**,161 99-100

34 Demlow TA, Quinn SF, Franzini DA, Rosencranz DR, Szumowski J, Kim J MR imaging of the prostate with endorectal surface coil technique and whole mount correlation *Radiology* **1993**,189(P) 251(Abstract)

35 Hricak H, White S, Vigneron DB, et al Carcinoma of the prostate gland MR imaging with pelvic phased-array coils versus integrated endorectal-pelvic phased- array coils *Radiology* **1994**,193 703-709

36 Greenes RA, Begg CB Assessment of diagnostic technologies methodology for unbiased estimation from samples of selectively verified patients *Invest Radiol* **1985**,20 751-756

37 Langlotz CP, Schnall MD, Pollack H Staging of prostatic cancer Accuracy of MR imaging *Radiology* **1995**,194 645-646

38 Lu-Yao GL,Greenberg ER Changes in prostate cancer incidence and treatment in USA *Lancet* **1994**,343 251-254

Interlude I
Amyloidosis of the Seminal Vesicles Simulating Tumor Invasion of Prostatic Carcinoma on Endorectal MR Images

G. Jager[1], E. Ruijter[2,3], J. de la Rosette[2], C. van de Kaa[3]

Departments of [1]Radiology, [2]Urology and [3]Pathology, University Hospital Nijmegen, The Netherlands

Abstract

Amyloid deposits within the seminal vesicles are a common finding at autopsy. The incidence increases with age. Amyloid deposits can mimic tumor extension into the seminal vesicles due to prostate or bladder cancer on T2-weighted Magnetic Resonance (MR) images. We describe a case of seminal vesicle amyloidosis demonstrating the MR appearance and the characteristic pathologic findings. Recognizing seminal vesicle amyloidosis may prevent overstaging prostate cancer on MR images.

Introduction

Amyloid deposits within the seminal vesicles are a common finding at autopsy. The reported incidence ranged from 9-16% [1,2] in an unselected population of men over the age of 50. The incidence increased with age and was found in 21% of men over 75 year [2]. Despite the high incidence, only two reports in the radiologic literature have described the Magnetic Resonance (MR) appearance of seminal vesicle amyloidosis [3,4]. In both cases, amyloid deposits were misinterpreted as tumor extension into the seminal vesicles due to prostate or bladder cancer. With the increasing use of MR as a staging modality, more men with vesicula amyloidosis will undergo such an examination. Recognizing this entity may prevent overstaging the tumor. We describe a patient in whom seminal vesicle amyloidosis was misinterpreted as extension of prostate cancer into the seminal vesicles on MR images obtained with an endorectal coil.

Case Report

A 61-year old, previously healthy man was referred to the urologic department because of a palpable nodus in the right lobe of the prostate. Transrectal ultrasound examination demonstrated a hypoechoic region in the base of the prostate extending into both seminal vesicles. Biopsies revealed bilateral moderately differentiated adenocarcinoma of the prostate. MR images were obtained with a 1,5 T Siemens SP system (Siemens, Erlangen, Germany), using a Medrad®

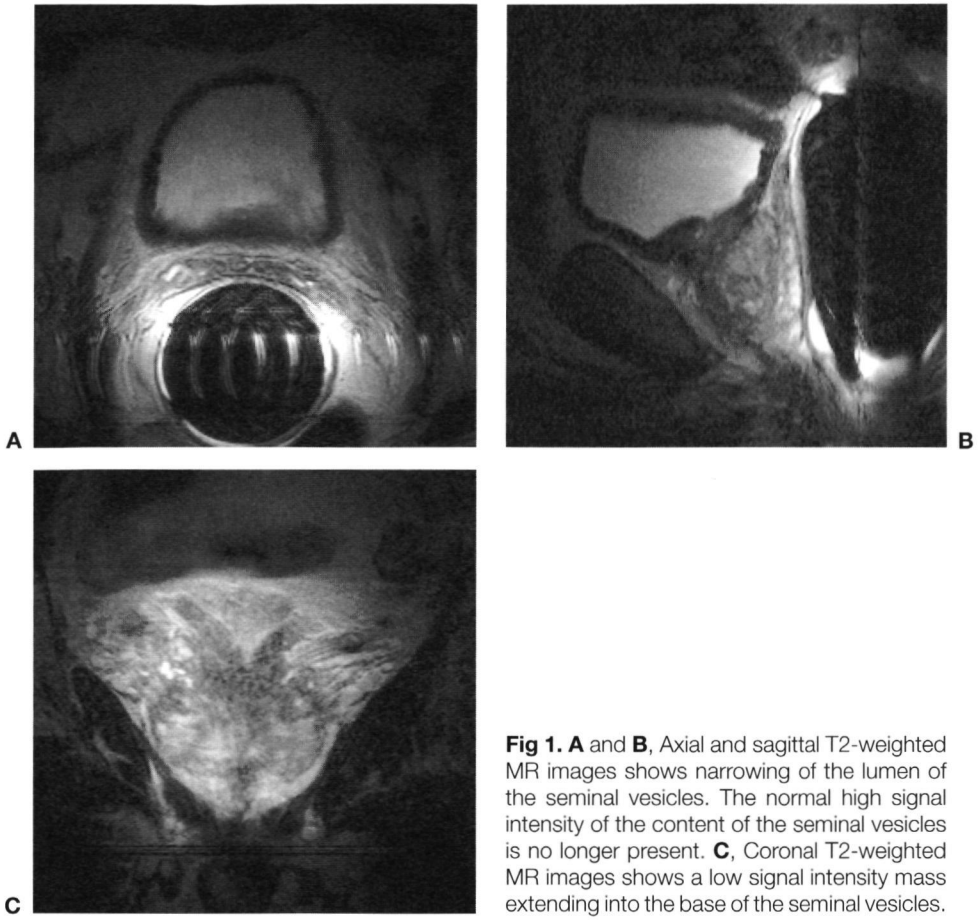

Fig 1. A and **B**, Axial and sagittal T2-weighted MR images shows narrowing of the lumen of the seminal vesicles. The normal high signal intensity of the content of the seminal vesicles is no longer present. **C**, Coronal T2-weighted MR images shows a low signal intensity mass extending into the base of the seminal vesicles.

(Pittsburgh, PA, USA) endorectal coil by using a 26 cm field of view, 5-mm section thickness, 1-mm intersection gap, with a 512 x 216 matrix. Axial T1 (TR 420 / TE 22) and axial, sagittal and coronal FSE T2-weighted images TR 2940, TE 160, 13 echotrains) were performed.

The T2-weighted demonstrated an area of low signal intensity bilaterally in the base of the prostate (fig 1a,b,c). This was interpreted as prostate cancer extendeding into the base of both seminal vesicles. Because radical surgery is not the treatment of choice in patients with seminal vesicle invasion, additional ultrasound guided needle biopsies of the prostatoseminal vesicular junction were obtained. One of the three cores demonstrated moderately differentiated adenocarcinoma. Seminal vesicle epithelum was not present. One core showed small eosinophilic deposits at the end of the biopsy. In retrospect, this deposit was amyloid material. Because seminal vesicle invasion could no be confirmed with these biopsies, radical prostatectomy was thought to be the best treatment.

Following radical prostatectomy, the specimen was fixed with formalin and embedded in paraffin. Four-micron thick tissue sections were stained with hema-

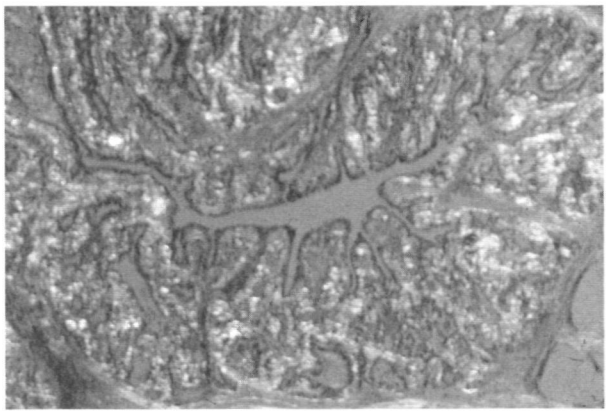

Fig 1. D. Histopathologically specimen (**100x**) at the level of the ejaculatory ducts. Hugh amounts of amyloid are easily recognized as amorph eosinophilic material, that shows a characteristic apple-green birifrigence in polarized light after staining with Congo red.

toxylin and eosin. The specimen showed moderately differentiated bilateral adenocarcinoma of the base of the prostate. The tumor volume was 2.0 cc. Because routine stains showed amorphic eosinophilic material in the wall of the seminal vesicles suspect for amyloidosis, additional staining with Congo-red was performed. The deposits showed a positive staining reaction with apple-green birefrigence in polarized light characteristic of amyloid (fig 1d). The amyloid deposits were found exclusively around the collecting ducts of the seminal vesicles in the base of the prostate and in the muscular layer of both seminal vesicles. Tumor invasion into the seminal vesicles was excluded histologically.

Discussion

The appearance of normal seminal vesicles is a grape-like configuration with a homogeneous hyperintense content on T2-weighted MR images. The most important MR criterion for tumor invasion into the seminal vesicle is an abnormal low signal intensity within the lumen of the seminal vesicle [5]. Focal thickening of the wall of the seminal vesicle is also considered a criterion for seminal vesicle invasion [6]. The accuracy for detecting seminal vesicle involvement on endorectal coil images varies. A high specificity (85-97%) and a low sensitivity (21%-63%) [7-9] have been reported. An explanation for false-positive seminal vesicle invasion by cancer may be biopsy-related haemorrhage [10]. However, this can be diagnosed on T1-weighted images because of the high signal intensity of the hemorrhagic breakdown products. False-positive findings may also be due to chronic inflammation, and history of pelvic irradiation [11]. Finally, low signal intensity of the seminal vesicles on T2-weighted images may be the result of stones in the lumen of the seminal vesicles.

Deposits of amyloid in the seminal vesicles as the cause of false-positive findings on MR images has only been described in two reports. Kaj et al. [4] reported a patient with a noninvasive bladder carcinoma in whom seminal vesicle amyloidosis was misinterpreted as tumor extension into the seminal vesicles, resulting in an unnecessary cystectomy. Ramchandani et al. [3] described a patient in whom seminal vesicle amyloidosis was interpreted as metastatic extension of prostate

cancer on MR images obtained with an endorectal coil In this case the correct diagnosis was made with ultrasound-guided needle biopsies

Amyloid deposits in the seminal vesicles (localized senile amyloidosis) is considered a localized disorder Considering the high frequency of prostatitis and the local nature of amyloidosis these two entities may be related The disorder is rarely associated with systemic AA amyloidosis Histopathologically amyloid is easily recognized as amorph eosinophilic material, that shows a characteristic apple-green birifrigence in polarized light after staining with Congo red (fig 1d) Both seminal vesicles are usually symmetrically involved [2]

As in the previously reported cases, the low signal intensity of the seminal vesicles in the reported case was caused by narrowing of the lumen and thickening of the wall of the seminal vesicles due to amyloid deposits The radiologic appearance may be indistinguishable from that of tumor It is suggested that gadolinium may be helpful in making the diagnosis because amyloid does not enhance, whereas tumor invasion shows enhancement [4]

Because false-positive results may deny potentially curable patients an operation, MR imaging cannot have a high percentage of false positive results Considering the high incidence of seminal vesicle amyloidosis, the diagnosis of tumor invasion in the seminal vesicles should be confirmed with additional ultrasound-guided biopsies Radiologist, urologist and pathologist should be familiar with this disorder to suggest the right diagnosis

References

1 Coyne JD, Kealy WF Seminal vesicle amyloidosis morphological, histochemical and immunohistochemical observations *Histopathology* **1993** 22 173-176

2 Pitkanen P, Westermark P Cornwell III GG, Murdoch W Amyloid of the seminal vesicles a distinctive and common localized form of senile amyloidosis *Am J Pathol* **1983**,11 64-69

3 Ramchandani P, Schnall MD, LiVolsi VA, Tomaszewski JE, Pollack HM Senile amyloidosis of the seminal vesicles mimicking metastatic spread of prostatic carcinoma on MR images *AJR* **1993**,161 99-100

4 Kaji Y, Sugimura K, Nagaoka S, Ishida T Amyloid deposition in seminal vesicles mimicking tumor invasion from bladder cancer MR Findings *J Comput Assist Tomogr* **1992** 16 989-991

5 Bezzi M, Kressel HY Allen KS, et al Prostatic carcinoma staging with MR imaging at 1 5 T *Radiology* **1988** 169 339 346

6 Narayan P, Vigneron DB, Jajodia P, et al Transrectal probe for 1H MRI and 31P MR spectroscopy of the prostate gland *MRM* **1989**,11 209 220

7 Chelsky MJ, Schnall MD, Seidmon EJ, Pollack HM Use of endorectal surface coil magnetic resonance imaging for local staging of prostate cancer *J Urol* **1993**,150 391 395

8 Quinn SF, Franzini DA, Demlow TA, et al MR imaging of prostate cancer with an endorectal surface coil technique correlation with whole-mount specimens *Radiology* **1994**, 190 323-327

9 Tempany CMC, Zhou X, Zerhouni EA, et al Staging of prostate cancer results of radiology diagnostic oncology group project comparison of three MR imaging techniques *Radiology* **1994**,192 47-54

10 Mirowitz SA Seminal Vesicles biopsy related hemorrhage simulating tumor invasion at endorectal MR imaging *Radiology* **1992**,185 373-376

11 Secaf E, Nuruddin RG, Hricak H, Demas B MR Imaging of the seminal vesicles *AJR* **1991**,156 989-994

4 Pelvic Adenopathy in Prostate and Bladder Carcinoma: MR Imaging with a Three-dimensional T1-weighted Magnetization Prepared-rapid Gradient-echo Sequence

G. Jager[1], J. Barentsz[1], G. Oosterhof[2], J. Witjes[2], J. Ruijs[1]

Departments of [1]Radiology and [2]Urology, University Hospital Nijmegen, The Netherlands

Abstract

Objective

The purpose of this study was to evaluate a magnetization-prepared rapid gradient-echo (MP-RAGE) sequence as a three-dimensional (3D) T1-weighted MR imaging technique to reveal lymph node metastases from carcinoma of bladder and prostate.

Subjects and Methods

Using a 3D T1-weighted MP-RAGE sequence, MR images of 134 consecutive patients with prostate carcinoma (n=63) or urinary bladder carcinoma (n=71) who were scheduled for radical prostectomy or radical cystectomy were correlated with histopathologic findings after fine-needle aspiration biopsy (FNAB) (n=6), open or laparoscopic pelvic lymph node dissection (PLND) (n=127), or autopsy (n=1). MR imaging was used 10 times to guide FNAB in 9 patients.

Results

The sensitivity, specificity, accuracy, and positive predictive value of the technique were 75%, 98%, 90%, and 94%, respectively. Thin slice (1.2-mm) multiplanar reconstructed images correctly revealed pathological nodes in 33 patients. However, MR failed to reveal microscopic metastatic deposits in normally sized nodes in 11 patients. Two other patients had enlarged nodes without metastasis. Furthermore, MR-guided FNAB revealed metastases in six patients of nine patients, but failed to do so in the other three patients.

Conclusions

MR imaging with a 3D MP-RAGE sequence was accurate in revealing nodal metastases from carcinoma of the prostate and bladder. Therefore this imaging technique can be used to select patients for MR-guided biopsy or laparoscopic PLND.

Introduction

The purpose of this study is to evaluate the diagnostic accuracy of using a three-dimensional (3D) magnetization-prepared rapid gradient-echo (MP-RAGE) MR technique for staging regional lymph nodes in patients with prostate or bladder carcinoma.

Subjects and Methods

One hundred and thirty-four consecutive patients with biopsy proven prostate carcinoma (n = 63, mean age 64, years 48-73) or invasive urinary bladder carcinoma (n=71, 55 males, 16 females, mean age 59 years, range 38-75) were considered suitable candidates for curative surgery on basis of clinical stage, local and regional MR staging, and their general condition.

In patients with prostate carcinoma, clinical stage was based on digital rectal examination, transrectal ultrasound, PSA (mean 8.2 range 2.4–40) and histologic tumor grade (9 good, 42 moderately, and 12 poorly differentiated). All patients with bladder cancer had biopsy proven muscle invasion. Nine patients had moderately, and 64 patients had poorly differentiated tumors.

MR imaging was done using 1.5-T magnet (Magnetom 63/48 SP/4000; Siemens, Erlangen, Germany) and a Helmholtz double surface coil. To reduce bowel motion, patients received 0.5 mg of glucagon IV before the examination. To reduce respiratory motion, an adjustable belt was wrapped around the abdomen producing slight abdominal compression. In the 3D MP-RAGE implementation that was used, T1 weighting was obtained by means of a 180° inversion pulse for magnitude preparation. For each of the phase-encoding steps in the second dimension, the inversion preparation was applied and then the rapid gradient-echo data acquisition was carried out; the latter step extended into the phase encoding for the third dimension. The sequence parameters were: 10/4/500 (TR/TE/inversion time); flip angle, 10°; matrix size, 192 x 256; field of view (FOV), 25 cm; two acquisitions; and voxel size, 1.0 x 1.3 x 1.6 mm. A total of 128 contiguous images were obtained in 9 min. From this image set, off-line multiplanar reconstruction of images in specific planes were performed depending on the preference of the investigator. A plane parallel to the external iliac vessels was always included. In patients with bladder carcinoma the 3D-MP-RAGE sequence was part of local staging [1], in patients with prostate carcinoma the sequence preceded local staging with an endorectal surface coil. Image interpretation was done by two experienced investigators who were unaware of the clinical and surgical findings except that the patient was a candidate for prostatectomy or cystectomy. The image quality was assessed good or poor as described before [1]. The investigators performed multiplanar reconstructions of the MP-RAGE data in what they considered to be the optimal plane. In the first 40 patients, all reconstructions were done independently by both investigators. Later, as the study proceeded, the prostate and bladder carcinoma reconstructions were each done by a single reader. When in doubt, independent double

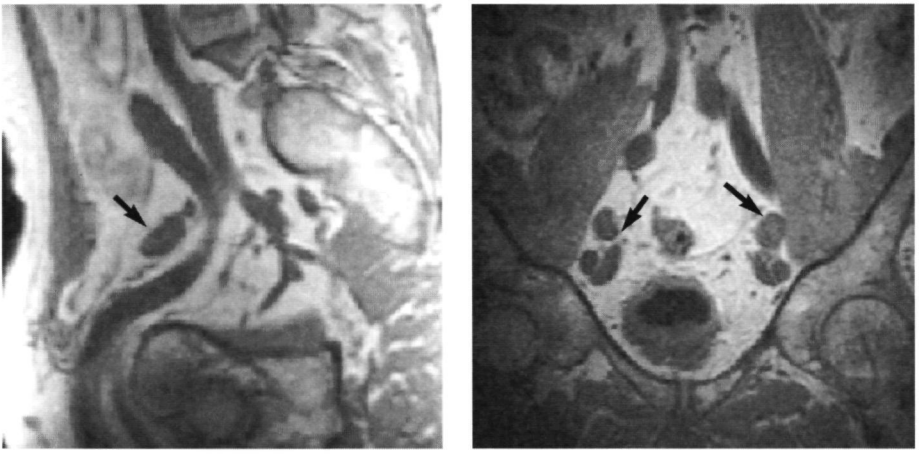

Fig. 1. Lymph node metastases in a 54-year-old patient with T3b bladder carcinoma. Reconstructed three-dimensional magnetization prepared-rapid gradient echo image in plane parallel to right external iliac vessel **A**, and in a slightly angulated coronal plane **B**, reveals enlarged lymph node (arrow) along course of iliac vessels (diameter, 12 mm). Histology following fine-needle aspiration biopsy revealed metastatic deposits.

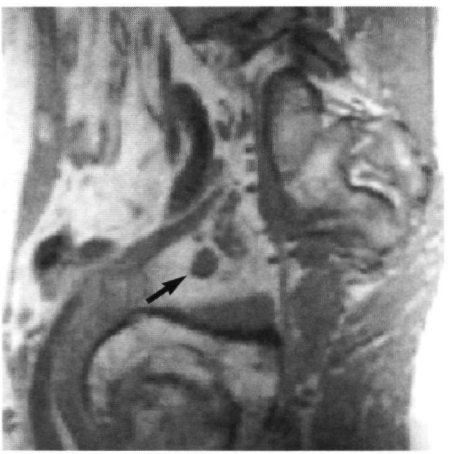

Fig. 2. 65-year-old men with localized prostate cancer and iliac metastases. Reconstructed three-dimensional magnetization prepared-rapid gradient echo image in a plane parallel to the right external iliac vessel reveals a round obturator node with a diameter of 9.3 mm (arrow). Histology following laparoscopic lymph node dissection revealed metastatic deposit.

reading was performed. Consensus was achieved in all cases. In determining sizes of lymph nodes, maximal long axis and minimal axial measurements were obtained. The minimal axial size was defined in a plane perpendicular to the long axis through the thickest part of the node. From these measurements an index was calculated: the shortest axial size was divided by the long axis. Lymph nodes were considered pathological when the minimal axial diameter was 10 mm or more (Fig. 1) or when the minimal axial diameter was between 8 mm and 10 mm and the index exceeded 0.8 (a round node) (Fig 2). The signal intensity of lymph nodes was not considered diagnostic for nodal metastases [2].

In nine patients, MR-guided biopsies of suspected enlarged nodes with a 18-gauge MR compatible needle (Löfkin; Medicor, Türkenfield, Germany). In one

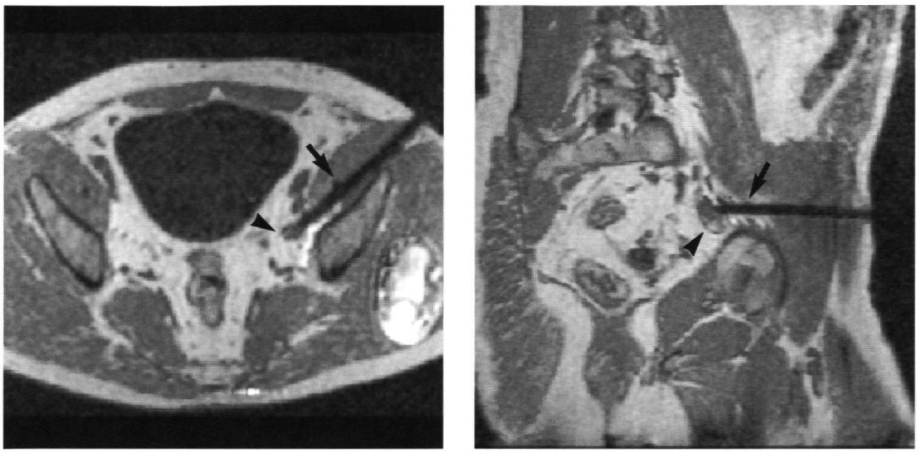

Fig. 3. 57-year-old man with bladder carcinoma and lymph node metastases. Fast reconstructed three-dimensional magnetization prepared-rapid gradient echo image reconstructions in transversal **A**, and multiple angulated plane **B**, obtained during fine-needle aspiration biopsy. Needle tip (arrow) and lymph node (arrow head) are visible. Phase wrap of patient's wrist is visible within the left gluteal muscle.

patient, the procedure was repeated after an inconclusive result. To determine the ideal percutaneous approach, multiple angulated images were reconstructed. The position of the needle tip was checked with a transaxial and sagital two-dimensional spin echo scan with these: 200/15 (TR/TE); matrix size, 192 x 256; FOV, 25 cm, and contiguous slice thickness, 5mm. We also used a fast 3D MP-RAGE sequence with these parameters: 10/4/500 (TR/TE/inversion time); flip angle, 10°; FOV, 25 cm, matrix size, 128 x 256 (Fig. 3). The procedure took 30–60 minutes and was done on outpatients.

The MR findings were compared with histopathologic findings after FNAB in six, open or laparoscopic PLND in 127, and autopsy in one patient.

Results

Overall

Lymph nodes with an axial diameter of 3 mm could be visualised (Fig. 4). Initially, multiplanar reconstructions were performed in 20 min: after a learning curve, we did them in 10 min. Results of nodal staging are presented in Tables 1 and 2.

MR imaging revealed lymph node metastases in 33 of 44 patients. MR imaging failed to depict metastases in 11 patients with non-enlarged nodes. No metastatic disease was found in two patients with enlarged nodes.

The MR technique proved to have a sensitivity of 77%, a specificity of 94%, an accuracy of 98%, and a positive predictive value of 95%.

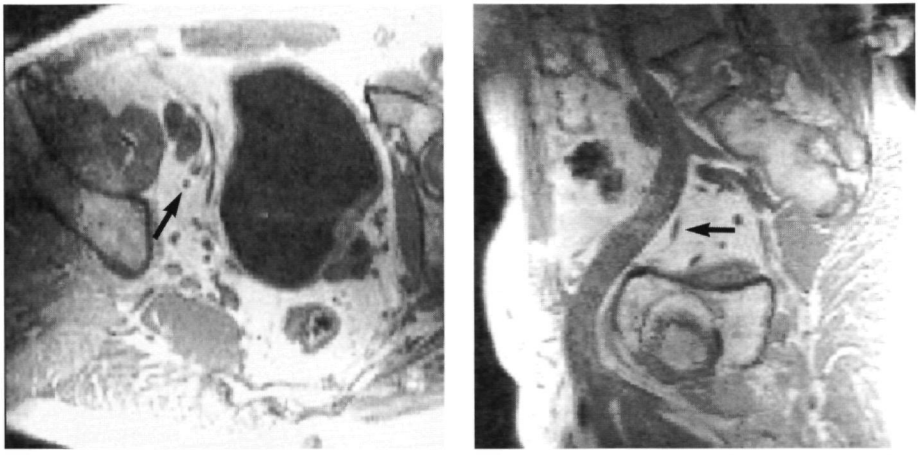

Fig. 4. 52-year-old man with prostate cancer. Reconstructed three-dimensional magnetization prepared-rapid gradient echo image 3D MP-RAGE reconstructions in coronal **A**, and plane parallel to the right external iliac vessel **B**. Small lymph nodes (arrows) with a diameter of 3mm can be depicted along course of vessels. Histology following open lymph node dissection revealed no metastatic deposits.

Table 1. Results of pelvic lymph node staging in patients with prostate carcinoma

		Pathology		
	Results	No Metastases	Metastases	Totals
MR imaging	No metastases	47	6	53
	Metastases	1	9	10
	Totals	48	15	63

The MR technique proved to have a sensitivity of 60%, a specificity of 98%, an accuracy of 89%, a positive predictive value of 90%, and a negative predictive value of 89%.

Table 2. Results of pelvic lymph node staging in patients with bladder carcinoma

		Pathology		
	Results	No Metastases	Metastases	Totals
MR imaging	No metastases	41	5	46
	Metastases	1	24	25
	Totals	42	29	71

The MR technique proved to have a sensitivity of 83%, a specificity of 98%, an accuracy of 92%, a positive predictive value of 96%, and a negative predictive value of 89%.

Prostate carcinoma

The MR pelvic lymph node findings in 63 patients with prostate carcinoma is correlated with pathological examination in Table 1. Metastases were revealed correctly in nine patients. In these patients, 15 enlarged lymph nodes were shown with a mean diameter of 11 mm (range, 8–18 mm). In three of these patients

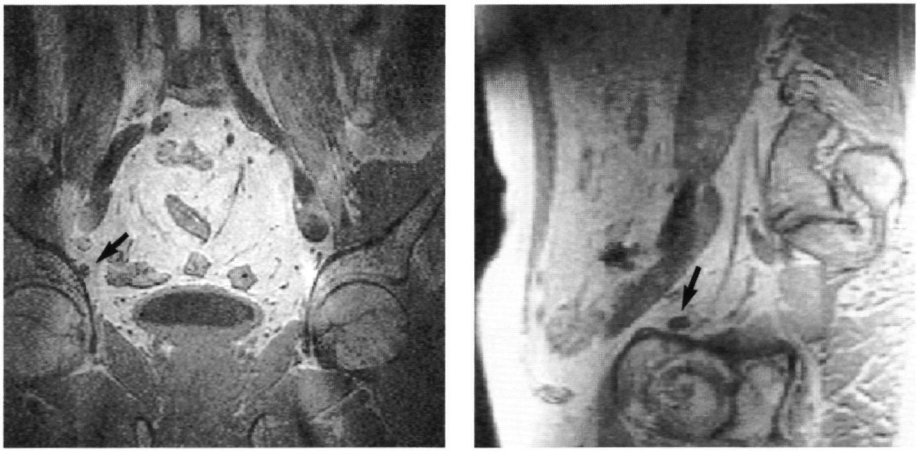

Fig. 5. 58-year-old man with prostate cancer and a false-negative node at MR examination. Reconstructed three-dimensional magnetization prepared-rapid gradient echo image MR images in coronal **A** and plane parallel to right external iliac vessel **B**. Lymph node with a diameter of 6.2 mm is visible (arrow). This node contained metastatic deposits at pathologic examination.

lymph node metastases were present in round nodes with a diameter of 8 or 9 mm. In six patients, lymph node metastases were present in normal sized nodes. The diameter of the largest false-negative node was 6.2 mm (Fig. 5). In the one patient with a false-positive lymph node, we measured a diameter of 9.5 mm on reconstructed MR images.

Bladder carcinoma

The MR pelvic lymph node findings in 71 patients with invasive bladder carcinoma is correlated with pathological examination in table 2. Metastases were predicted correctly in 24 patients. In these 24 patients 39 enlarged lymph nodes were detected. The mean axial diameter was 12 mm (range, 8.5–18 mm). Metastases in five patients were predicted correctly because of the round shape of those metastases. The diameter of the involved nodes was 8.5–9.5 mm. In one patient with false-positive nodes, the minimal axial diameter of the largest node measured 15 mm. However, this node did not contain metastatic disease.

In nine patients with enlarged nodes, MR imaging was used to guide FNAB. All patients appeared to have metastases. In four patients, insufficient aspirated material precluded diagnosis. These cases were classified as false-negative. In one of these patients the procedure was repeated with sufficient material aspirated for diagnosis. In six patients tumor cells could be demonstrated following MR-guided FNAB. All failures occurred in the first five procedures, suggestive a "learning curve" for this procedure.

Discussion

Nodal staging accuracy of MR imaging

Evaluation of local and regional lymph nodes is done in patients who are candidates for radical prostatectomy or cystectomy. The finding of lymph node metastases obviates surgery.

Surgical pelvic lymph node dissection (PLND) is the most invasive and reliable method establishing the presence of metastatic disease in pelvic lymph nodes. However, frozen section has been reported to be false negative in 33% of patients [3]. Laparoscopic PLND is less invasive and almost as accurate in sampling lymph nodes (90%). However, this method requires more skill and experience and if no lymph nodes metastases are found a second operation is necessary [4].

Computed tomography (CT) and magnetic resonance (MR) are reported to be the most accurate non-invasive techniques for nodal staging. Reported accuracies rates obtained from literature show a wide range. For CT the sensitivity varies from 0% to 100%, and the specificity varies from 44% to 100% [5,6]. For MR the sensitivity varies from 0% to 100% and the specificity varies from 94% to 100% [7-9]. Compared with CT, MR has better soft tissue contrast and the potential of multiplanar imaging without the use of IV contrast. MR imaging may therefore be potentially more accurate than CT scanning, but currently both imaging methods are considered similar in their ability to facilitate nodal staging [2,5]. However, the most optimistic results were obtained with routine axial imaging with CT [6]. The CT technique proved to have a sensitivity of 78%, a specificity of 97%, and an accuracy of 94%.

MR imaging is considered superior in local staging of prostate carcinoma [10] and slightly better in local staging of bladder carcinoma [1,2]. Because we use MR imaging for local staging in patients with prostate and bladder cancer we investigated if MR imaging is appropriate in nodal staging. Then local and nodal staging can be done in one session.

On the other hand, CT provides the opportunity to do fine-needle aspiration biopsy (FNAB) more easily [6]. FNAB is a minimal invasive method to determine lymph node metastases histologically. The mean reported sensitivity of FNAB is 70% [5].

We investigated the value of a 3D MR technique in evaluating the presence of nodal metastases in patients with prostate or bladder carcinoma. Because we obtained thin slices in multiple directions, the minimal axial diameter could be determined correctly. The multiplanar reconstruction allowed us to evaluate the nodal shape. By defining the maximal normal size for a round node as 8 mm instead of 1 cm, the number of true-positives increased from 25 to 33 and there was one more false-positive. These findings concur with a study of Vinicombe et al. [11] who suggest a lower limit of normal size for pelvic lymph nodes. They suggested 7 mm for internal iliac, 8 mm for obturator, 9 mm for external iliac locations and 10 mm for external iliac locations. Oyen et al. [6] also suggest lower limits of normal size lymph node. They consider every asymmetrical lymph node with a diameter of 6 mm or more abnormal. Retrospectively, we had adapted 6

mm as the upper size limit of normal, 18 patients with normal lymph nodes would have been judged pathological (false-positives) and in one patient with a true-positive node of 6.2 mm would have been correctly classified (Fig 3). For this reason we chose 8 mm as the upper limits of normal size pelvic lymph nodes. Reconstructions in every desired plane prevented us from over-estimating the size of the node which can result from measuring the node in a plane not perpendicular to the long axis. This may explain the relatively low number of false-positive lymph nodes in our series.

Nodal staging in prostate carcinoma

The presence of lymph node metastases in patients with prostate carcinoma is highly related to tumor grade and clinical stage. The chance of a patient with a well differentiated T1a tumor having lymph node metastases is zero [12,13], whereas a patient with a poorly differentiated T3 tumor has a reported probability of having nodal metastases between 68% [14] and 93% [12]. Lymph node metastases can also be assessed by prostate specific antigen (PSA) level [13,15].

Because of an increasing trend to perform surgery on patients with earlier stage prostate carcinoma, the incidence of positive lymph nodes has decreased to 5%-15% [16]. Therefore, routine use of PLND is no longer considered justified in all patients [13]. Also, the diagnostic yield from imaging in nodal staging is considered too low for routine use [13]. Cost-effective analysis carried out by Wolf et al. [5] pointed out that imaging should be restricted to patients with a high probability of having lymph node metastasis. They stated that when the probability of positive nodes, based on PSA, grade and clinical stage, was 32% the sensitivity of the imaging method should be 36% to be beneficial, when the sensitivity was 25% as in their series prior probability should be 45%. On condition that FNAB was performed with a sensitivity of 70%.

We achieved a high sensitivity in our series of patients. Because metastases may occur in normally sized nodes the sensitivity of imaging cannot be 100%. In a series of 39 lymph node metastases, 14 metastases were present in lymph nodes even smaller than 1 mm! Of these, seven were not recognised at frozen section [3].

One has to keep in mind that the study subjects are restricted to those patients whose true disease status is verified by pathological examination (verification bias). For example if the confidence of clinicians in MR-staging increases, the need for pathological confirmation decreases. A patients with obvious T3c disease (seminal vesicle invasion) and enlarged lymph nodes will no longer undergo FNAB. Therefore the number of true-positive nodes becomes lower. In addition the real prevalence of disease has effect on the reported figures. For example, in our hospital MR staging is no longer indicated in patients with low-grade tumors, who have a PSA concentration lower 10 ng/ml. For this reason we expect a lower number of true-negative results.

Nodal staging in bladder carcinoma

The presence of lymph node metastases is related strongly with tumor stage. Lymph node metastases in patients with superficial tumors (less than T3) are rare but, if the deep muscle layer is involved (T3A), or if there is extravesicular invasion the incidence of lymph node metastases rises to 20–30%, and 50–60%, respectively [17]. Although some authors advocate radical cystectomy even when the patient has microscopic metastases [18], radical cystectomy is not justified if lymph node metastases are detected [19].

The sensitivity of nodal staging in patients with bladder carcinoma was better than in patients with prostate carcinoma. The difference between these two groups of patients is also present in the compilation of results obtained from the literature. For prostate cancer and for bladder cancer the overall reported sensitivity for nodal staging with MR imaging is 32% [5,7,8,10,20-25] and 64% [9,19,26-32], respectively.

The 3D MP-RAGE sequence in our hospital an integral part of bladder carcinoma staging. Therefore, nodal staging does not affect the costs of staging.

In patients with bladder carcinoma laparoscopic PLND is no longer done because of the chances of tumor seeding. In patients with positive lymph node on MR imaging we have now started doing MR-guided FNAB.

Fine needle aspiration biopsy

FNAB of pelvic lymph nodes has been performed under sonography [33], CT [6], or lymphangiography [34] guidance. The reported sensitivity varies from 50% to 100% with an average of 70% [5]. In this preliminary study of MR-guided FNAB, we achieved a sensitivity of 60% in 10 procedures, obviating the need for radical cystectomy in six of nine patients. False-negative results were obtained in the first patients done. Compared with CT, MR-guided FNAB has no advantages, it is more time-consuming and more expensive. With the development of new open-configurating, superconducting MR imagers, which allow direct access to the patient during the procedure [35], and MR compatible puncture devices, we expect some of these problems will be overcome.

Conclusion

Nodal staging using the 3D MP-RAGE technique is excellent compared to other MR studies and to most CT studies. Therefore, local and nodal staging should be integrated in one MR examination. We advise MR staging in all patients with bladder carcinoma with muscular invasion who are considered surgical candidates and in candidates for radical prostatectomy who have biopsy Gleason score of ≥ 7 (moderately and poorly differentiated tumors) and PSA concentration ≥ 10 ng/ml. If a lymph node is considered positive a fine needle biopsy is advised.

Acknowledgment

The authors thank Dr. Janet Husband for reviewing the manuscript

References

1 Barentsz JO, Jager GJ, Mugler JPIII, et al Staging urinary bladder cancer value of T1-weighted three-dimensional magnetization prepared-rapid gradient-echo and two-dimensional spin-echo sequences *AJR* **1995**,164 109-115
2 Husband JE Review staging bladder cancer *Clin Radiol* **1992**,46 153-159
3 Davis GL Sensitivity of frozen section examination of pelvic lymph node for metastatic prostate carcinoma *Cancer* **1995**,76 661-668
4 Guazzoni G, Montorsi F, Bergamaschi F, et al Open surgical revision of laparoscopic pelvic lymphadenectomy for staging of prostate cancer the impact of laparoscopic learning curve *J Urol* **1994**,151 930-933
5 Wolf JS, Cher M, dalla'Era M, Presti JC, Hricak H, Carroll PR The use and accuracy of cross-sectional imaging and fine needle aspiration cytology for detection of pelvic lymph node metastases before radical prostatectomy *J Urol* **1995**,153 993-999
6 Oyen RH, Van Poppel HP, Ameye FF, Van de Voorde WA, Baert AL, Baert LV Lymph node staging of localized prostatic carcinoma with CT and CT-guided fine-needle aspiration biopsy prospective study of 285 patients *Radiology* **1994**,190 315-322
7 Kier R, Wain S, Troiano R Fast spin-echo MR imaging of the pelvis obtained with a phased array coil value in localizing and staging prostatic carcinoma *AJR* **1993**,161 601-606
8 Biondetti PR, Lee JK, Ling D, Catalona WJ Clinical stage B prostate carcinoma staging with MR imaging *Radiology* **1987**,162 325-329
9 Narumi Y, Kadota T, Inoue E, et al Bladder tumors Staging with gadolinium-enhanced oblique MR imaging *Radiology* **1993**,187 145-150
10 Hricak H, Dooms GC, Jeffrey RB, et al Prostatic carcinoma staging by clinical assessment, CT and MR imaging *Radiology* **1987**,162 331-336
11 Vinnicombe SJ, Norman AR, Nicolson V, Husband JE Normal pelvic lymph nodes evaluation by CT scanning after bipedal lymphangiography *Radiology* **1995**,194 349 355
12 Smith JA, Seaman JP, Gleidman RG, Middleton RG Pelvic lymph node metastases from prostate cancer influence of tumor grade and stage in 452 consecutive patients *J Urol* **1982**,130 290-292
13 Narayan P, Fournier G, Gajendran V, et al Utility of preoperative serum prostate-specific antigen concentration and biopsy gleason score in predicting risk of pelvic lymph node metastases in prostate cancer *Urology* **1994**,44 519-524
14 Donohue RE, Mani JH, Whitesel JA Pelvic lymph node dissection guide to patient management in clinically locally confined adenocarcinoma of prostate *Urology* **1982**,20 559-565
15 Bluestein DL, Bostwick DG, Bergstralh EJ, Oesterling JF Eliminating the need for bilateral pelvic lymphadenectomy in select patients with prostate cancer *J Urol* **1994**,151 1315-1320
16 Petros JA, Catalona WJ Lower incidence of unsuspected lymph node metastases in 521 consecutive patients with clinically localized prostate cancer *J Urol* **1992**,147 1574-1575
17 van der Werf-Messing, B, Schroeder, R H and Bush, H Bladder In *Textbook of cancer*, edited by Halman, K.E London Chapman and Hall, 1982, p 457-474
18 Lerner SP, Skinner DG, Lieskovsky G, et al The rationale for en bloc pelvic lymph node dissection for bladder cancer patients with nodal metastases long-term results *J Urol* **1993**,149 758-765
19 Barentsz JO, Debruyne FM Ruijs SHJ *Magnetic resonance of carcinoma of the urinary bladder* Boston, London Kluwer, **1990**
20 Hricak H, White S, Vigneron DB, et al Carcinoma of the prostate gland MR imaging with pelvic phased-array coils versus integrated endorectal-pelvic phased-array coils *Radiology* **1994**,193 703-709

21. Bezzi M, Kressel HY, Allen KS, et al. Prostatic carcinoma: staging with MR imaging at 1.5 T. *Radiology* **1988**;169:339-346
22. Hammerer P, Huland H, Sparenberg A. Digital rectal examination, imaging, and systematic-sextant biopsy in identifying operable lymph node-negative prostatic carcinoma. *Eur Radiol* **1992**;22:281
23. Mukamel E, Hannah J, Barbaric Z, de Kernion JB. The value of computed tomography scan and magnetic resonance imaging in staging prostatic carcinoma: comparison with clinical and histological staging. *J Urol* **1986**;136:1231-1233
24. Rifkin MD, Zerhouni EA, Gatsonis CA, et al. Comparison of magnetic resonance imaging and ultrasonography in staging early prostate cancer. Results of a multi-institutional cooperative trial. *N Engl J Med* **1990**;323:621-626
25. McSherry SA, Levy F, Schiebler ML, Keefe B, Dent GA, Mohler JL. Preoperative prediction of pathological tumor volume and stage in clinically localized prostate cancer: comparison of digital rectal examination, transrectal ultrasonography and magnetic resonance imaging. *J Urol* **1991**;146:85-89
26. Buy J-N, Moss AA, Guinet C, et al. MR staging of bladder carcinoma: correlation with pathologic findings. *Radiology* **1988**;169:695-700
27. Rholl KS, Lee JKT, Heiken JP, Ling D, Glazer HS. Primary bladder carcinoma: evaluation with MR Imaging. *Radiology* **1987**;163:117-121
28. Amendola MA, Glazer GM, Grossman HB, Aisen AM, Francis IR. Staging of bladder carcinoma: MRI-CT-surgical correlation. *AJR* **1986**;146:1179-1183
29. Bryan PJ, Butler HE, LiPuma JP, Resnick MI, Kursh ED. CT and MR imaging in staging bladder neoplasms. *J Comput Assist Tomogr* **1987**;11:96-101
30. Tavares NJ, Demas BE, Hricak H. MR imaging of bladder neoplasms: correlation with pathologic staging. *Urol Radiol* **1990**;12:27-33
31. Tanimoto A, Yuasa Y, Imai Y, et al. Bladder tumor staging: comparison of conventional and gadolinium-enhanced dynamic MR imaging and CT. *Radiology* **1992**;185:741-747
32. Kim B, Semelka RC, Ascher SM, Chalpin DB, Carroll PR, Hricak H. Bladder tumor staging: comparison of contrast-enhanced CT, T1- and T2-weighted MR Imaging, dynamic gadolininium-enhanced imaging, and late gadolinium-enhanced imaging. *Radiology* **1994**; 193:239-245
33. Nagano T, Nakai Y, Taniguchi F, et al. Diagnosis of paraaortic and pelvic lymph node metastasis of gynecologic malignant tumors by ultrasound-guided percutaneous fine-needle aspiration biopsy. *Cancer* **1991**;68:2571-2574
34. Chagnon S, Cochand-Priollet B, Graeil M, et al. Pelvic cancers: staging of 139 cases with lymphography and fine-needle aspiration biopsy. *Radiology* **1989**;173:103-106
35. Schenck JF, Jolesz FA, Roemer PB, et al. Superconducting open-configuration MR Imaging system for image-guided therapy. *Radiology* **1995**;195:805-814

Interlude II
Sensitivity of Frozen Section Examination of Pelvic Lymph Nodes for Metastatic Prostate Carcinoma

G. Jager

Letter to the Author

I read with particular interest the article of Davis [1] about the sensitivity of frozen section examination of pelvic lymph nodes for metastatic carcinoma. The section in which the results are of frozen section are compared with imaging techniques found in MEDLARS literature research deserves comment.

The conclusion of the author that "...Frozen section analysis ... is more sensitive for the diagnosis of prostate carcinoma in pelvic lymph nodes than is MRI because more than half of the metastases are smaller than the 1,0-cm resolution limit of the MRI", may be misleading and is not correct

The upper limit of the spatial resolution of Magnetic Resonance Imaging (MRI) and Computed Tomography (CT) is much smaller than 1 cm. It depends on many factors such as field of view, matrix size, slice thickness, image quality (signal-to-noise ratio, motion artifacts) and contrast between the object and surrounding structures. Using a three-dimensional imaging technique we achieved an in-plane resolution of 1.3 x 1.0 mm and were able to visualize lymph nodes with a diameter of 4 mm [2].

Also the literature search on imaging techniques is incomplete. The reviewed number of articles on CT and MRI is far too low, e.g the review does not obtain the article of Rifkin et al. [3] which includes more patients (185) investigated with MRI than the compilated data of the articles cited by the author.

In general, it is believed that MRI is equal to CT for lymph node imaging. The advantage of CT over MRI is that fine needle aspiration of a nodal mass may be more easy to perform. In contrast to lymphangiography where metastases are visible as filling defects of 4 mm or more [4], MRI and CT do not allow direct visualization of lymph node metastases. The main criteria to assess the presence of lymph node metastases is the axial diameter of the lymph node. Perhaps the author confused "resolutions limit" with what is considered as the upper limit of normal sized lymph node. However, criteria for positive lymph nodes are arbitrary. In the cited articles the upper border of normal varies from 1.0 cm [5,6] to 1.5 cm [7,8]. There is a general tendency to lower the upper limit of normal. Recently, Vinnicombe et al. [9], who found only 2% of normal lymph nodes have a short axis diameter of more than 1 cm, suggested that the sensitivity of CT in depicting lymph nodes may be improved by adopting lower limits of normal. These may become 7 mm for internal iliac, 8 mm for obturator, 9 mm

for common iliac and 10 mm for external iliac nodes. Using a 3-dimensional imaging technique we could add the shape of the node in the judgement; round nodes with a diameter of 8 mm and an index of 0,8 (shortest axial diameter divided by the long axis) or less were considered abnormal. With these criteria the figures for sensitivity, specificity and accuracy were 58%, 96%, and 92% (will be presented at the 81th annual meeting of the Radiologic Society of North America). Van Poppel et al. [10] consider even nodes of 6 mm on CT positive. Calculated figures for sensitivity, specificity and accuracy were 77,8%, 96,6%, and 93,7%. When fine needle aspiration biopsy was performed to evaluate suspected nodes the calculated figures were 77,8%, 100% and 96,5%. These figures are unique and may be not representative for imaging in general.

However, the argument that frozen section is more sensitive than CT or MRI does not implicate that there is no place for imaging as is suggested in the abstract and on page 665. Nodal metastases detected by imaging will considerably save financial costs, morbidity, hospital stay, and patients discomfort. However, only 10% of patients who are candidates for surgical cure have metastatic nodal disease [11,12]. Therefor cross-sectional imaging is not indicated for all patients. It should be restricted for patient who are at high risk for having lymph node metastases depending on PSA, stage and the Gleason biopsy score. Wolf et al. [13] have estimated that when the sensitivity of imaging was 36% (baseline derived from literature), imaging would be beneficial when the probability of metastases was 32% and when suspected lymph nodes will be confirmed by fine needle aspiration biopsy.

In conclusion, imaging is still of value in a selected group of patients who are at high risk for nodal metastases to prevent them from an unnecessary operation. In my opinion, in this group of patients, the upper limit of normal should be lower than 1 cm.

References

1. Davis GL. Sensitivity of frozen section examination of pelvic lymph node for metastatic prostate carcinoma. *Cancer* **1995**;76:661-668
2. Barentsz JO, Jager GJ, Mugler JPIII, et al. Staging urinary bladder cancer: value of T1-weighted three-dimensional magnetization prepared-rapid gradient-echo and two-dimensional spin-echo sequences. *AJR* **1995**;164:109-115
3. Rifkin MD, Zerhouni EA, Gatsonis CA, et al. Comparison of magnetic resonance imaging and ultrasonography in staging early prostate cancer. Results of a multi-institutional cooperative trial. *N Engl J Med* **1990**;323:621-626
4. Strijk SP, Debruyne FM, Herman CJ. Lymphography in the management of urologic tumors. *Radiology* **1983**;146:39-45
5. Hricak H, Dooms GC, Jeffrey RB, et al. Prostatic carcinoma: staging by clinical assessment, CT and MR imaging. *Radiology* **1987**;162:331-336
6. Bezzi M, Kressel HY, Allen KS, et al. Prostatic carcinoma: staging with MR imaging at 1.5 T. *Radiology* **1988**;169:339-346
7. Biondetti PR, Lee JK, Ling D, Catalona WJ. Clinical stage B prostate carcinoma: staging with MR imaging. *Radiology* **1987**;162:325-329
8. Kier R, Wain S, Troiano R. Fast spin-echo MR imaging of the pelvis obtained with a phased-array coil: value in localizing and staging prostatic carcinoma. *AJR* **1993**;161:601-606

9 Vinnicombe SJ, Norman AR, Nicolson V, Husband JE Normal pelvic lymph nodes evaluation by CT scanning after bipedal lymphangiography *Radiology* **1995**,194 349-355
10 Van Poppel HP, Oyen RH, Van de Voorde WA, Baert AL Radical prostatectomy for localized prostate cancer *Eur J Surg Oncol* **1992**,18 456-462
11 Petros JA Catalona WJ Lower incidence of unsuspected lymph node metastases in 521 consecutive patients with clinically localized prostate cancer *J Urol* **1992** 147 1574 1575
12 Narayan P, Fournier G, Gajendran V, et al Utility of preoperative serum prostate specific antigen concentration and biopsy gleason score in predicting risk of pelvic lymph node metastases in prostate cancer *Urology* **1994** 44 519-524
13 Wolf JS, Cher M, dalla Era M, Presti JC, Hricak H, Carroll PR The use and accuracy of cross sectional imaging and fine needle aspiration cytology for detection of pelvic lymph node metastases before radical prostatectomy *J Urol* **1995**,153 993-999

Author's Reply

Gustave L Davis M D
Department of Pathology and Laboratory Medicine
Bridgeport Hospital
Bridgeport

I thank Dr Jager for his comments He is correct regarding my confusion between the spatial resolution limit of the imaging technique and the criteria for metastasis (the axial diameter of the lymph node) The purpose of my study was to assess the diagnostic efficiency of frozen section and then compare the results with the only other modality available for the direct assessment of lymphnode metastases prior to prostatectomy- imaging

I did miss the 1990 article by Rifkin et al [1] which indicates that magnetic resonance imaging and computed tomography had high specificity (96%) but very low sensitivity (4%) for the diagnosis of lymph node metastases "because neither technique has the ability to identify microscopic spread of disease [1]" In 1995, using either a 4-mm resolution limit lymphangiography or 6-mm limit for computed tomography, the best imaging technique cited by Dr Jager, 18 of 39 or 22 of 39 patients in my series still would not have been detected due to the microscopic size of their metastases below these respective resolution limits Accepting Dr Jager's criticism, I would change the conclusion of the paper to "Frozen section analysis is more sensitive for the diagnosis of prostate carcinoma in pelvic lymph nodes than are imaging techniques because 46% of the metastases in our series are smaller than the lowest (4 mm) resolution limit of the imaging techniques to be reported by Barentsz et al [2]"

Imaging is of value in identifying patients who are at high risk for lymph node metastases to prevent them from an unnecessary operation [3] Regardless of imaging technique or user, with an upper limit of normal lower than 1 cm, half of our patients with metastases would still be missed and we are therefore unable to identify them in advance of lymphadenectomy

The rapid changes taking place in both the diagnosis and treatment of prostate cancer are reflected in editorials and articles concerned with prostate specific antigen (PSA), biopsy grade, and treatment variables in the literature

[3-8] concurrent with the submission and publication of my paper. Imagers face the same dilemma as surgeons; how to select patients who will benefit by use of a procedure. Strategies for detecting lymph node metastases [7,8], including imaging with or without fine-needle aspiration of "positive" lymph node metastases and two-stage (open or laparoscopic) lymphadenectomy, attempt to preselect patients at risk for lymph node metastases by means of PSA, biopsy grade, and clinical staging.

Can current clinical or laboratory parameters preselect patients who are at risk for lymph node metastases? Using PSA levels and biopsy grade, we have been unable, retrospectively, to differentiate false-negative frozen-section patients (microscopic lymph node disease) from true positive patients (unpublished data). Only at the extremes of PSA and grade can we predict lymph node metastases with greater efficiency than by frozen section and, for the majority of the patients, there is no relation between PSA and biopsy grade, and size of the metastasis. Metastasis do not necessarily result in lymph node enlargement.

As prostate cancer is diagnosed "earlier," I anticipate that a greater proportion of metastases will be occult [9], for the diagnosis of which current routine clinical laboratory tests and imaging are inadequate. The application of new diagnostic technology (such as polymerase chain reaction amplification [10] for detection of currently occult cancer cells in the blood stream or tissue obtained with minimally or noninvasive techniques with imaging localization) is needed for the accurate and cost-effective staging and treatment of prostate cancer.

References

1. Rifkin MD, Zerhouni EA, Gatsonis CA, et al. Comparison of magnetic resonance imaging and ultrasonography in staging early prostate cancer. Results of a multi-institutional cooperative trial. *N Engl J Med* **1990**,323 621-626
2. Davis GL Sensitivity of frozen section examination of pelvic lymph node for metastatic prostate carcinoma. *Cancer* **1995**;76:661-668
3. Campbell SC, Klein EA, Levin HS, Piedmonte MR. Open pelvic lymph node dissection for prostate cancer: a reassessment. *Urology* **1995**,46.352-355
4. Blute ML Refining the early detection and staging of prostate cancer [editorial]. *J Urol* **1995**;154 1401-1402
5. Flanigan RC. Prostate cancer [editorial]. *J Urol* **1995**;154.1084
6. Narayan P, Fournier G, Gajendran V, et al. Utility of preoperative serum prostate-specific antigen concentration and biopsy gleason score in predicting risk of pelvic lymph node metastases in prostate cancer. *Urology* **1994**,44 519-524
7. Van Poppel HP, Ameye FE,, Oyen RH, Van de Voorde WA, Baert LV Accuracy of combined computerized tomography and fine needle aspiration cytology in lymph node staging of localized prostatic carcinoma *J Urol* **1994**,151·1310-1314
8. Wolf JS, Cher M, dalla'Era M, Presti JC, Hricak H, Carroll PR. The use and accuracy of cross-sectional imaging and fine needle aspiration cytology for detection of pelvic lymph node metastases before radical prostatectomy *J Urol* **1995**;153:993-999
9. Bretton PR, Melamed MR, Fair WR, Cote RJ Detection of occult micrometastases in the bone marrow of patients with prostate cancer *Prostate* **1994**,25.108-114
10. Foss AJE, Guille MJ, Occleston NL, Hykin PG, Hungerford JL, Lightman S. The detection of melanoma cells in the peripheral blood by reverse transcription-polymerase chain reaction. *Br J Cancer* **1995**,72.155-159

Part II
New Developments

5 Dynamic Turbo-FLASH Subtraction Technique for Contrast-enhanced MR Images of the Prostate: Correlation with Histopathology

G. Jager[1], E. Ruijter[2,3], C. van de Kaa[3], J. de la Rosette[2], G. Oosterhof[2], J. Thornbury[4], J. Ruijs[1], J. Barentsz[1]

Department of [1]Radiology, [2]Urology and [3]Pathology, University Hospital Nijmegen, The Netherlands; [4]Department of Radiology, University of Wisconsin-Madison, USA

Abstract

Purpose

To assess the role of single-slice gadolinium enhanced dynamic subtracted (DS) magnetic resonance (MR) imaging in improvement of the accuracy of fast spin echo (FSE) endorectal coil (ERC) MR imaging in the staging and localizing of prostate cancer.

Materials and Methods

ERC MR imaging was performed in 57 patients with clinically localized prostatic carcinoma. Conventional T1-weighted Spin-Echo (SE), Fast-Spin-Echo (FSE) T2-weighted, single slice DS-Turbo-FLASH (TF) following bolus injection of 0.1 mmol gadopentetate dimeglumine/kg body weight (time resolution one image every 1.2 or 2.4 seconds), and late post contrast T1-weighted SE sequences were obtained. Retrospective interpretation of the MR images was performed blindly by two independent readers. Onset and steepest slope of enhancement were graded. Results were compared with the corresponding slice of the other sequences with respect to tumor involvement and capsular penetration. The findings were correlated with corresponding postoperative histopathologic section.

Results

As visualized on DS-TF images, prostate cancer was characterized by early and rapidly accelerating enhancement compared to surrounding tissues. Poorly differentiated tumors showed the earliest and greatest rate of enhancement. Sensitivity, specificity and accuracy to depict tumor involvement for the two readers were 74% and 73%, 79% and 83%, and 77% and 78%. On FSE MR images the sensitivity, specificity and accuracy to depict tumor involvement for the two readers were 57% and 58%, 88% and 82%, and 73% and 71%, respectively. With DS-TF images, capsular penetration was better depicted for both readers in 6 and 9 patients respectively, but worse in 0 and 2 patients respectively. Overall staging was better in 5 and 7 patients. Tumor was better delineated in 7 and 8 patients.

Conclusion

Tumor was better depicted and delineated when DS-TF images were included than at routine ERC images, including late post-contrast images. Also staging results were better.

Introduction

MR imaging is considered to be an effective tool for staging of prostatic cancer [1]. However, it is also stated that the technique adds little to the traditional data based on information gained by clinical staging completed with information obtained from biopsies such as tumor grade, number and lengths of cores containing malignancy, and involvement of seminal vesicles [2-4].

The use of gadopentetate dimeglumine (gadolinium-DTPA) to increase the diagnostic information of MR imaging, has been described in the literature [5-10]. The results suggest that post-contrast T1-weighted images do not provide additional information compared with T2-weighted images, but that it may be useful in evaluating seminal vesicle invasion in equivocal cases [6,10]. Therefore, the use of gadolinium is not warranted for routine staging of prostatic cancer. Brown et al. [8] evaluated early phase T1-weighted bolus enhanced MR imaging for the evaluation of prostatic carcinoma. They found that information provided by T1-weighted images during the early phase of contrast enhancement enables the best delineation of tumor within the gland.

Experience with Dynamic Subtraction-Turbo FLASH (DS-TF) MR imaging in bladder and breast cancer indicated that malignant lesions demonstrate an earlier and faster enhancement compared to benign lesions [11,12]. The diagnostic value of fast dynamic contrast enhancement in prostate cancer has not been evaluated previously. The aim of the present study is to evaluate the complementary diagnostic value of single slice DS-TF MR imaging in patients with prostate cancer.

Subjects and Methods

Patients

The patient population consisted of 57 patients with clinically localized prostate cancer who underwent DS-TF MR imaging complementary to the routine staging MR examination of the prostate. The examinations were performed between August 1993 and February 1996. Only patients who underwent radical prostatectomy were included in this study. Patients who received hormonal treatment before surgery were excluded from this study. Patients mean age was 64 years (range 48-73). Biopsies preceded the MR imaging by an average of three weeks. Patients underwent radical prostatectomy within three weeks after imaging. All prostatectomies were performed on patients in whom no lymph node metastases were found on laparoscopic lymph node dissection prior to the operation or by frozen section examination during the operation.

MR Technique

All images were obtained with a 1.5T Siemens Magnetom SP system (Siemens, Erlangen, Germany), using a Medrad® ERC (Medrad, Pittsburgh, PA). The coil was inserted with the patient in the lateral decubitus position and inflated with 50-100 cc of air. Peristalsis was suppressed by IV administering 1 mg glucagon. A tight band was wrapped around the patients abdomen to decrease respiratory movement.

First, a sagittal T1-weighted localizing image was obtained to confirm coil positioning and to select locations for the axial images. Axial T1-weighted images (420/22[TR/TE], two acquisitions) as well as axial, sagittal and coronal FSE T2-weighted images (2940/160[TR/TE], echo-train lengths of 13, three acquisitions) were acquired. All examinations were performed using a 4- or 5-mm section thickness with a 0.8-1.5 mm gap, 26-cm field of view, and a 512 x 216 matrix. An equalizing processing after application and a filter algorithm to compensate for near-field effect were also used. We changed the phase encoding gradient to decrease motion artifacts over the prostate.

The section for the gadolinium enhanced MR images was selected from the T2-weighted axial FSE images. A section was chosen in which tumor and normal prostatic tissue was likely to be present. When no tumor was visible a level demonstrating normal anatomic details or benign prostatic hyperplasia (BPH) was chosen. In this section during I.V. bolus injection of 0.1 mmol Gd-DTPA/kg body weight (Magnevist®; Schering, Berlin, Germany), 63 images using a single-section turbo FLASH (Fast Low Angle Shot) magnetization-prepared sequence were acquired (7/3/15 [TR/TE/TI], 10 flip angle, 128 x 256 matrix, 200-mm FOV, 1 cm section thickness) with a speed of 1 image per 2.5 seconds in 15 patients (two acquisitions) and a speed of 1 image per 1.25 seconds in the remaining 42 patients (one acquisition). Finally multi-slice axial late post contrast T1-weighted SE images (420/22[TR/TE], two acquisitions) were obtained.

The dynamic single section images were transferred to a diagnostic HP work station. At our department a computer program was developed to subtract the TF images, and to calculate color coded time-, negative and positive slope, and maximal signal intensity images (Fig. 1) [11,12]*. In time-images, the beginning of enhancement of prostatic tissue in relation to the beginning of arterial enhancement is color coded, and projected over the unenhanced image. The beginning of enhancement was defined as an increase of 10 arbitrary units (A.U.) above the base noise line. In the positive slope-image the slope of maximal signal intensity increase is color coded. The negative slope image displays the wash-out of contrast material. The maximal signal intensity images display maximal enhancement 45 seconds after the beginning of arterial enhancement. Time-signal intensity curves were made in operator defined regions of interest (ROI) to determine enhancement patterns of iliac vessels and benign and malignant prostatic tissue.

---

* Note: The subtraction technique is commercially available on most MR systems. The software program for time-, slope, and maximal signal intensity images is available from the authors on request.

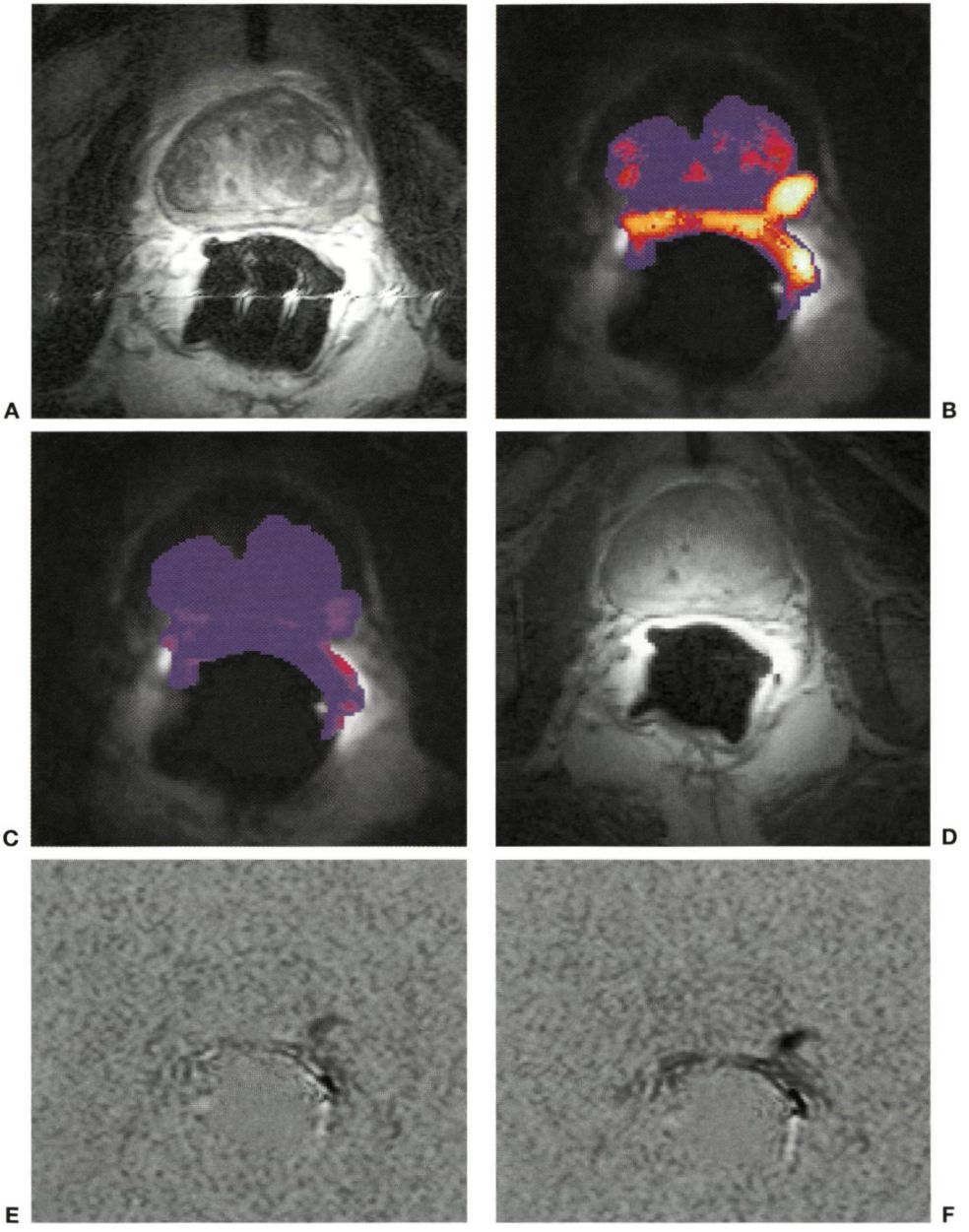

Fig. 1. 63-year-old man with poorly differentiated tumor at the left side.
A, FSE image, note small low-signal-intensity area in the peripheral zone at left side.
B, Time-images demonstrate very early and rapid enhancement.
C, negative slope image demonstrates a relative high wash out.
D, T1-weighted post-contrast image demonstrates a relative low signal intensity.
E-G, subtracted images show early and rapid enhancement of the tumor. There is also some enhancement outside the contour of the prostate. This was interpreted as capsular perforation by one reader.

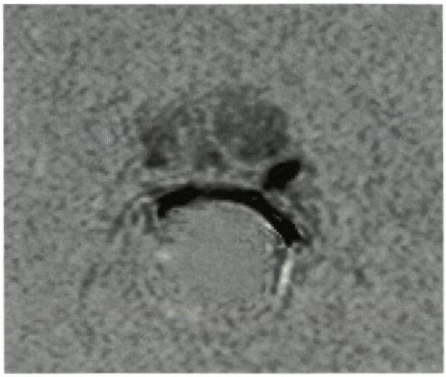

G

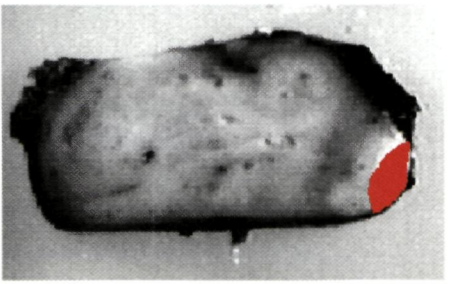

H

Fig. 1. H, Histopathologic specimen shows small poorly differentiated tumor at the right side (red), there was no capsular penetration.

MR image evaluation

The T2-weighted FSE, the T1-weighted post-contrast and the subtracted images were interpreted independently by two observers investigators (G.J.J. and J.O.B.) who were blinded to clinical findings, laboratory and imaging results.

The T2-weighted, the T1-weighted post-contrast images, and DS-TF images were interpreted for tumor presence, location, and capsular penetration. At the level of the DS-TF images the prostate was divided into 4 areas: peripheral zone left and right and central zone left and right. The presence of tumor was scored on a five-point scale (1 = definitely absent, 2 = probably absent, 3 = indeterminate , 4 = probably present, 5 = definitely present). The presence of capsular penetration was scored on a three-point scale (1 = no, 2 = indeterminate, 3 = yes). Regions representing cancer were outlined in a diagram.

On T2-weighted images, an area in the peripheral zone with a relatively low signal intensity zone was considered to represent malignancy. Low signal-intensity areas in the central zone were not interpreted as being malignant. If a low signal area intensity showed high signal on the corresponding T1-weighted image, the area was considered to be haematoma. The criteria for capsular perforation were: disruption of the prostatic capsule, infiltration of the periprostatic fat, low-signal-intensity stranding, and involvement of the neurovascular bundle. A bulge in the contour or capsular thickening was interpreted as "probably" (on the three-point scale = 2) capsular perforation [13].

The onset and slope of enhancement were assessed on hard copies made of the subtraction set. The onset of enhancement in relation to the onset of arterial enhancement was registered in seconds, the slope of enhancement was scored on a three-point scale (1 = slow, 2 = normal, 3 = fast).

On the subtracted images a lesion was considered to represent malignancy if the slope of enhancement was faster and the onset was earlier relative to the adjacent prostatic tissue. Enhancement outside the contour of the prostate was considered to represent capsular penetration (Fig 2.)

Using these criteria the additional value of the turbo-FLASH technique was evaluated.

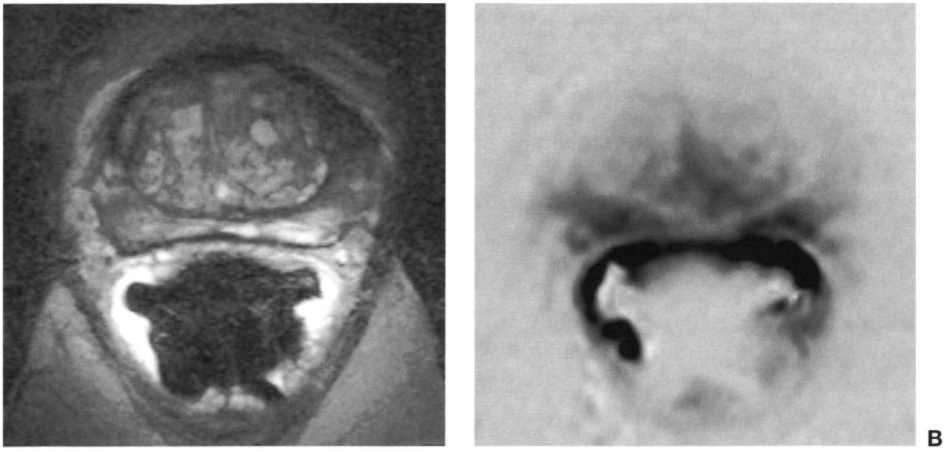

Fig 2. 63-year-old-man with tumor involvement on the right side.
A, T2-weighted FSE image demonstrates retraction of capsule on the left side which was not interpreted as capsular penetration. **B,** DS-TF image shows enhancement outside the contour of the prostate. This appeared to be capsular penetration on final pathologic examination.

Pathologic examination

The prostatectomy specimens were in toto fixed overnight in a solution of 10% neutral buffered formalin. Step-sections were made at 4 mm intervals in a plane parallel to the base of the prostate, which corresponded to the slices used on axial MR imaging. After separating the step-sections into right and left halves, all sections were routinely embedded in paraffin. Tissue sections of 4 μm were prepared and stained with haematoxylin and eosin. Regions representing cancer were outlined on the glass cover and retraced onto a diagram of the axial histologic sections that extended from the base to the apex of the prostate. Measurements were multiplied by a factor 1.1 to correct for tissue shrinkage due to fixation.

Data Analysis

Analysis of the correlation of MR findings and histopathology were performed by two radiologists (G.J.J., J.O.B.) and one pathologist (E.T.G.R). The MR images were correlated with tumor maps based on the histopathologic sections. The level of the DS Turbo-FLASH images was determined by its location between the apex and base of the prostate. The corresponding slice of the tumor map was then adjusted. Because of the difference between slice thickness of the Turbo-FLASH images (10 mm) compared to the FSE images and the pathologic examination (4 mm), tumor maps of adjacent slices were also considered.

Penetration through the capsule was compared for each quadrant.

Statistical analysis

The McNemar test (exact distribution) was used to evaluate the differences in assessing tumor presence and capsular penetration by both techniques.

Cohen's Kappa (κ) analysis was used to test for agreement between both rea-

ders with respect to the presence and absence of tumor and capsular penetration. (κ <0.40 = poor;κ >0.4,<0.75 = good;κ >0.75 = strong).

When sensitivity and specificity figures for tumor presence and for capsular penetration were calculated; score 4-5 and score 3, respectively were considered present.

Additional diagnostic value

The overall additional diagnostic value of DS-TF images to routine MR imaging was determined as follows: major improvement of the diagnostic performance was present when DS-TF correctly depicted up or down staging (T2->T3, T3->T2), minor improvement was present when the estimated area of tumor involvement as determined on the DS-TF images became within the 25% range of the actual tumor (Fig 3 and 4). Diagnostic performance was defined worse (major) when DS-TF depicted incorrectly up or down staging, and worse (minor) when the estimated area of tumor involvement as determined on the DS-TF images, exceeded the 25% range of the actual tumor area correlated with the corresponding step section histology slice. Additional information of DS-TF images that did not change the final staging result was called minor. For example, DS-TF depicted capsular penetration not depicted on FSE images, but FSE already depicted seminal vesicle invasion (T3c).

Results

Correlating MR images with histopathologic findings

The correlation between MR images and the corresponding histopathologic section was difficult in most patients. The most caudal section of MR images was 0.5–1.5 centimeter more distal than the most apical section of the prostatectomy specimen. Also the angle by which the sections were cut in both techniques was never exactly the same for either technique (difference, 5°–15°). Furthermore, the shape of the prostate changed after surgery and fixation, compared with the shape of the gland within the body at the time of imaging. Also making correlation difficult was the fact that prostate tumors are very irregular and often demonstrate fingerlike projection with ill defined margins that did not display on MR images of 4 or 5 or 10 millimeters (whereas the histologic sections were only 4 μm thick). We tried to overcome these problems using tumor maps, which gave a good three-dimensional picture of the prostate and were of help in assessing the corresponding level.

Characterizing enhancement patterns

Differences in enhancement within the prostate were best visible in the early phase of the first pass of gadolinium. However, most glandular tissue of the prostate displayed early enhancement and there was a considerable variation be-

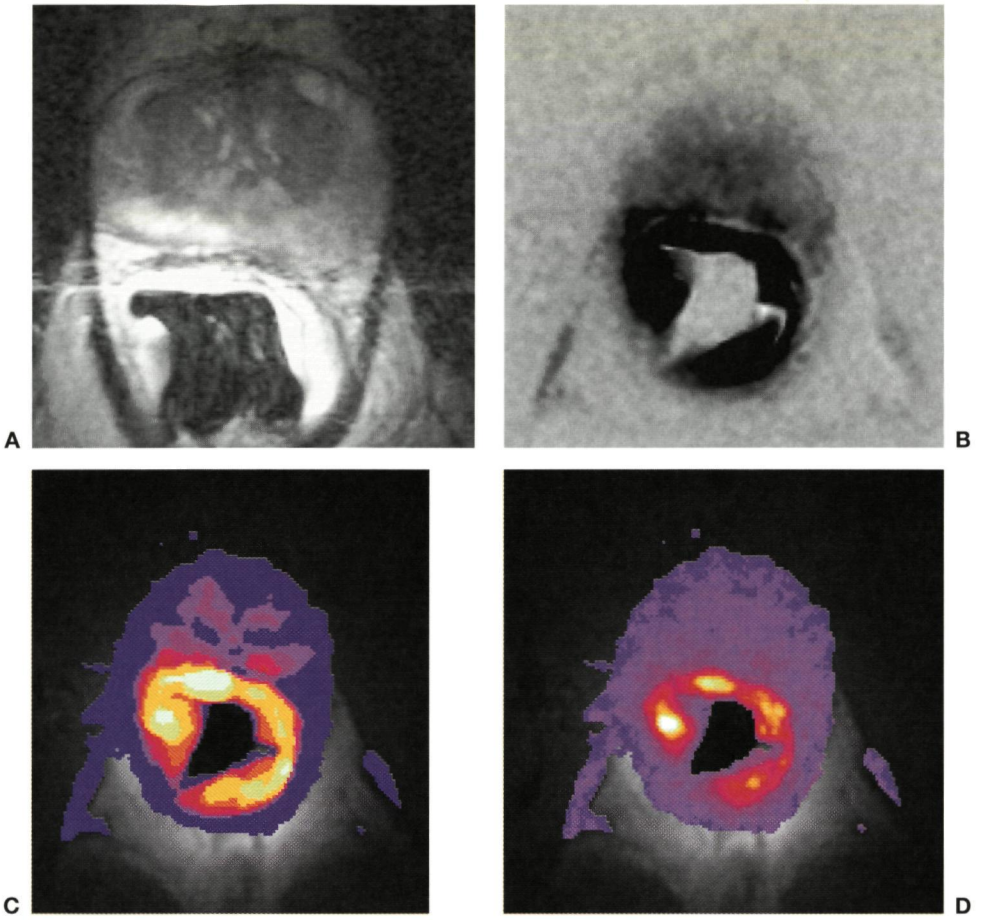

Fig 3. 66-year-old-man with prostate cancer.
A, T2-weighted FSE image demonstrate low signal intensity on the left side and bulging of the contour. **B,C,D,** Subtracted, time and slope image show late and slow enhancement. No tumor was found at final pathologic examination.

tween the start of enhancement of the external iliac artery (t = 0) and the start of enhancement of prostatic tissue. Therefore, the onset of enhancement was judged relative to the adjacent prostatic tissue. We were also not able to characterize the signal intensity-time curve (slope of enhancement) for malignant or benign lesions. Therefore relative differences in slope values in the selected slice were used to differentiate between benign and malignant lesions.

Interobserver agreement

Interobserver agreement for the interpretation of MR images with and without DS-turbo-FLASH was strong. Cohen's Kappa was respectively 0.79 and 0.78.

Both observers agreed that non-dynamic T1-weighted post contrast images did not provide additional information compared with T2-weighted FSE images.

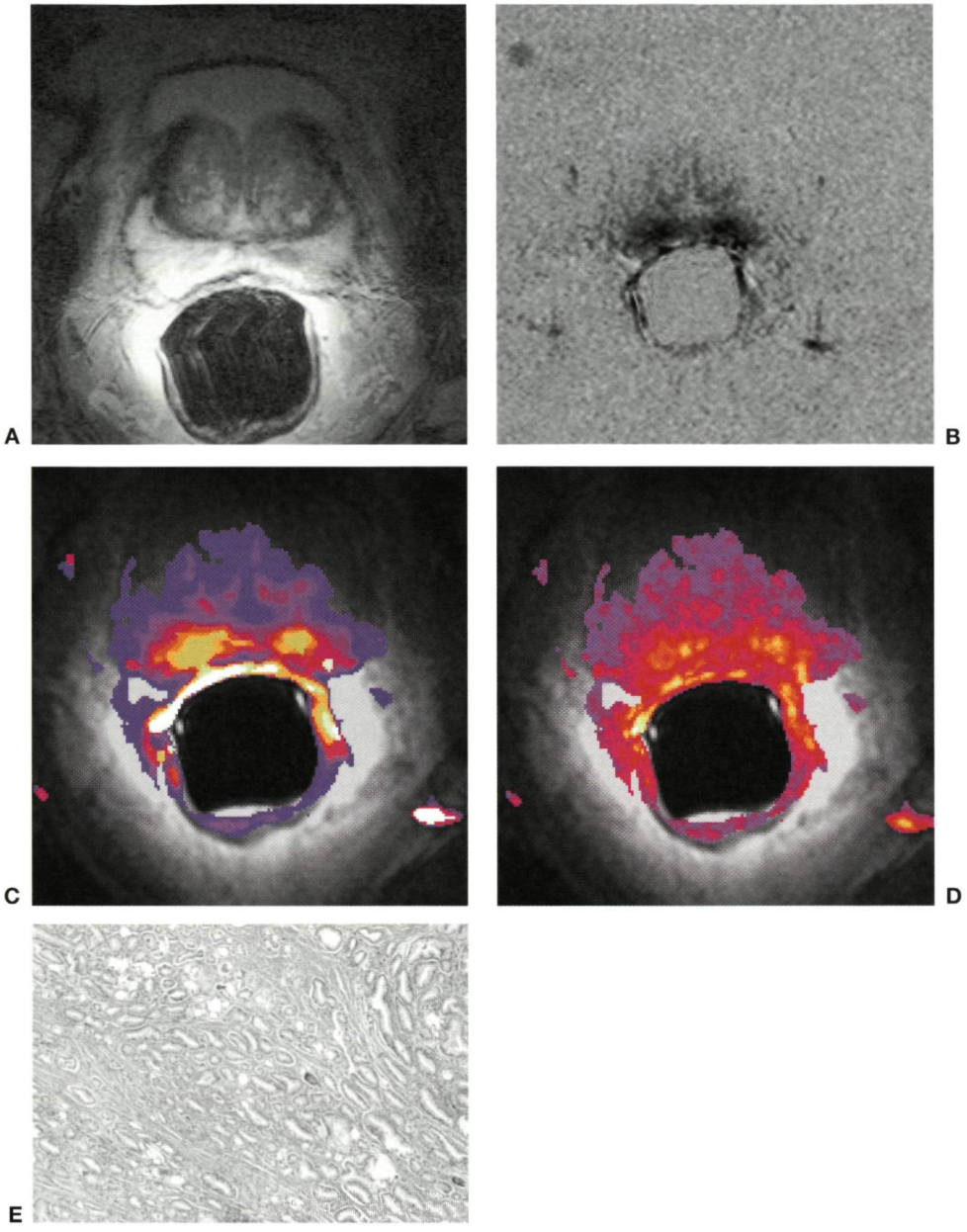

Fig 4. 57-year-old-man with prostate cancer.
A, T2-weighted FSE image demonstrate small low signal intensity on the left side
B,C,D, Subtracted, time and slope image show early and rapid enhancement of the peripheral zone. At final pathologic examination tumor location was almost symmetrically bilateral, corresponding with the area of rapid enhancement.
E, Photograph of histopathologic section (haematoxylin and eosin stain; magnification 20x) shows moderately differentiated tumor on both sides.

Detection of tumor

A total of 228 quadrants were identified, rated and analyzed. Tumor was present in 102. The results for predicting tumor presence with and without DS-TF images are presented in Table 1. The sensitivity was 57% and 58% for FSE images and 74% and 73% for DS-TF images, respectively (P = not significant). The specificity was 88% and 82% for FSE images and 79% and 83% for DS Turbo-FLASH images, respectively (P = not significant). The accuracy was 73% and 71% for FSE images and 77% and 78% for DS Turbo-FLASH images respectively (P = not significant).

Tumor volume

In 17 (30%) and 18 (32%) patients the area of tumor involvement estimated with FSE images fell within a 25% range of the actual area of tumor involvement, respectively. With DS Turbo-FLASH images the estimated tumor volume fell within a 25% range in 23 (40%) and 25 (44%) patients (P not significant).

Capsular penetration

In 19 different quadrants capsular penetration was present at histopathologic examination in 14 patients. In the remaining two hundred and nine quadrants, capsular penetration was absent, including one site where capsular penetration could not be evaluated because the surgeon incised the capsule. FSE images correctly depicted capsular penetration in 4 and 3 quadrants, respectively. There were two false-positive sites. DS-TF images correctly depicted capsular penetration in 9 and 10 quadrants, respectively. With DS-TF there were one and two false-positive quadrants. Therefore capsular penetration was predicted more accur-

Table 1. Sensitivity and specificity for tumor localization for FSE and DS-TF images

	sensitivity for tumor localization Routine		DS-TF	
pathology tumor present	Reader I	Reader II	Reader I	Reader II
PZ (n=72)	74%(53)	76%(55)	81%(58)	83%(60)
CZ (n=30)	17%(5)	13%(4)	57%(17)	47%(14)
total (n=102)	57%(58)	58%(59)	74%(75)	73%(74)
	specificity for tumor localization			
pathology tumor absent	routine		DS-TF	
PZ (42)	64%(27)	52%(22)	57%(24)	74%(31)
CZ (84)	98%(82)	96%(81)	90%(76)	87%(73)
total (126)	88%(109)	82%(103)	79%(100)	83%(104)

Note: Numbers are in parentheses PZ = peripheral zone, CZ = Central zone. The accuracy was 73% and 71% for FSE images and 77% and 78% for DS Turbo-FLASH images respectively (P = not significant).

Table 2. Additional diagnostic value of dynamic subtracted turbo-FLASH images.

Diagnostic Performance with DS Turbo-FLASH	Observer (I)	Observer (II)
Better (major)	5	8
Better (minor)	13	12
Equal	34	30
Worse (minor)	5	6
Worse (major)	0	1

Note. Diagnostic performance was defined better (major) when DS-TF images correctly depicted up or down staging (T2->T3, T3->T2), and worse (major) when DS-TF incorrectly depicted up or down staging in addition to complete routine imaging. Minor improvement or deterioration was defined when the estimated area of tumor involvement of the selected slice became, respectively within or out the 25% range of the actual tumor area, or when depicted capsular penetration did not change final stage.

ately by DS-TF by both readers in 6 and 9 quadrants in 6 (11%) and 9 (16%) of patients respectively, but less accurately in respectively 0 and 2 quadrants in 2 (4%) of the patients (P = not significant). Three other patients had capsular penetration at a different level than DS-TF images. Capsular penetration was depicted in one of these three at FSE images.

Tumor grade

Ten patients had poorly differentiated tumors. All were recognized by DS-TF. Five of these showed the most steepest enhancement from all lesions, and the earliest (within one image) (Fig. 1). These numbers however, were too small for statistical analysis. There were no differences in enhancement between good and moderately differentiated tumors.

Additional diagnostic value

The overall additional diagnostic value of DS-TF images to routine MR imaging is summarized in Table 2. We achieved overall major improvement in 5 and 7 patients respectively, and overall minor improvement 8 and 6 patients respectively.

Discussion

The merit of MR imaging is in the local staging of prostate cancer. Although microscopic capsular penetration may not be demonstrated on T2-weighted images, MR may be helpful in selecting patients with a potential resectable disease [404,307]. However, more accurate staging is needed.

Several studies have addressed the use of contrast material in MR imaging of the prostate [148,48,151,344,405,376,345]. In the normal prostate the central zone enhances more than the peripheral zone. Both enhance homogeneously. In the presence of BPH, the enhancement pattern of the central gland is marked-

ly inhomogeneous [48,344]. BPH may occasionally arise within the peripheral zone of the prostate leading to an inhomogeneous enhancement.

Prostate cancer is frequently reported to show increased enhancement compared to adjacent glandular tissue, especially in the peripheral zone; in the central zone the difference is less obvious [344].

Reported studies suggest that contrast enhancement in prostate cancer is of limited value and may be only helpful in cases of seminal vesicle invasion [48,345].

Brown et al. [344] evaluated bolus enhanced MR imaging in prostatic carcinoma. They showed that early phase contrast enhanced images enables best the definition of tumor within the gland in 50% of patients and demonstrated capsular spread more clearly in 80% of the patients. In that study no pathologic correlation could be obtained.

We evaluated the enhancement of the prostate cancer during the first pass of contrast with fast dynamic imaging with a temporal resolution of one image per 1.2 or 2.4 seconds following IV bolus administration of contrast.

Malignant breast, bladder and bone tissue have demonstrated early and fast enhancement. The enhancement pattern can be characterize by the onset of enhancement [169,146], or by the slope of enhancement [162]. Our findings indicate that prostate cancer also enhances early and that differences in enhancement are visible in the early phase of the first pass. However, due to a large variation in the onset and slope of enhancement among patients and minor differences between the onset of enhancement of carcinoma and benign tissue, we were not able to define a cut-off time nor a slope value to differentiate benign from malignant prostatic tissue. Therefore, the onset and slope of enhancement were judged relative to adjacent prostatic tissue.

Because we used subjective signs, independent double reading was performed to test for inter-observer variability. There appeared to be strong agreement between both readers for the interpretation of both FSE and DS-TF images. This in contrast to other studies which reported high inter-observer variation in estimating tumor location, volume and capsular penetration of the prostate [56,171]. The high agreement of our readers may be due to the study design. The slice of the DS turbo-FLASH images was chosen in a plane that was likely to consist both cancer and normal tissue on the T2-weighted FSE image.

Reported figures for detecting tumors with MR imaging are in general poor especially for central gland tumors [90,68]. With DS-TF the sensitivity for localization of tumors was consistently better than with FSE images. It was confirmed that tumors located ventrally and centrally on histopathologic examination were easily missed on T2-weighted images. With DS-TF there were 12 and 10 more true-positive centrally located tumors but also 6 and 8 more false-positive tumors.

Tumor volume is a predictor of pathologic stage [116]. Except for one study performed with an external array coil [54], studies performed with ERC coil [404] and body coil MR imaging reported a poor correlation between MR tumor volume and the volume as calculated from the pathologic specimen [61,67,43,55]. Studies evaluating post contrast T1-weighted images also reported

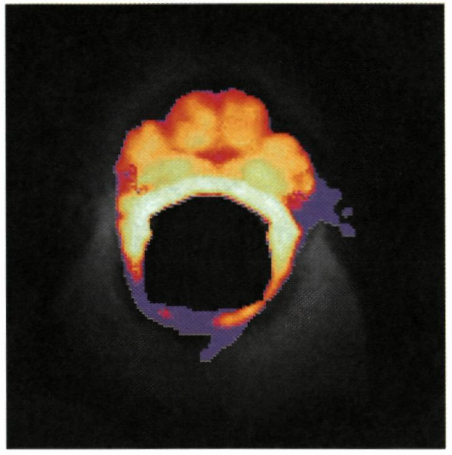

A

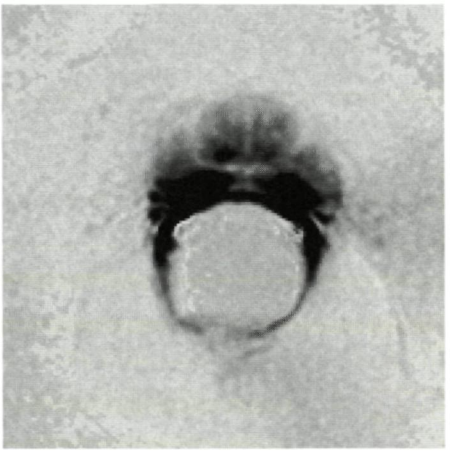

C

Fig 5. 52-year-old-man with very small focus of prostate cancer (0,4cc).
A and **B,** Time and maximal signal intensity images show symmetrically rapid and early enhancement.
C, Pathologic specimen of the corresponding section show BPH. No tumor was present.

poor correlation between the estimated and calculated volume [48]. Brown et al. [345] found better correlation during the early phase of enhancement but in this study pathologic confirmation was not obtained.

Compared to FSE images, DS-TF images estimated the area of tumor involvement better in 10-12% of the patients. However, in only 30%-32% of patients the area of tumor involvement estimated with FSE images fell within a 25% range of the actual area of tumor involvement. One reason for overestimating tumor volume on DS-TF images was rapid enhancement of BPH in the central zone (Fig. 5). This error can be avoided when symmetrical central enhancement is not considered as cancer. In an overview, Schiebler et al. [109] stated that body coil MR imaging gives unsatisfactory results in detecting capsular penetration. The detection of capsular penetration improved with ERC MR (sensitivity 67%) compared to body coil MR (sensitivity 44%) in the same patient cohort [58]. Results of recent studies with ERC MR, however, showed a limited accuracy for detecting capsular penetration as low as 33% [114,173,148,171,404].

In the present study the sensitivity for capsular penetration was 21% and 16% with FSE, and 47% and 53% with DS-TF, respectively. These figures appeared not to be statistical significant. The low sensitivity for capsular penetration with FSE is due, at least for a part, to the fact that we only studied one level, preferably in

which capsular penetration was not obvious. False-positive results on DS-TF images may be due to enhancement of a capsular artery. The vessel may be differentiated from tumor by a different enhancement curve (Fig. 1).

T2-weighted MR images do not provide information about tumor grade, another predictor of clinical outcome. A noteworthy finding of the present study was that DS-TF depicted all poorly differentiated tumors and that five of them showed the earliest and fastest enhancement of all lesions. These numbers are however too small for statistical analysis. These findings seems to be in contradiction with the findings of Yoshizako et al. [405], who reported that poorly differentiated tumors demonstrated less enhancement on contrast-enhanced T1-weighted images compared to moderately differentiated tumors. However, we also observed that rapid enhancing tumors demonstrated relatively low signal intensity on late post-contrast images (Fig. 1D) which may be explained by the high wash-out of contrast material from the tumor (Fig. 1C).

Our study demonstrates that the results of MR imaging with DS-TF were consistently better than routine MR imaging although routine use of single slice DS-TF images did not significantly improve tumor localization and staging results. The results of the DS-TF may however, be improved. In the first place there was a learning curve. Secondly, a number of examinations was carried out in patients in whom clinical stage was obvious from FSE images. In these cases DS-TF images did not provide additional information. Thirdly, the single slice imaging technique we used only allows evaluation in one plane. Better delineation of tumor and tumor volume may become possible, when with echo-planar imaging a dynamic multi-slice technique can be performed with a time resolution of minimal 3 seconds. Also the spatial resolution is considerable less than with FSE images and the slice is twice as thick. Another limiting factor of our technique was the ERC dependent variation of signal intensity throughout the prostate gland. Especially lesions located ventrally are difficult to recognize because they show relative less enhancement. This problem may be overcome with the introduction of a combined endorectal phased array coil. Also easily applicable corrections for the coil profile may be helpful.

Conclusion

This study demonstrates that prostate cancer shows early and rapid enhancement and that with fast imaging and the use of a subtraction technique tumor assessment can be improved. Further improvement of the technique however, may be achieved by application of a multislice sequence and by correction for the sensitivity profile of the ERC throughout the prostate gland.

References

1 Schiebler ML, Schnall MD, Pollack HM, et al Current role of MR imaging in the staging of adenocarcinoma of the prostate *Radiology* **1993**,189 339-352
2 Denis LJ, Murphy GP, Schroeder FH Report of the consensus workshop on screening and global strategy for prostate cancer *Cancer* **1995**,75 1187-1207
3 Perrotti M, Kaufman Jr,R P , Jennings TA, et al Endo-rectal coil magnetic resonance imaging in clinically localized prostate cancer is it accurate? *J Urol* **1996**,156 106-109
4 Bostwick DG, Qian J, Bergstralh EJ, et al Prediction of capsular perforation and seminal vesicle invasion in prostate cancer *J Urol* **1996**,155 1361 1367
5 Quinn SF, Franzini DA, Demlow TA, et al MR imaging of prostate cancer with an endorectal surface coil technique correlation with whole-mount specimens *Radiology* **1994**,190 323-327
6 Mirowitz SA, Brown JJ, Heiken JP Evaluation of the prostate and prostatic carcinoma with gadolinium-enhanced endorectal coil MR imaging *Radiology* **1993**,186 153-157
7 Sommer FG, Nghiem HV, Herfkens R, McNeal JE Gadolinium-enhanced MRI of the abnormal prostate *Magn Reson Imaging* **1993**,11 941-948
8 Brown G, Macvicar DA, Avton V, Husband JE The role of intravenous contrast enhancement in magnetic resonance imaging of prostatic carcinoma *Clin Radiol* **1995**,50 601-606
9 Yoshizako T, Sugimura K, Kaji Y, Moriyama M, Wada A Prostate and prostatic carcinoma comparison of gadolinium-enhanced MR images and histopathologic findings *Nipon Igaku-Hoshasen Gakkai-Zasshi* **1995**,55 545-549(Abstract)
10 Huch Böni RA, Boner JA, Lütolf UM, Trinkler F, Pestalozzi DM, Krestin GP Contrast-enhanced endorectal coil MRI in local staging of prostate carcinoma *J Comput Assist Tomogr* **1995**, 19 232-237
11 Boetes C, Barentsz JO, Mus RD, et al MR characterization of suspicious breast lesions with gadolinium-enhanced TurboFLASH subtraction technique *Radiology* **1994**,193 777-781
12 Barentsz JO, Jager GJ, van Vierzen PBJ, et al Staging urinary bladder cancer after transurethral biopsy the value of fast dynamic contrast-enhanced MR imaging *Radiology* **1996**,(In Press)
13 Jager GJ, Ruijter ETG, van de Kaa CA, et al Local staging of prostate cancer with endorectal MR imaging correlation with histopathology *AJR* **1996**,166 845 852

6 Proton MR Spectroscopy of the Normal Human Prostate with an Endorectal Coil and a Double Spin-echo Pulse Sequence

A. Heerschap, G. Jager, M. van der Graaf, J. Barentsz, J. Ruijs
From the Department of Radiology, University Hospital Nijmegen, The Netherlands

Abstract

This report describes the use of an endorectal coil and a double spin-echo pulse sequence for localized ^{1}H MR spectroscopy of the normal prostate in volunteers. The spectra showed well-resolved signals for citrate, (phospho)choline and creatine protons. Additional signals were assigned to taurine and myo-inositol protons. J-modulation of the main and outer peaks of citrate could be monitored *in vivo*. Apparent relaxation times T_1 and T_2 have been estimated for the methyl protons of cholines and creatine. An effective T_1 relaxation time was estimated for the main peaks of the citrate multiplet. Ratios of the integrals of these resonances have been evaluated and tissue contents of choline and creatine were estimated using the H_2O signal as an internal reference.

Spectroscopic imaging experiments revealed a lower relative citrate signal in central parts of the prostate than in peripheral parts.

Keywords: human prostate, magnetic resonance spectroscopy, metabolites, spectroscopic imaging.

Introduction

Proton magnetic resonance spectroscopy (^{1}H MRS) has been mostly applied to the brain in human studies. To extend its use to other parts of the human body seems less trivial. Problems involved in abdominal application of ^{1}H MRS are related to the deep location and movement of some tissues of interest. Furthermore, dominating triglyceride signals, either from the target tissue itself or from adjacent adipose tissue, often obscure resonances of relevant metabolites.

With the advent of endorectal RF coils [1,2], the potential of ^{1}H MR of the human prostate has improved substantially and several groups have explored the use of such coils to obtain ^{1}H MR spectra of the human prostate [3-5]. The most prominent metabolite signal in these spectra is that of citrate, a compound abundantly present in the healthy prostate. The tissue content of citrate has been reported as a potential marker for prostate pathology, in particular to discriminate between the presence of adenocarcinomas and benign prostate hyperplasia (BPH) [6-13]. The intensity of the methyl proton signal of (phospho)cholines in

^{1}H MR spectra of the prostate may also serve this purpose [5,12,13]. Localized ^{1}H MRS of the human prostate based on magnet field gradient techniques has been initiated employing the STEAM (Stimulated Echo Acquisition Method) sequence [4,9,13] and the PRESS (Point Resolved Spectroscopy) sequence [5,14].

In this paper we report on the application of a double spin-echo (or PRESS) sequence [15,16] in combination with endorectal coils in ^{1}H MRS of the prostate of healthy volunteers. At an echo time of 135 ms well-resolved spectra were obtained showing major signals for citrate, choline compounds and creatine. Minimal contamination of these spectra with broad components facilitated the quantitation of metabolite levels. Furthermore, high quality ^{1}H MR spectra were obtained in multiple locations of the human prostate by extending PRESS volume localization with phase-encoding gradients to collect a spectroscopic imaging data set.

Materials and Methods

Volunteers

This study was approved by the local ethical committee. After informed consent was given 12 volunteers participated in this study. Of these volunteers 8 were examined with single volume localization, of which 3 were investigated twice. Four were examined in studies employing spectroscopic imaging. The ages of the volunteers ranged from 25 to 46. None of the volunteers had a history of genito-urinary disease or showed any signs of clinical prostate disease. MR images obtained of the prostates were interpreted as being normal. The volunteers were examined in the supine position. A belt was applied around the lower abdomen with slight compression to reduce respiratory motion. No antiperistaltic drugs were used.

MR Imaging

MR examinations were performed on a 1.5 T MR system (Magnetom SP, Siemens, Erlangen, Germany) employing a body radio-frequency coil for excitation. For MR signal reception a disposable endorectal probe (MEDRAD®, Pittsburg, USA) holding a surface coil with approximate length of 75 mm and width of 35 mm, was inserted. The probe was inflated with 50–100 ml of air to ensure tight positioning of the coil adjacent to the prostate. To visualize the prostate multiple slice MR imaging was performed in 3 orthogonal planes employing a turbo spin-echo (TSE) sequence (slice thickness: 5 mm, 1 mm interslice distance, field-of-view: 260 mm, matrix: 260*512, acquisitions: 2, Te: 160 ms, Tr: 2940 ms).

Single voxel MR spectroscopy

Based on these images volumes were selected for localized ^{1}H MRS employing a double spin-echo slice selective sequence (90°_τ_180°_T_180°_(T-τ)_Acquisition)

with echo times (2T) between 30 and 270 ms. The delay time τ was 11 ms. The length of the sinc-shaped RF pulses was 2.56 ms and the bandwidth of the 180° pulses was adjusted to select the same effective slice thickness as for the 90° pulse. The slice selective gradients were 2.67 mT/m, and EXORCYCLE phase cycling was applied. Field homogeneity was optimized for the selected volume using the resonance of water protons. For the detection of metabolite signals a chemical shift selective method [17] was used to suppress the water resonance and 2K data points were acquired with a spectral width of 1000 Hz. The nominal dimensions of the voxels were 1.5*1.5*1.5 cm (3.4 cc) except in two cases where voxels with nominal dimensions of 1.6*1.6*1.6 cm (4.1 cc) and 1.8*1.8*1.8 cm (5.8 cc) were selected. The scan repetition time ranged from 1.6 to 4.5 s and the number of scans from 96 to 256. In addition a spectrum without water suppression was obtained for eddy current correction and for referencing purposes.

To estimate apparent T_2-relaxation times of metabolite proton spins *in vivo,* spectra were recorded at 4 different echo times between 65 and 270 ms. For the estimation of the apparent T_2 relaxation time of water proton spins, 7 spectra were recorded without water resonance suppression at echo times between 30 and 270 ms.

Inversion recovery experiments to obtain apparent T_1 relaxation times were performed by the same pulse sequence used for localization, preceded by a non-selective 180° inversion pulse (650 µs). The echo time was 135 ms and the repetition time 3 s. Five or six spectra were recorded at different delay times between the inversion pulse and the localization sequence ranging from 50 to 1000 ms. In the same way inversion recovery experiments were performed without water suppression. The repetition time was set to 6 s and delay times ranged from 50 to 2500 ms (number of delay times investigated 6–8).

Besides these experiments with volunteers, inversion recovery experiments were also performed on a phantom (described below). Thirteen measurements were performed with inversion delay times between 40 and 1600 ms at a Tr of 6 s.

Spectroscopic imaging (SI)

In the SI experiments a transversal slice of 10 (or 11) mm thickness, 40 mm in the left-right and 30 mm in the anterior-posterior direction was selected for localized ^{1}H MRS by the double spin-echo sequence described above with an echo time of 135 ms. In these experiments τ was 14.5 ms, the pulse lengths were 5.12 ms, the slice selection gradient in the z-direction 3 mT/m and in the other directions 1.4 mT/m. Gradients for phase encoding in two directions were applied during 1 ms in the τ period, to obtain a set of SI data within the preselected volume. The field-of-view was 160 mm. Data was encoded in a 16 * 16 matrix resulting in nominal voxels of about 1.0 cc. For the spectral dimension 1K data points were acquired with a spectral width of 1 kHz. A total of 512 scans (2 scans per phase-encoding step) were acquired with a Tr of 1.6 sec resulting in an acquisition time of 13.6 min. For eddy current correction and referencing purposes also an SI experiment without water suppression was performed.

Phantom

To test the performance of MRS acquisition methods a phantom was used. It consisted of a glass sphere with an outer diameter of 10 cm filled with a citrate solution prepared according to the average composition of expressed human prostatic fluid as reported by Kavanagh [18]. It contained 90 mM sodium citrate, 8.8 mM $ZnCl_2$, 16.7 mM $MgCl_2$, 18.8 mM $CaCl_2$, 63 mM KCl at pH 6.7. For referencing and phasing purposes 13.6 mM glycine and 10 mM sodium acetate were added. The sphere was placed in a container filled with sunflower oil, to mimic the presence of periprostatic fat, which was positioned on the endorectal surface coil.

Post-processing

Post-processing of single volume measurements consisted of zerofilling to 4K data points and filtering as indicated in the figures. Eddy current correction was performed according to Klose [19] by a software procedure provided by the manufacturer. After this procedure usually only minor phase correction was necessary.

In the case of spectroscopic imaging, post-processing consisted of Fourier transformation to spatial and frequency dimensions applying zerofilling to 2 K data points and a Gaussian filter for the frequency dimension. No k-space filtering was used. Eddy current correction was performed as for the single voxel measurements.

For fitting of signals in the frequency domain NMR1 software (New Methods Research, Inc., Syracuse, New York) was used. Apparent T_1 and T_2 relaxation time values were derived by fitting the integrals of resonances to a single exponential function.

Average values are presented with standard deviations (±SD). Chemical shifts are given in parts per million (ppm).

Results

Single volume measurements

Spatial origin of spectra

By histology the most simple subdivision of the prostate gland is in a central part (including transition zone tissue) and a peripheral part of which the latter part occupies about 70% of the normal prostate gland [20]. In order to minimize signal contributions of periprostatic triglycerides the volumes for MR spectroscopy in this study were located in the central part of the prostate mainly containing central zone / transition zone tissue. From inspection of the MR images the contribution of peripheral zone tissue to the selected volumes was estimated to be between 15 and 25% for nominal volumes of 3.4 cc. In two examinations, with nominal voxels of 4.1 and 5.8 cc the contribution of the peripheral zone to the

selected volume was estimated to be 30–40%. Because a part of the peripheral zone included in the voxels was closest to the endorectal surface coil, the actual contribution of signal intensity from this zone to the spectra will be somewhat larger.

Homogeneity

In the present volunteer studies we have encountered little problems with prostate movement. If tissue movement occurs, this usually becomes manifest during the shimming procedure. One examination failed due to bad shimming results. Shimming values of all other 10 single voxel examinations performed at an echo time of 135 ms ranged from 3.5 to 10 Hz (full-width-half-maximum) with an average value of 6.2 ± 1.8 Hz.

Assignment of spectral components

Figure 1 shows a water resonance image of a transversal slice through the prostate of a volunteer also displaying the outline of the voxel selected for MR spectroscopy. The spectrum obtained from this voxel at an echo time of 135 ms is shown in Fig. 2. Assignments are indicated in the spectrum. These are based on previous high-resolution NMR studies of perchloric acid extracts of prostate specimens [12]. The most dominating metabolite resonance in the spectrum originates from citrate. At 1.5 T the 4 proton spins of citrate behave as a strongly coupled AB system with nearly identical chemical shifts showing 4 resonances of which the two central ones are most intense at the present experimental conditions [14]. *In vivo* usually only one peak is visible containing both these central components. However, at shimming values of about 5 Hz (or less) the separate resonance components of citrate start to get resolved (see below). In addition to citrate resonances all spectra showed peaks that could be assigned to the methyl protons of creatine and cholines. When referencing the creatine resonance to a chemical

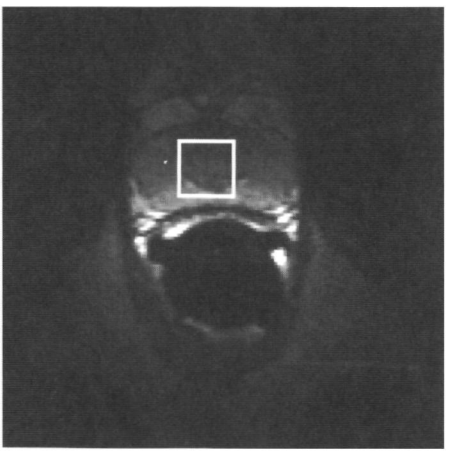

Fig. 1. Transversal MR image (T2-weighted) showing the prostate of a 28-year-old-volunteer. The volume selected for ^{1}H MR spectroscopy is indicated by a box. It has a nominal volume of 3.4 cc (1.5 * 1.5 * 1.5 cm).

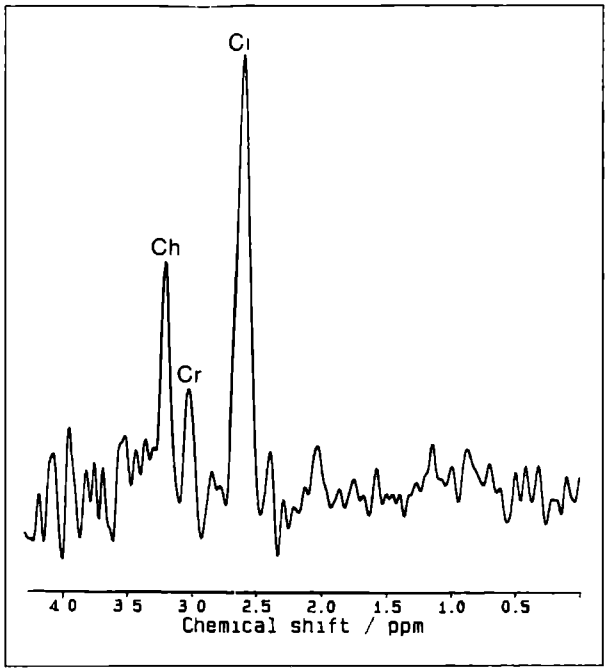

Fig. 2. ^{1}H MR spectrum of the volume shown in fig. 1. This spectrum has been obtained with an echo time of 135 ms, a Tr of 1600 ms and 256 scans. The half-width of the water resonance was 6 Hz Zerofilling to 4K and a Gaussian filter (maximum at 96 ms and half-width 148 ms) was applied to the FID before FT. No baseline correction was used. The indicated resonance assignments are Ci for the central citrate component, Cr for the methyl protons of creatine and Ch for the methyl protons of (phospho-)choline.

shift position of 3.03 ppm, we find in spectra obtained at Te = 135 ms, an average position (n–10) for the choline peak at 3.21 ± 0.01 ppm, for the central position of citrate at 2.63 ± 0.01 ppm and for the position of the water resonance at 4.68 ± 0.02 ppm. According to the extract studies the choline peak originates mainly from phosphocholine and choline compounds. Resonances of taurine, inositol, ethanolamine and polyamine protons may also contribute to signal intensity at 3.20–3.25 ppm [12,13]. The spectrum in figure 2 shows very little contribution of triglyceride signals between 1.7 and 0.5 ppm. In some of the spectra signals in this region were more intense. These likely originate from periprostatic fat as verified by taking spectra of voxels located more to the periphery of the prostate which showed an increased intensity of these resonances. In the spectra with minimal triglyceride signals no indication for a signal of lactate was observed which should be visible as an inverted doublet at about 1.33 ppm at an echo time of 135 ms.

At this echo time occasionally some additional weak resonances are observable which we tentatively assign, on the basis of prostate extract studies [12], to protons of taurine (3.2-3.4 ppm), glutamate/glutamine (2.0–2.5 ppm) and inositol (3.54 ppm). These become better discernible at shorter echo times. See for instance the spectra in figure 3 obtained at echo times of 100 and 65 ms. At echo times between 65 and 100 ms it is still possible to obtain spectra with resolved resonances for citrate, cholines and creatine, but for spectra at Te below 65 ms resolution becomes worse and therefore these spectra are more difficult to analyse. Usually, there is more signal contribution of triglycerides between 1.7 and 0.5 ppm at shorter echo times.

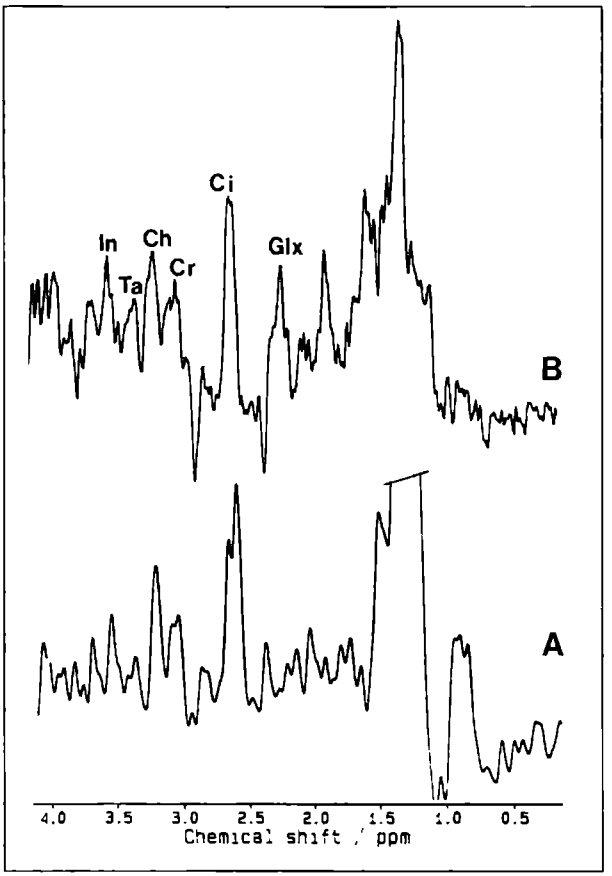

Fig. 3. MR spectra of the prostate of two volunteers obtained at different echo times. Nominal volumes were 3.4 cc. Tr was 2000 ms. Processing was performed as for Fig. 2. Further details: Spectrum **A**. Te = 100 ms. Gaussian filter with maximum at 96 ms and half-width 160 ms. Spectrum **B**. Te = 65 ms. Gaussian filter with maximum at 160 ms and half-width 160 ms.
In = inositol
Ta = taurine
Ch = (phospho) choline
Cr = creatine
Ci = citrate
Glx = glutamine/ glutamate

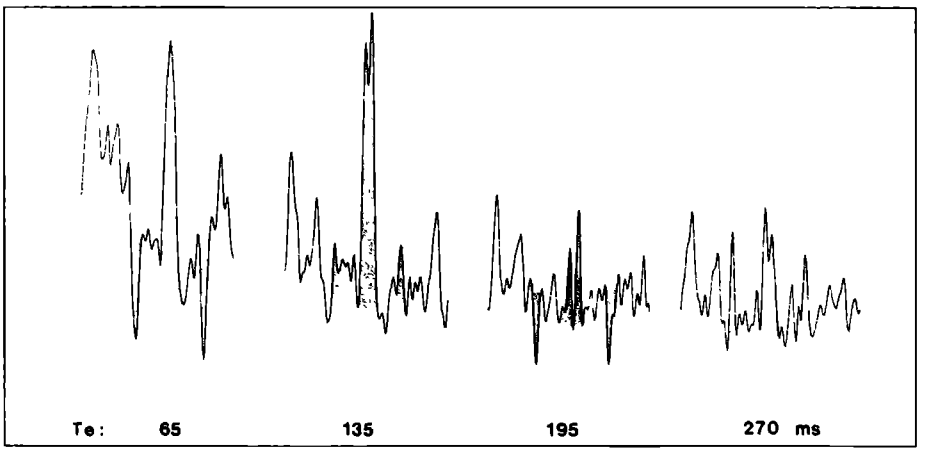

Fig. 4. MR spectra of the prostate of a volunteer obtained at different echo times. Nominal size of the selected volume was 5.8 cc. The Tr was 2000 ms. To aid visualization of the modulation of citrate resonances only the spectral part between 2.2 and 3.3 ppm is plotted. The multiplet of citrate is shaded grey. Echo times are indicated below the spectra. The same Gaussian filter was applied to all the spectra.

J modulation of the citrate signal in vivo

At shimming values of about 5 Hz width for the water resonance at half height, occasionally it became possible to observe the smaller outer signals of citrate at approximately 15–16 Hz from the central peaks Figure 4 shows the spectral region between 2 2 and 3 3 ppm with the citrate resonances at various echo times The outer peaks and the splitting of the main peak of citrate, at echo times of 135 ms and more, are well visible As described previously [14], the main citrate component shows slow modulation at 1 5 T, both *in vitro* and *in vivo* In addition, the present data (see fig 4) show that the faster modulation of the outer peaks seen *in vitro* [14] also occurs *in vivo* At the present timing of the PRESS sequence the main citrate resonances have a relative maximal signal amplitude at an echo time of approximately 130 ms, while the amplitudes of the outer peaks are minimal [14,21]

Apparent relaxation times

In 3 volunteers we have been able to perform inversion recovery experiments to get an estimate of the effective T_1 of the proton spins of some compounds In the localization scheme Te was set to 135 ms Figure 5 shows spectra of such an experiment Resonance integrals were determined by computer integration as described in the next section The mean effective T_1 obtained from these experiments was 339 ± 42 ms for the main component of the citrate signal complex and 837 ± 89 and 864 ± 98 ms for the methyl protons of cholines and creatine, respectively By the same procedure the mean effective T_1 of the water proton spins in the same volume elements of the 3 volunteers was 1481 ± 109 ms For comparison the effective T_1 value of the main resonance component of citrate in the phantom was also determined at Te = 135 ms This T_1 increases with temperature e g. at 22 °C a value of 360 ± 5 ms and at 32 °C a value of 534 ± 8 ms was found

Apparent T_2 relaxation times of metabolite resonances were derived from PRESS localisation experiments with 4 different echo times (from 65 to 270 ms) as shown in fig 4 The mean values obtained for the choline and creatine signals were 227 ± 61 ms and 209 ± 97 ms respectively (n=3) To estimate the apparent T_2 of H_2O spins 5 or 6 different echo times between 30 and 270 ms were used An average apparent T_2 value of 98 ± 9 ms was found (n=4) To derive a T_2-relaxation time for the citrate methylene proton spins is more difficult as its signals follow a complicated J modulation using a PRESS localization scheme[14,22] The treatment of this problem for the interpretation of *in vivo* MR results will be the subject of a separate publication

Quantitation

The good resolution of the spectra obtained at an echo time of 135 ms allowed evaluation of the integrals of the resonances of cholines and creatine and of the main component of the citrate multiplet

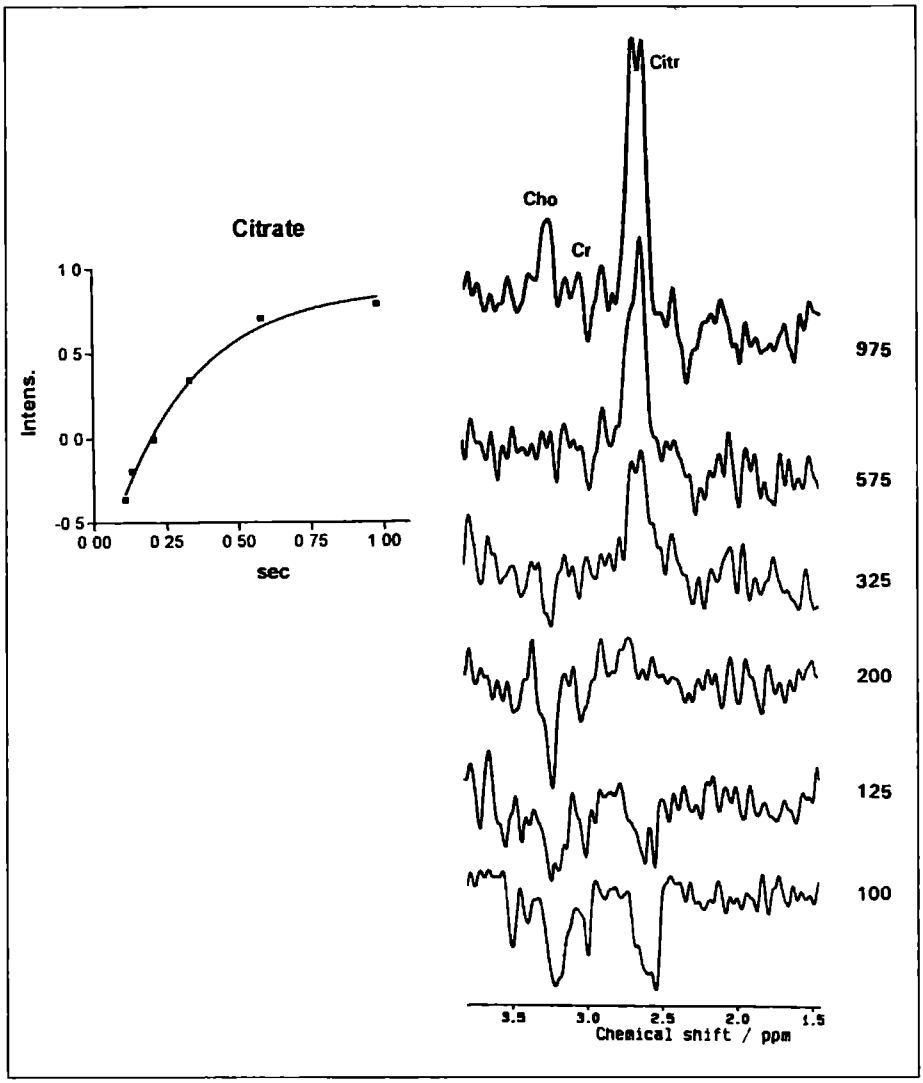

Fig. 5. Spectra of an inversion recovery experiment of the prostate of a volunteer. The nominal size of the selected volume was 4.1 cc. The echo time was set to 135 ms, Tr to 3 s and 96 scans were accumulated for each spectrum The delay times (ms) between the inversion pulse and the first slice selective 90° pulse are indicated in the figure. Zerofilling to 4K and a Gaussian filter were applied. The same phasing was used for all spectra. These were plotted without baseline correction The inset shows the fit of the integrals of the main citrate resonances to a single exponential function Cho = (phospho) choline, Cr = creatine, Citr = citrate.

Integration of resonances in the frequency domain was performed in two different ways after Gaussian filtering and phasing. Gaussian filtering consisted of a 2 Hz Lorentzian line width removal and a 4 Hz Gaussian linewidth broadening. Usually only minor baseline correction was needed. In the first approach signals were fitted to a Gaussian model function. In the second approach the

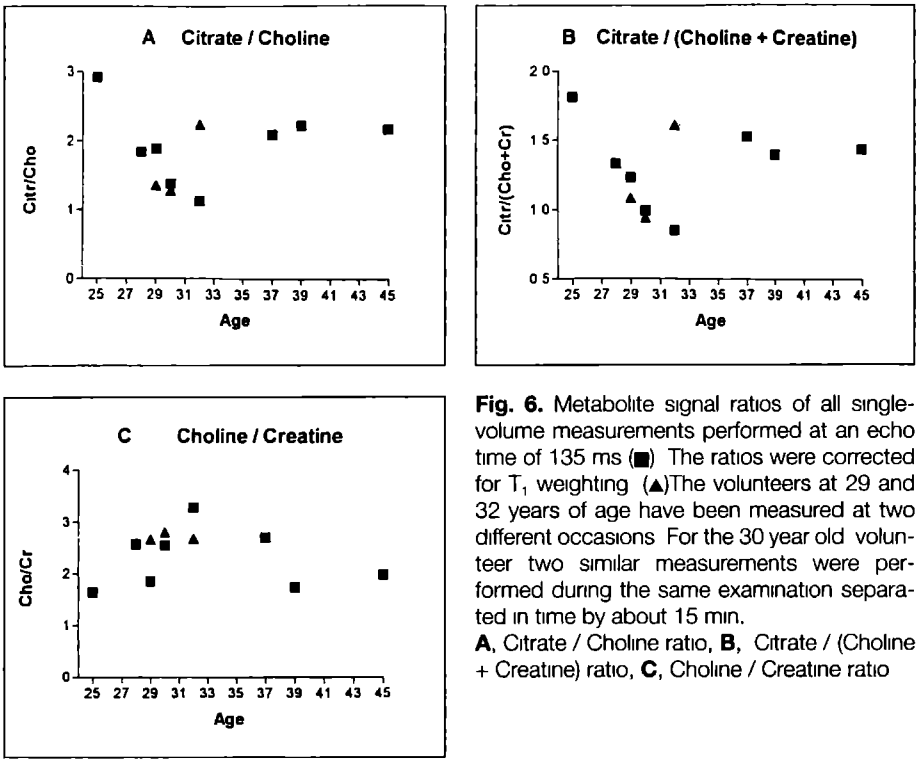

Fig. 6. Metabolite signal ratios of all single-volume measurements performed at an echo time of 135 ms (■) The ratios were corrected for T_1 weighting (▲)The volunteers at 29 and 32 years of age have been measured at two different occasions For the 30 year old volunteer two similar measurements were performed during the same examination separated in time by about 15 min.
A, Citrate / Choline ratio, **B**, Citrate / (Choline + Creatine) ratio, **C**, Choline / Creatine ratio

signal areas were obtained by computer integration. Integration of the main resonances of citrate was performed between the spectral limits of 2.49 and 2.77 ppm, of the creatine methyl peak between 2.96 and 3.11 ppm, of the choline methyl peak between 3.12 and 3.30 ppm, and of the water resonance between 4.42 and 4.94 ppm. The data were first evaluated as signal ratios. Since repetition times of the experiments varied between 1.6 and 4.5 s, the resonance integrals have been corrected with the effective T_1 values given above. Fig. 6 displays individual values for the ratios of citrate and cholines, cholines and creatine, and citrate and the sum of cholines and creatine, as obtained by the signal fitting procedure. Note that the highest citrate ratios are observed for the two largest volumes measured. In the volunteer at 25 years of age a nominal voxel size of 5.8 cc was measured and in the second measurement of the volunteer at 32 years a nominal voxel size of 4.1 cc was selected. The lowest citrate ratio was determined for the volume estimated to be the least contaminated with peripheral zone tissue: i.e. in the first measurement of the volunteer at 32 years of age.

See Table 1 (column I) gives the average values of ratios obtained from all single voxel examinations at an echo time of 135 ms. The ratio calculations from computer integration of signals gave very similar results: i.e. citrate/choline, citrate/(choline + creatine) and choline/creatine were 2.10 ± 0.74, 1.47 ± 0.49 and 2.44 ± 0.50, respectively. Column II gives the average ratios only including spectra from nominal volumes of 3.4 cc.

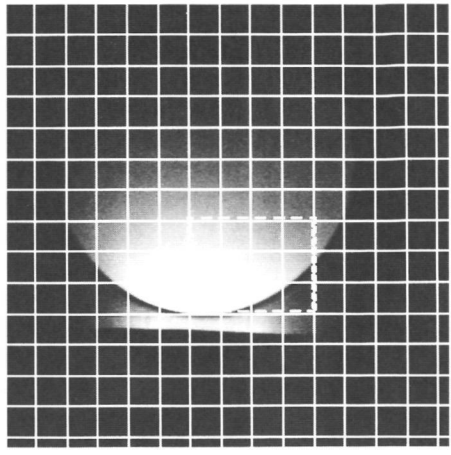

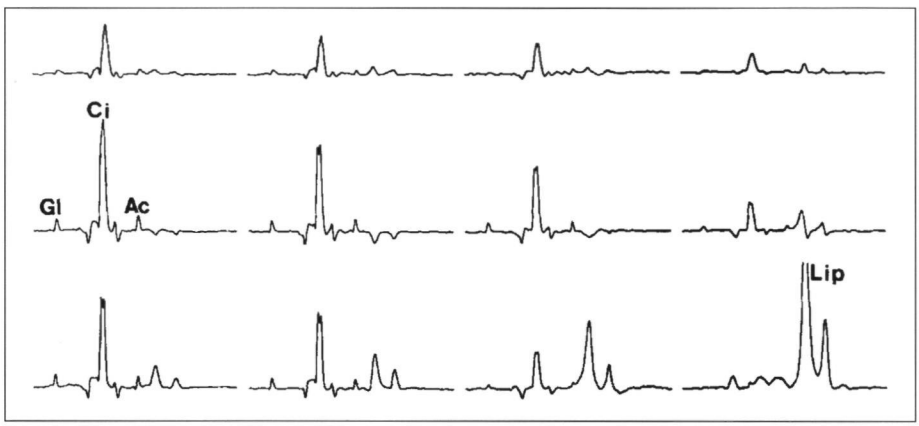

Fig. 7. A, Transversal MR image of the test phantom. At the same position an 11 mm thick slice was selected for spectroscopic imaging. The grid indicates voxels from which spectra have been acquired. The dashed line delineates the preselected volume which is both in the sphere and the container. **B**, ^{1}H MR spectra of the voxels in the pre-selected volume. The orientation is the same as in figure 7A. The nearly coinciding main citrate signals (Ci), and signals of acetate (Ac) and glycine (Gl) are indicated in the middle left voxel. The major lipid signals are indicated by 'Lip' in the lower right voxel. Spectra are plotted from 0–4 ppm

Because we also have recorded the H_2O signal for all volumes of which a spectrum was obtained, it is in principle possible to estimate tissue concentrations of metabolites using water as an internal reference. For this estimation it was assumed that the water content of prostate tissue is 83% and the tissue density 1.02 kg/L [23]. Furthermore, it was arbitrarily assumed that 10% of tissue water is not recovered in the H_2O resonance of the MR recording at Te = 135 ms because of a short T_2, e.g. due to macromolecular binding and other interactions, similar as described for brain MR studies [24]. By these calculations the average prostate tissue concentrations (per litre tissue volume) of cholines and creatine were estimated to be 3.1 ± 0.7 and 4.4 ± 0.8 mM respectively (n=10).

Spectroscopic imaging (SI) measurements

Phantom study

Figure 7a shows a transversal MR image of the phantom also displaying the preselected volume and the grid with SI voxels. The MRI intensity distribution within

the sphere follows the sensitivity profile of the endorectal coil. Fig. 7b shows spectra obtained from the voxels within the preselected volume. The spectrum in the lower right corner only shows signal intensity arising from lipid protons of sunflower oil as expected for its location. Spectra of voxels completely located within the sphere show signals for citrate, glycine and acetate. Signal intensity varies as a function of the sensitivity of the surface coil. Notice that the outer lines of the citrate multiplet are nearly in antiphase which is in contrast with the single voxel measurements where the outer lines are more in phase. This is due to the difference in time between the 90° and first 180° slice selection pulses. The small, sometimes inverted lipid signals seen in the SI spectra are attributed to voxel bleeding. Spectra of voxels located partly in the sphere and partly outside show signal contributions of citrate, glycine and acetate compounds and of lipids according to their partial volume extent of sphere and container. These results illustrate the quality of localisation by the present SI approach.

Volunteer studies

For the preselected volumes chosen in this study (about 12 cc) we obtained a H_2O resonance linewidth at half maximum just below 10 Hz which appeared to be sufficient to obtain well-resolved signals in most voxels of the spectroscopic images.

Figure 8 displays a transversal T_2-weighted image through the prostate of a volunteer of 32 years at a level close to the veramontanum. Anatomical details such as peripheral zone, central gland and capsule are visible. Due to the young age of the volunteer the prostate is relatively small and distinction between peripheral zone and central gland is less prominent than usually seen at older age. The grid projected on the image identifies voxels from which spectra are displayed in figure 9. These voxels have been obtained after extrapolating spatial data from a 16 * 16 to a 32 * 32 matrix by zerofilling in two dimensions in k-space prior to Fourier transformation.

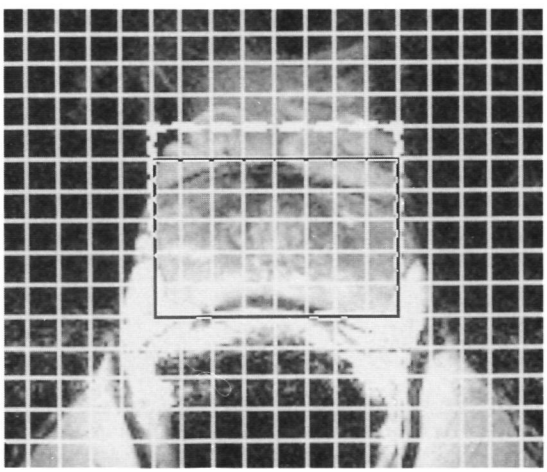

Fig. 8. Transversal MR image showing the prostate of a 32 year old healthy volunteer. The slice thickness was 5 mm. Spectroscopic imaging was performed for an 11 mm thick transversal plane. It was centered at the same position, but extended about 3 mm at either side beyond the MRI slice borders. The preselected PRESS volume is indicated by the white dashed box. Zerofilling in the spatial dimensions has been performed from a 16 x 16 to a 32 x 32 matrix. The volume with voxels from which spectra are displayed in figure 9 is indicated by a solid black box.

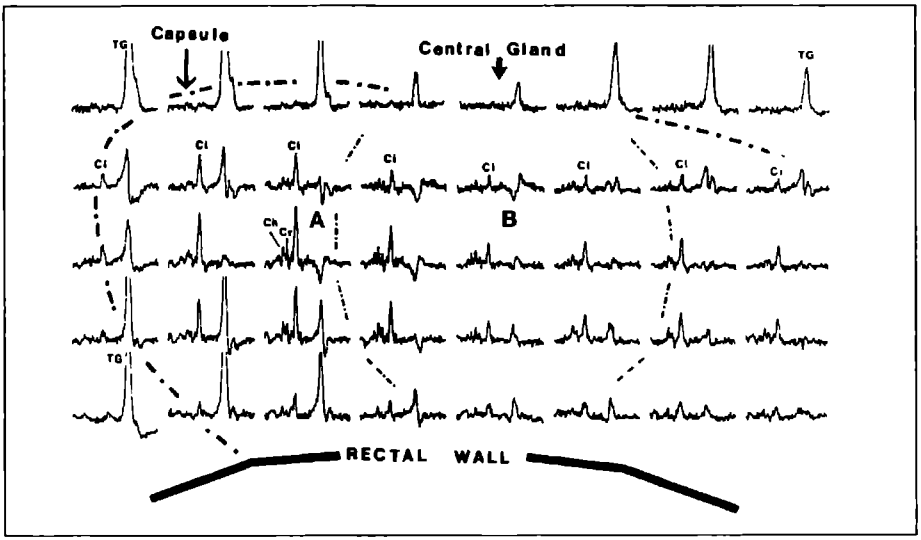

Fig. 9. Spectra of an SI data set from the voxels as shown in fig. 8 (black box). The maximum of the Gaussian filter applied was 64 ms and the half-width 256 ms. To aid interpretation the most prominent features of prostate anatomy are indicated schematically. Triglyceride signals are indicated by TG in the top corner spectra and in the bottom left spectrum. In the second row the central citrate resonance in the spectra are indicated by Ci. In the spectrum labelled A the methyl resonances for creatine (Cr) and choline (Ch) are indicated. Spectra are plotted from 0.1 to 4.1 ppm.

Figure 9 shows spectra from voxels in the black lined block in figure 8. Other voxels from the pre-selected volume show almost only signals for periprostatic fat. Typical spectral profiles observed in the selected data set appear to be related to prominent features of the human prostate. High triglyceride signals are observed outside the prostate or at the capsule. So most of the intensity in the upper row comes from triglycerides and very little from prostate metabolites. Note the relative decrease of the triglyceride signal in the two middle spectra of this row which coincide with the location of the anterior fibromuscular band which has a low signal intensity on T_1 and T_2 weighted MRI [25,26]. The left column also shows spectra mainly with signals of methylene triglyceride protons of periprostatic fat. In the second row from above signals of metabolites in the prostate become visible such as those for citrate methylene protons (at 2.63 ppm) and choline and creatine methyl protons (at 3.21 and 3.03 ppm, respectively). Citrate signals are not observed outside the prostate.

Figure 10 shows enlargements of spectra from the peripheral part of the prostate (A) and from the central gland area (B). Well-resolved resonances for methylene protons of citrate and for methyl protons of creatine and (phospho)cholines can be observed. The central gland area in the selected slab predominantly is composed of the transition zone of the prostate, but it also includes a part of the central zone, the urethra, periurethral tissue and the fibromuscular band [25,26]. Notice that in both spectra the outer lines of citrate are nearly in antiphase, similar as found for the citrate signal in the phantom study.

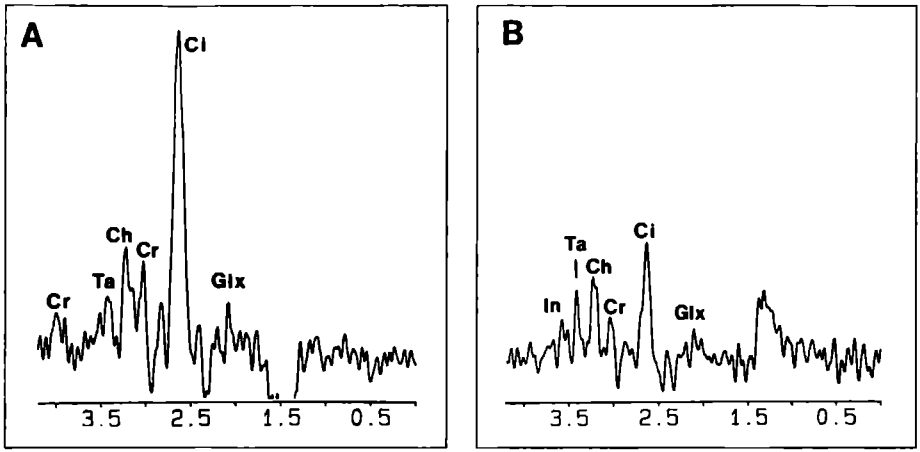

Fig. 10. A, ^{1}H MR spectrum of the peripheral part of the prostate. It is a blow-up from the spectrum labelled A in the third row of fig 9. **B,** ^{1}H MR spectrum of the central prostate gland. This spectrum is a blow-up of a spectrum from the same row labelled B. In = inositol, Ta = taurine, Ch = (phospho) choline, Cr = creatine, Ci = citrate, Glx = glutamine/glutamate.

Spectroscopic images of similar quality as shown above were obtained from the prostate of 3 other volunteers (age 40–46 years). In all 4 volunteers voxels of 1 cc were selected both from the peripheral zone and the central / transition zone. In the latter voxels contamination with peripheral zone tissue was estimated to be less than 10%. The citrate/cholines, citrate/(cholines + creatine) and cholines/creatine signal integral ratios were determined by fitting of the spectral lines to Gaussian model functions. T_1 corrections were performed assuming similar apparent T_1 values for proton spins in peripheral and central gland as those determined in the single voxel measurements. The T_1 corrected values are in Table I, columns III and IV. The citrate signal ratios are significantly higher in peripheral gland compared to the central gland. The values for average citrate ratios of the central gland (column III) are closest to the values of citrate ratios obtained from single voxels (column II), which were deliberately positioned in the center of the prostate.

Pulse lenghts and value in the PRESS sequence used for single volume acquisition are different from those used for SI experiments. Because this may affect the citrate signal we have compared both sequences in a study of the phantom. In these experiments the area of the main citrate signal with respect to those of the acetate and glycine resonances differed not more than 10% between both acquisition methods.

Discussion

In this study it is demonstrated that high quality ^{1}H MR spectra can be recorded of the human prostate by the application of PRESS localization and an endorectal surface coil. Results are presented of normal prostates in volunteers at an age before BPH starts to occur.

Most experiments were performed with a timing of the PRESS sequence (i.e. Te = 135 ms) which is nearly optimal for refocussing of the main multiplet signals of citrate and which in principle enables one to identify lactate signals if present. Spectra obtained at this echo time are also sufficiently depleted of broad components to enable quantitative evaluation of metabolite signals. ^{1}H MRS of volumes carefully located in the center of the prostate demonstrate that it is possible to obtain spectra with little or no signals between 0.5 and 2 ppm. High signal intensity in this chemical shift range, often seen in ^{1}H MR spectra of the prostate *in vivo*, is likely dominated by contamination of triglyceride signals from periprostatic fat.

The spectra obtained at Te = 135 ms show almost only signal intensity for the methyl protons of cholines and creatine next to the dominating peak of citrate methylene protons. The presence of signals of these compounds could be anticipated from *in vitro* extract studies, e.g. [8,10–12]. However, these studies also revealed the presence of other compounds in prostate tissue at comparable amounts, e.g. inositol, taurine, glutamine and glutamate and possibly polyamines. Due to T_2 relaxation and/or J modulation their signals are much attenuated in spectra obtained at Te = 135 ms. However, at shorter echo times additional signals appear which can be assigned to some of these compounds. In this respect the situation is much the same as for ^{1}H MR spectra of the brain obtained by the PRESS sequence. At longer echo times signals for choline, creatine and N-acetylaspartate are essentially the only signals remaining in the spectra.

In ^{1}H NMR spectra of extracts of normal prostate tissue significant signals are observed for lactate [12,13]. However, the present *in vivo* results, obtained by single voxel acquisition at TE=135 ms, give no indication for such signals. Lactate may have become "NMR invisible" *in vivo*, for instance due to macromolecular binding, but more likely its presence in *in vitro* spectra is a consequence of the biopsy procedure.

A study concerning normal prostate has been reported in which PRESS was used for localization in conjunction with a Helmholtz coil for signal reception [14]. In concurrence with our findings no signs for the presence of a lactate signal in spectra of the prostate were observed. Furthermore, slow J modulation of the main peaks of citrate *in vivo* was demonstrated. Due to improved resolution both this slow modulation as well as the faster modulation of the outer peaks of citrate could be monitored in the present study.

It is known that substantial amounts of divalent cations such as Mg^{2+}, Ca^{2+} and Zn^{2+} are present in prostatic fluid [18]. As observed in ^{1}H NMR of citrate solutions both the spin-spin coupling constant and the chemical shift positions of citrate signals are sensitive to pH, but much more to complexation of citrate with these cations [27]. The chemical shift position of citrate signals measured *in vivo* are similar to those measured *in vitro* in the presence of divalent cations which indicates that also in the prostate, citrate is complexed to these ions.

In a few volunteers apparent relaxation times for water and metabolite proton spins in the prostate have been estimated. T_1 and T_2 relaxation times for water proton spins are close to values published previously by Kjaer et al. [28]. Recently

spatially more precise T_2 measurements have been made showing a longer T_2 relaxation time for the peripheral zone as compared to the central zone [29]. Our T_2 value is closest to that reported for the central zone which is in agreement with the location of the volumes from which the measurements have been made. The apparent T_1 and T_2 relaxation times estimated for choline and creatine methyl proton spins are equal or somewhat shorter than T_1 and T_2 relaxation times of the corresponding proton spins in ^1H spectra of the adult human brain [30]. For citrate methylene proton spins a relatively short effective T_1 value is found. As citrate efficiently binds divalent cations [27] this may be caused by trace amounts of paramagnetic ions. The estimation of these relaxation times provides starting values to set sequence timing in ^1H MRS studies of the prostate and to enable quantification of compound levels.

Presently, little quantitative data of localized ^1H MR spectroscopy of the healthy human prostate *in situ* is available. Most studies have been performed using the STEAM localization sequence [4,9,13,29,31]. In a recent paper by Kurhanewicz et al. [32] quantitative data on the ratio of the citrate signal with respect to signal intensity at the choline and creatine position in spectra of zonal regions of healthy volunteers are presented using both STEAM and PRESS. Although experimental and processing conditions are somewhat different from ours the mean ratios in both studies are fairly similar. Some estimates of the tissue content of citrate in the prostate have been made by localized ^1H MRS [5,29], but adequate evaluation of the complex citrate signal and correction for J-modulation and T_2 relaxation for this purpose have not been fully realized yet.

Levels for choline and creatine compounds in the prostate have not been reported up till now. The concentrations for cholines and creatine in the prostate estimated by MRS in the present study are different from those determined for brain tissue by the same method. The estimated choline concentration is higher and the creatine concentration lower than in brain (see for instance [30]). A substantial part of creatine in the prostate is phosphorylated [12,33,34]. The most likely locations for creatine are the various smooth muscle components in the prostate: i.e. stromal and capsular muscle cells and myoepithelial cells surrounding prostatic acini.

Previously, we have performed ^1H NMR of an extract of a normal prostate tissue specimen [12]. We have reanalysed data of this sample to enable comparison with the present *in vivo* results. From a fully relaxed ^1H NMR spectrum obtained from the sample at pH 7 the total creatine signal intensity (Cr) was determined. Furthermore the signal intensity between 3.15 and 3.28 ppm was determined including contributions of all methyl protons of various choline compounds (Cho) but excluding contributions of taurine, inositol and phosphoethanolamine protons. A Cho/Cr ratio of 1.81 was found which is only slightly lower than the Cho/Cr ratio obtained by *in vivo* MRS measurements at Te=135 ms. Because Cho and Cr methyl proton spins have similar T_2 values, this indicates that the majority of signal intensity at about 3.2 ppm seen in spectra obtained *in vivo* at Te=135 ms originates from choline compounds.

The results of the spectroscopic imaging experiments show that high quality spectra can be obtained simultaneously from multiple locations in the prostate.

The present acquisition time to record a SI data set with good signal-to-noise at a nominal resolution of 1 cc was 13 6 min at a Tr of 1600 ms Obviously, based on the estimations of the effective T_1 relaxation times of the main resonances a better signal-to-noise per unit time can be achieved and thus spatial resolution may be enhanced The acquisition of ^{1}H MR spectra of the human prostate at a spatial resolution below 1 cc has been demonstrated to be possible [32,35] Such resolution may be needed to match with the complex anatomy of the human prostate and with the heterogeneity of prostate pathology

Variations in resonance intensity for distinct morphological locations in the prostate become visible at a spatial resolution of about 1 cc Most striking is the lower relative level of the citrate signal in spectra from the central/ transition zone as compared to the peripheral zone Recently, a similar difference in citrate signal levels between peripheral zone and central/transition zone has been observed in other MRS studies [29,32] The average citrate content in the peripheral part of the prostate appears to be twice of the amount in the central part [29] The same increase is found for the relative citrate signal in the present study A higher citrate level in the peripheral zone presumably is related to the presence of more glandular elements in this area [25] This also explains why in the single volume measurements the citrate ratios are the highest in cases with most contributions of peripheral zone tissue

In conclusion, this study on healthy individuals shows that with PRESS localization and an endorectal coil, it is possible to perform detailed MR spectroscopic investigations of a number of metabolites in relevant parts of the human prostate Data obtained in this way may serve as a reference for clinical applications of ^{1}H MRS to BPH and prostate cancer [32,35].

Acknowledgments

We thank Dr Sauter and co-workers at Siemens Erlangen, Germany for providing us with an elementary proton spectroscopic imaging pulse sequence and post-processing software Furthermore, we thank Ing H J van den Boogert for technical assistance and Dr W M M J Bovée (Technical University Delft) for useful discussions This study was supported by the Dutch Cancer Society

References

1 M D Schnall, R I Lekinski, H M Pollack, Y Imai, H Y Kressel Prostate MR imaging with an endorectal surface coil *Radiology* **172**, 570 - 574 (1989)

2 P Narayan, D B Vigneron, P M Jajodia, C M Anderson, M W Hedgcock, E A Tanagho, T L James Transrectal probe for ^{1}H MRI and ^{31}P MR spectroscopy of the prostate gland *Magn Reson Med* **11**, 209 220 (1989)

3 M A Thomas, P Naravan, J Kurhanewicz, P Jojadia, M W Weiner ^{1}H MR Spectroscopy of normal and malignant human prostates *in vivo J Magn Reson* **87**, 610 - 619 (1990)

4 M Schnall, R Lenkinski, B Milestone, H Kressel Localized ^{1}H spectroscopy of the human prostate *in vivo, in* "Proc , SMRM, 9th Annual Meeting, New York, 1990," pg 288

5 A Heerschap, G Jager, A de Koster, J Barentsz, J de la Rosette, F Debruyne and J Ruijs ^{1}H MRS of prostate pathology, *in* "Proc , SMRM, 12th Annual Meeting, New York, 1993," pg 213
6 I C Costello and R B Franklin Concepts of citrate production and secretion by prostate 1 Metabolic relationships *The Prostate* **18**, 25 - 46 (1991)
7 K R Halliday, C Fenoglio-Preiser, L O Sillerud Differentiation of human tumors from nonmalignant tissue by natural abundance ^{13}C NMR spectroscopy *Magn Reson Med* **7**, 384 - 411 (1988)
8 A H Fowler, A A Pappas, J C Holder, A F Finkbeiner, G V Dalrymple, M S Mullins, J R Sprigg, R A Komoroski Differentiation of human prostate cancer from benign hypertrophy by *in vitro* ^{1}H NMR. *Magn Reson Med* **25**, 140 - 147 (1992)
9 P Narayan, J Kurhanewicz Magnetic resonance spectroscopy in prostate disease diagnostic possibilities and future developments *The Prostate* Supplement **4**, 43 - 50 (1992)
10 J Kurhanewicz, R Dahiya, J M McDonald, I H Chang, T L James, P Narayan Citrate alterations in primary and metastatic human prostatic adenocarcinomas ^{1}H magnetic resonance spectroscopy and biochemical study *Magn Reson Med* **29**, 149 - 157 (1993)
11 M L Schiebler, K K Miyamoto, M White, S J Maygarden, J L Mohler *In vitro* high resolution 1H spectroscopy of the human prostate benign prostatic hyperplasia, normal peripheral zone and adenocarcinoma *Magn Reson Med* **29**, 285 - 291 (1993)
12 F B Cornel, G A H J Smits, G O N Oosterhof, H F M Karthaus, F M J Debruyne, J A Schalken, A. Heerschap Characterization of human prostate cancer, benign prostate hyperplasia and normal prostate by *in vitro* ^{1}H and ^{31}P magnetic resonance spectroscopy *J Urol* **150**, 2019 - 2024 (1993)
13 J Kurhanewicz, D B Vigneron, S J Nelson, H J Hricak, J M McDonald, B Konety, P Narayan Citrate as an *in vivo* marker to discriminate prostate cancer from benign hyperplasia and normal prostate peripheral zone detection via localized proton spectroscopy *Urology* **45**, 459 466 (1995)
14 F Schick, H Bongers, S Kurz, W-I Jung, M Pfeffer, O Lutz Localized proton MR spectroscopy of citrate *in vitro* and of the human prostate *in vivo* at 1 5 T *Magn Reson Med* **29**, 38 - 43 (1993)
15 R J Ordidge, M R Bendall, R L Gordon, A Connelly Volume selection for in vivo biological spectroscopy *In* "Magnetic Resonance in Biology and Medicine" (G Govil, C L Khetrapal, A Saran, Eds), 386 - 397, Tata McGraw-Hill, New Delhi, 1985
16 P A Bottomley Spatial localization in NMR spectroscopy *in vivo Ann NY Acad Sci* **508**, 333 - 348 (1987)
17 A Haase, J Frahm, W Hänicke, D Matthaei ^{1}H NMR chemical shift selective (CHFSS) imaging *Phys Med Biol* **30**, 341 - 344 (1985)
18 J P Kavanagh Sodium, potassium, calcium, magnesium, zinc, citrate and chloride content of human prostatic and seminal fluid *J Reprod Fert* **75**, 35 41 (1985)
19 U Klose *In vivo* proton spectroscopy in presence of eddy currents *Magn Reson Med* **14** , 26 - 30 (1990)
20 J E McNeal Normal histology of the prostate *Am J Surg Pathol* **12** , 619 - 633 (1988)
21 K Straubinger, F Schick, O Lutz Computer-algebra calculations and measurements on AB spin systems for double-spin-echo sequences *MAGMA* **3**, 109 118 (1995)
22 R V Mulkern, J L Bowers Caculating spectral modulations of AB systems during PRESS acquisitions *Magn Reson Med* **30**, 518 - 519 (1993)
23 Report of the Task Group on the Reference Man, International Commission on Radiological Protection, no 23 New York, Pergamon Press, Oxford (1981)
24 I Ernst, R Kreis, B D Ross Absolute quantitation of water and metabolites in the human brain I compartments and water *J Magn Reson series B*, **102** , 1 - 8 (1993)
25 H Hricak, G C Dooms, J E McNeal, A S Mark, M Marotti, A Avallone, M Pelzer, E C Proctor, E A Tanagho MR imaging of the prostate gland normal anatomy *Am J Roentgenol* **148**, 51 - 58 (1987)
26 M D Schnall, M Berzi, H M Pollack, H Y Kressel Magnetic Resonance Imaging of the prostate *Magn Reson Quart* **6**, 1 - 16 (1990)

27 M van der Graaf & A Heerschap Effect of cation binding on the proton chemical shifts and the JAB coupling constant of citrate *J Magn Reson* Series B, 112, 58-62 (1996)
28 L Kjaer, C Thomsen, P Iversen, O Henriksen *In vivo* estimation of relaxation processes in benign hyperplasia and carcinoma of the prostate gland by magnetic resonance imaging *Mag Reson Imaging* **5**, 23 - 30 (1987)
29 M Lowry, D J Manton, I W Turnbull, S J Blackband, A Horsman Quantitative proton MRS assessment of citrate heterogeneity in normal prostate *MAGMA* **2**, 483 - 485 (1994)
30 R Kreis, T Ernst, B D Ross Development of the human brain *in vivo* quantification of metabolite and water content with proton magnetic resonance spectroscopy *Magn Reson Med* **30**, 424 - 437 (1993)
31 M L Schiebler, M D Schnall, H M Pollack, R E Lenkinski, J F Tomaszewski, A J Wein, R Whittington, W Rauschning, H Y Kressel Current role of MR imaging in the staging of adenocarcinoma of the prostate *Radiology* **189**, 339 - 352 (1993)
32 J Kurhanewicz, D B Vigneron, H Hricak, P Narayan, P Carrol, S J Nelson Three-dimensional H-1 MR Spectroscopic imaging of the in situ human prostate with high (0 24-0 7cm^3) spatial resolution *Radiology* **198**, 795 - 805 (1996)
33 P Narayan, P Jajodia, J Kurhanewicz, A Thomas, J MacDonald, B Hubesch, M Hedgecock, C Anderson, T L James, E A Tanagho, M Weiner Characterization of prostate cancer, benign prostatic hyperplasia and normal prostate using transrectal ^{31}P phosphorus magnetic resonance spectroscopy a preliminary report *J Urology* **146**, 66 - 74 (1991)
34 J Kurhanewicz, A Thomas, P Jajodia, M Weiner, T I James, D Vigneron, P Narayan ^{31}P spectroscopy of the human prostate gland *in vivo* using a transrectal probe *Mag Reson Med* **22**, 404 - 413 (1991)
35 A Heerschap, G J Jager, M van der Graaf, J O Barentsz, J J M C H de la Rosette G O N Oosterhof, E T G Ruyter, S J Ruijs In-vivo proton MR Spectroscopy reveals altered metabolite content in malignant prostate tissue *Anticancer Res*, in press (1996)

7 In-vivo Proton MR Spectroscopy Reveals Altered Metabolite Content in Malignant Prostate Tissue

A. Heerschap[1], G. Jager[1], M. van der Graaf[1], J. Barentsz[1], J. de la Rosette[2], G. Oosterhof[2], E. Ruijter[2,3], J. Ruijs[1]

From the Departments of [1]Radiology, [2]Urology and [3]Pathology, University Hospital Nijmegen, The Netherlands

Abstract

Background

Recently the potentials of magnetic resonance (MR) methods for non-invasive diagnosis and therapy evaluation of prostate cancer have improved substantially. In this study proton MR spectroscopy (^{1}H MRS) is explored for the detection of cancer in the prostate.

Patients and Methods

Employing an endorectal probe localized ^{1}H MRS and contrast enhanced MR imaging were performed of the prostate of healthy volunteers and of patients with benign prostatic hyperplasia (BPH) and/or prostate cancer (PCa).

Results

^{1}H MR spectra of the human prostate show 3 major signals: i.e. for citrate, creatine and choline compounds. For cancer tissue the average citrate/ choline signal ratio is significantly lower than for BPH and non-cancerous peripheral and central zone tissue, but individual ratios overlap with ratios for normal central zone and BPH tissue. Low citrate/choline ratios in tumour tissue correspond with early MR contrast enhancement.

Conclusion

^{1}H MRS has potential for non-invasive detection and follow-up of tumours in the prostate.

Introduction

It is common practice to verify the presence of cancerous tissue in the prostate by histology of biopsy material. However, this analysis may be subject to sampling errors [1] and does not provide much information on spatial heterogeneity and multifocality. Non-invasive modalities such as computer tomography and transrectal ultrasound (without guided biopsies) have been of limited value for diagnosis and therapy evaluation of prostate cancer [2]. Also MR imaging (MRI) is still of little use to detect PCa and to determine its extension, although the more

recent introduction of endorectal and body phased-array radiofrequency detection coils have enabled better possibilities to stage PCa [3,4,5]. The potentials of MR may be further improved by the use of more advanced methods such as dynamic Gd contrast enhanced MRI or MR spectroscopy (MRS). Several groups have started to perform image-guided proton MRS (^{1}H MRS) of the human prostate with endorectal and/or phased-array coils [6-9]. In a ^{1}H MRS examination spectra can be obtained of particular locations in the prostate with proton signals of several metabolites. In this way it provides a metabolic window on prostate tissue which may be used for in-situ characterization, diagnosis and therapy evaluation of prostate cancer (PCa).

The most prominent metabolite signal in ^{1}H MR spectra of the prostate is that of citrate, of which the tissue content has been reported as a potential marker to discriminate between the presence of PCa and benign prostatic hyperplasia (BPH) [10-16]. In vitro studies of human prostate specimens have demonstrated that the relative intensity of the methyl proton signals of (phospho)choline compounds in ^{1}H MR spectra of PCa tissue is increased [15,16] and our preliminary results indicated that this could also be observed in vivo [8].

In this paper we report on results of the application of image-guided localized ^{1}H MRS in studies of the prostate of healthy volunteers, patients with BPH and/or with PCa. We applied and compared single and multiple voxel data acquisition methods. As elevation of choline and lowering of citrate levels appear to be associated with PCa, the citrate/choline (Ci/Ch) signal ratio plays a central role in the analysis of our data. Preliminary results on the combination of ^{1}H MRS and dynamic contrast enhanced Gadolinium (Gd) MR measurements are also presented.

Patients and Methods

Volunteers and patients

This study was approved by the local ethical committee and informed consent was obtained from all participants. Results of studies of 6 healthy volunteers aging from 32 to 54, without a history or clinical signs of prostate disease, are included in this report. MR images of the prostates were interpreted as being normal except for some slight hypertrophy of the oldest volunteer. Sixteen patients with BPH were included in this study (ages between 52 and 73). Furthermore, 23 patients suspected to have PCa, mainly on the basis of PSA levels (10 ng/ml or more) and ultrasonography, were investigated. The definitive diagnosis (PCa or not) was made on the basis of histological analysis performed on prostate tissue specimens obtained by needle biopsy or radical prostatectomy. Subjects were positioned supine in the magnet bore with a belt applied around the lower abdomen to reduce respiratory motion. Patients received 1 mg glucagon intravenously as antiperistaltic drug.

MR methods

MR examinations were performed on a 1.5 T MR system (Magnetom SP, Siemens, Germany) employing a body radio-frequency coil for excitation. For MR signal reception a disposable endorectal probe (MEDRAD®, Pittsburg, USA) holding a surface coil, was inserted. The probe was inflated with air to ensure tight positioning of the coil adjacent to the prostate.

MRI and MRS of the prostate was performed during the same patient examination which lasted about 1 hour. First multiple slice MR images were obtained in 3 orthogonal planes with a turbo spin-echo (TSE) sequence as described previously [5]. Guided by these images the prostate was inspected for the presence of areas likely to contain cancer tissue (hypo-intensity in the peripheral zone and anatomical deviations).

Localized ^{1}H MRS was performed with a double spin-echo slice selective pulse sequence (PRESS [17,18]) preceded by water signal suppression which first was turned off to optimize field homogeneity. The echo-time (Te) was 135 ms.

For single voxel MRS a voxel of nominal 1.5*1.5*1.5 cm (3.4 cc) was positioned in an area suspected to be tumour tissue, and if possible another voxel was studied in a non-cancerous area. The scan repetition time (Tr) ranged from 1.6 to 4.5 s and the number of scans from 96 to 256.

In the ^{1}H MR spectroscopic imaging (SI) experiments an axial slab of 10 mm thickness, 40 (or 50) mm in the left-right and 30 (or 40) mm in the anterior-posterior direction was selected using the PRESS sequence (Te = 120 - 135 ms) and positioned such that it contained a maximal amount of area suspected to be cancer tissue. Gradients for phase encoding in 2 directions were applied to obtain a multiple voxel SI data set within this preselected slab [19,20]. Data were encoded in a 16 * 16 matrix with a field-of-view of 144 or 160 mm, resulting in nominal voxels sizes of 0.8 or 1.0 cc. Per phase-encoding step 2 or 3 acquisitions were acquired with a Tr of 1.2 or 1.6 sec resulting in acquisition times of 13–15 min.

For eddy current correction and referencing purposes MRS experiments were also performed without water suppression.

In a number of patients suspected of PCa a dynamic Gd contrast enhanced inflow MR measurement was performed [21,22] after the MRS measurements. An axial slice of 10 mm thickness was selected through the suspected tumour region at exactly the same location as the SI slab or coinciding with the position of the single voxel. MR images were obtained by a turbo FLASH sequence (1–2 s/image) before and during inflow in the slice of Gd contrast, which was administered intravenously.

Post-processing was performed as described elsewhere [23]. Metabolite maps were reconstructed from the intensities of citrate and choline proton signals in SI spectra, showing spatial distributions of these compounds.

Chemical shifts are given in parts per million (ppm) with respect to the water resonance at 4.68 ppm. Signal integrals were determined by computer integration. All presented signal ratios for citrate and choline were corrected for T_1 weighting using an effective T_1 of 339 ms for citrate protons and of 837 ms for

choline protons as determined in a separate volunteer study [23]. Average values are presented with standard deviations (±SD).

Dynamic Gd contrast enhanced MR experiments are presented as dynamic subtraction (DS) images obtained by subtracting MR images recorded during Gd inflow in the slice from control images recorded before inflow.

Results

In figure 1A a T2 weighted MR image is shown of an axial plane through the prostate of a patient with PCa. An enlarged central gland (BPH) can be observed as a hypo-intense area including some hyper-intense nodular elements. The peripheral part of the prostate shows up as a hyper-intense zone except at the right side on this image where it is hypo-intense (solid box). This area was later demonstrated to be tumour tissue by histological examination. It showed earlier enhancement than other prostatic tissue on DS MR images (see arrow in Fig. 1B)). ^{1}H MRS was performed for voxels (see Fig. 1A) of which the spectra are shown in figures 1C and D. The spectrum in figure 1C, from a region assumed to house no cancer tissue, looks similar to spectra obtained from the peripheral zone of normal and most BPH prostates. It shows 3 major resonances. One at about 2.6 ppm originating from the methylene protons of citrate, one at about 3.0 ppm originating from the methyl group of creatine and one at about 3.2 ppm to which methyl groups of various choline containing compounds contribute. These assignments are based on previous ^{1}H MRS studies of perchloric extracts of prostate specimens [12-16]. The spectrum from the tumorous region (Fig. 1D) shows a strongly reduced citrate signal and an apparently increased choline and decreased creatine resonance.

Fifteen patients suspected of having PCa were examined by this single voxel approach. Two patients gave up further medical examinations after the MR investigation so that no definitive diagnosis is available and 3 were considered to have BPH after multiple biopsies. In 10 cases the presence of PCa was proven by histopathological examination of prostate material, either obtained by biopsy or radical prostatectomy [5]. After careful evaluation of the MR images and comparison with the histopathological results it was concluded that in 3 of these cases the voxels, with the aim to cover cancer tissue, were either located in an area with no apparent presence of cancer tissue or were mostly occupied with non-cancerous tissue (> 75%). For the 7 remaining cases it was estimated that the voxels mainly contained tumour tissue (> 50%). The citrate/choline signal ratio was determined from the spectra for further evaluation (see below).

In 3 patients suspected of having PCA a dynamic Gd MRI measurement was performed after the single voxel ^{1}H MRS examination showing relative fast enhancement in the area for which a low Ci/Ch signal ratio was determined.

Eight patients suspected to have PCa were investigated by 2D SI in an axial slab through the prostate using similar experimental parameters as for the single voxel measurements. In figure 2 results of a 2D SI and a dynamic Gd MR examination are shown of a PCa patient. Figure 2a and b show T_2 weighted MR

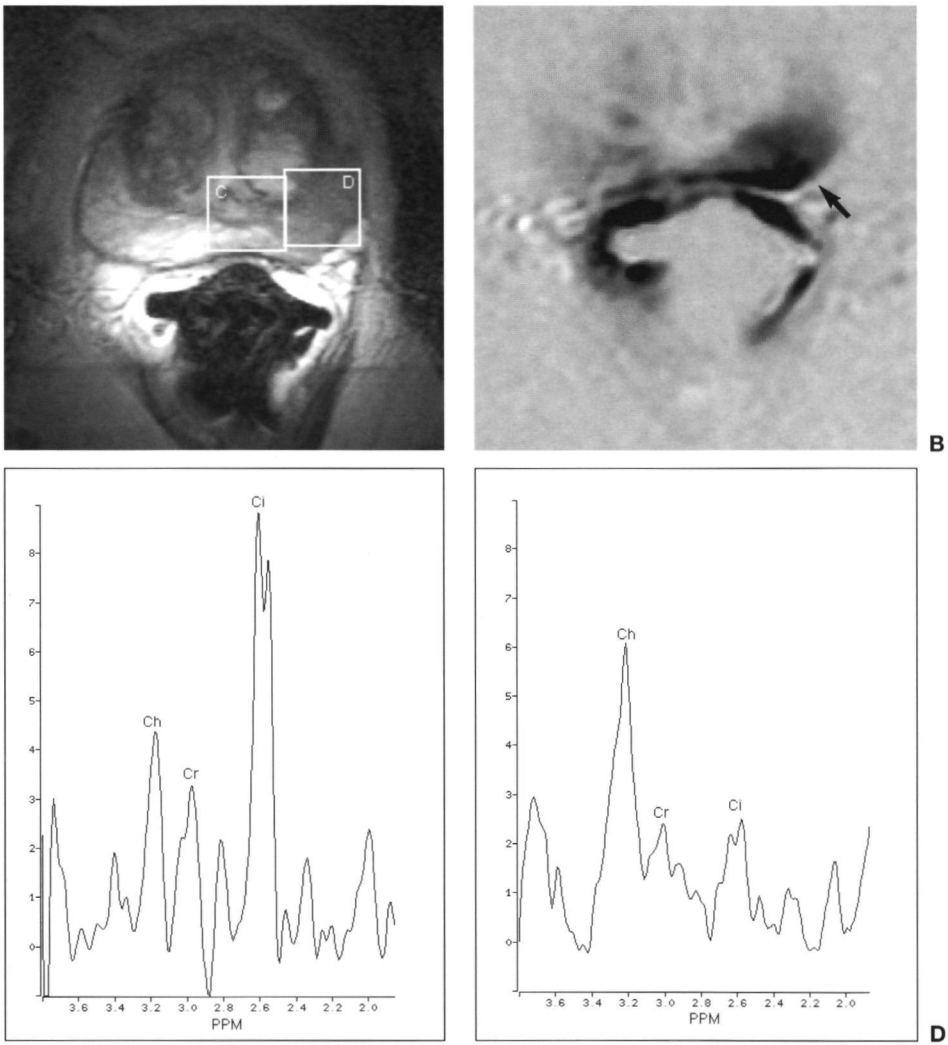

Fig. 1. Results of an MR examination of a patient with PCa (T3c, PSA 37 ng/ml). **A**, T_2 weighted axial TSE image of the prostate. Boxes indicate the size and location of two selected voxels for ^{1}H MRS. **B**, DS MR image showing focal enhancement (arrow) due to Gd contrast inflow in the tumour. The image is obtained at approximately 12 s after the start of inflow in the imaged slice. **C**, ^{1}H MR spectrum of the volume indicated by the dashed box. **D**, ^{1}H MR spectrum of the volume indicated by the solid box (tumor area). Ch = (phospho) choline, Cr = creatine, Ci = citrate.

images of an axial slice. Metabolic maps, reconstructed from signals of the SI data set are overlaid on these images. On the MR image a hypo-intense area in the peripheral zone is visible (arrow) extending into the prostate which was later identified as cancer tissue. The citrate metabolite map (fig. 2A) shows a relative low citrate level in this area. In contrast the choline metabolite map (fig. 2B) shows increased intensity. Furthermore, DS-MR images from a dynamic Gd MR investigation of the same slice showed fast enhancement in this area (fig. 2C).

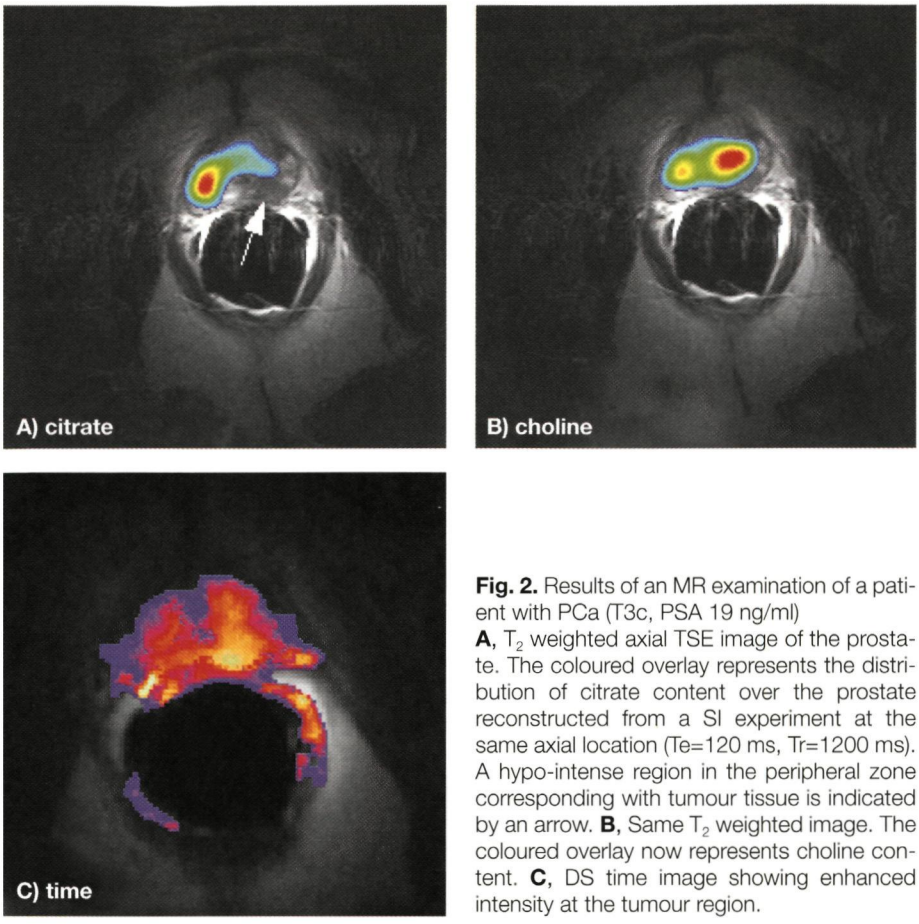

Fig. 2. Results of an MR examination of a patient with PCa (T3c, PSA 19 ng/ml)
A, T_2 weighted axial TSE image of the prostate. The coloured overlay represents the distribution of citrate content over the prostate reconstructed from a SI experiment at the same axial location (Te=120 ms, Tr=1200 ms). A hypo-intense region in the peripheral zone corresponding with tumour tissue is indicated by an arrow. **B**, Same T_2 weighted image. The coloured overlay now represents choline content. **C**, DS time image showing enhanced intensity at the tumour region.

Of the 8 patients suspected of PCa and investigated by SI, 5 were finally diagnosed as having PCa on the basis of biopsy material or radical prostatectomy specimens [5]. Of 1 patient no final diagnosis could be obtained, while histopathological examinations of biopsy material of 2 other patients showed no apparent malignancies. From the five SI data sets voxels were selected in identified cancerous areas and in areas assumed not to be affected by cancer. Ci/Ch signal ratios were determined from spectra of these voxels.

Although generally the experiments indicate increased choline signals in tumorous regions, in some cases the choline signal actually seemed to be decreased in such regions (with respect to the signal of water as an internal reference), but because the citrate signal decreased much more, the Ci/Ch signal ratio still served as a potential marker of malignancy.

The plot in figure 3 summarizes the evaluation of the Ci/Ch signal ratios derived from ^{1}H MR spectra of normal prostates, BPH and PCa patients. It shows average values of this ratio and standard deviations obtained from SI experiments of the normal prostates of healthy volunteers (n=6). The Ci/Ch signal ratio

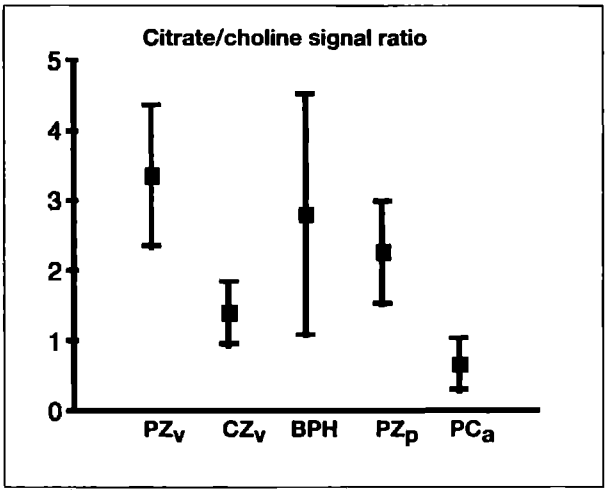

Fig. 3. Average Ci/Ch signal integral ratios (± SD) obtained from spectra of selected regions in the prostate. PZv : peripheral zone normal prostate (n=6). Method: SI; CZv: central zone normal prostate (n=6). Method: SI; BPH: mainly central gland (BPH region) of BPH patients (n=14). Method: SVS; PZp: normal peripheral zone of PCa and BPH patients (n=7). Method: SI; PCa: malignant tissue (n=12). Method: SI and SVS; SVS = single voxel spectroscopy; SI = spectroscopic imaging

values ranges from 2.2 to 5.4 for the peripheral zone and from 0.6 to 1.9 for the central zone. For BPH patients (n=14) the Ci/Ch signal ratio have been determined from single voxel measurements with mainly central gland tissue (BPH region) and shows a wide range of values: from 0.8 to 7.6. The range of values in non-tumour areas of peripheral zones of PCa and BPH patients determined with SI is from 1.7–3.5 (n=7)

The average Ci/Ch signal ratio obtained of all single voxel plus SI spectra from tumour regions (n=12) is significantly lower compared with each other group: peripheral zone, central zone and BPH regions (t tests: $p < 0.002$ for each comparison). However, the range of individual values (0.2–1.2) overlaps with the ratios obtained from central zone tissue in normal prostates and from BPH tissue.

Discussion

Citrate is highly abundant in the normal human prostate and mainly resides in the luminal space of the prostate [10]. For the normal prostate citrate signal levels are higher in ^{1}H MR spectra of the peripheral zone than in spectra of the central gland (including the transition zone and periurethral tissue) [9,23,24]. This is also evident in this study and is related with the different amount of citrate secreting elements in both parts of the prostate. The large variation of relative citrate signals for central gland BPH tissue is most likely caused by differences in glandular and stromal contributions. This study shows that decreased relative levels of citrate in cancer tissue of the prostate can be detected by in vivo ^{1}H MRS. Lower citrate levels found in cancerous tissue are presumably due to a reduction of citrate secreting epithelial structures [10,14,15].

Results from this and previous studies [8,15,16,24] indicate that the choline resonance is increased in cancerous areas of the prostate, but occasionally we have also observed reduced relative choline signals for PCa tissue in vivo.

Elevated signals for choline compounds have been reported from ^{1}H MRS studies of brain tumours [25] and are assumed to be related to a high proliferation rate of tumour cells.

The average T_1-corrected citrate/choline signal ratio, which we used for quantitative purposes, appears to be significantly reduced in tumour tissue compared to normal prostate and BPH tissue However, as there is overlap with values of BPH tissue and normal central zone, at the present status of MRS, the potential clinical applicability is restricted to peripheral zone tumours The results of this study generally are in good agreement with results published recently by Kurhanewicz et al [24] employing a similar MRS approach in 3 dimensions

One cause of failure to correctly place a volume of interest in a malignant region of the prostate by single volume MRS in a number of cases is due to the fact that conventional MRI is not very reliable in depicting prostate tumours. This shows that a multiple volume method for MRS enabling post-acquisition spatial evaluation, as efficiently provided by SI methods, is essential Preferentially, spectra should be obtained from voxels covering the whole prostate at high spatial resolution [24]

This study also demonstrates that T2-weighted MRI, ^{1}H MRS and dynamic Gd enhanced MRI can be combined in a single patient examination Dynamic Gd enhanced MRI has proven to be successful in the detection of some malignancies [21] This is based on the specific (transient) accumulation of the contrast compound in tumour tissue related to its typical neo-vascular characteristics Preliminary results indicate that it also improves prostate tumour detection (Chapter 5) ^{1}H MRSI in combination with dynamic Gd contrast enhanced MRI may be helpful to improve the characterization of cancer in prostate tissue

Acknowledgments

We thank Dr. K. Wicklow (Siemens, Erlangen, Germany) for providing us with post-processing software, Ing H J van den Boogert for technical assistance and Ing YA Heidkamp for help with data processing This study was supported by the Dutch Cancer Society (KUN 95-1016).

References

1 Bostwick DG, Cooner WH, Denis L, Jones GW, Scardino PT, Murphy GP The association of benign prostatic hyperplasia and cancer of the prostate Cancer 70 (suppl 1), 291 - 301, 1992
2 Jager GJ, Barentsz JO, Ruijter ETG, de la Rosette JJMCH, Oosterhof GON Primary staging of prostate cancer Eur Radiol 6, 134 - 139, 1996
3 Schiebler ML, Schnall MD, Pollack HM, Lenkinski RE, Tomaszewski JE, Wein AJ, Whittington R, Rauschning W, Kressel HY Current role of MR imaging in the staging of adenocarcinoma of the prostate Radiology 189, 339 - 352, 1993
4 Hricak H, White S, Vigneron D, Kurhanewicz J, Kosco A, Levin D, Weiss J, Narayan P, Carroll PR Carcinoma of the prostate gland MR imaging with pelvic phased-array coils versus integrated endorectal-pelvic phased-array coils Radiology 193, 703-709, 1994
5 Jager GJ, Ruijter ERMT, van de Kaa CA, de la Rosette JJMCH, Oosterhof GON, Thornbury

JR, Barentsz JO Local staging of prostate cancer with endorectal MR imaging correlation with histopathology AJR 166 845 - 852, 1996
6 Thomas MA, Narayan P, Kurhanewicz J, Jajadia P, Weiner MW ^{1}H MR Spectroscopy of normal and malignant human prostates *in vivo* J Magn Reson 87, 610 - 619, 1990
7 Schnall M, Lenkinski R, Milestone B, Kressel, H Localized ^{1}H MR spectroscopy of the human prostate *in vivo, in* "Proc , SMRM, 9th Annual Meeting, New York" pg 288, 1990
8 Heerschap A, Jager G, de Koster A, Barentsz J, de la Rosette J, Debruyne F, Ruijs J ^{1}H MRS of prostate pathology, *in* 'Proc , SMRM, 12th Annual Meeting, New York" pg 213, 1993
9 Lowry M, Manton DJ, Turnbull I W, Blackband SJ, Horsman A Quantitative proton MRS assessment of citrate heterogeneity in normal prostate MAGMA 2, 483 - 485, 1994
10 Costello LC and Franklin LB Concepts of citrate production and secretion by prostate 1 Metabolic relationships The Prostate 18, 25 - 46, 1991
11 Halliday KR, Fenoglio-Preiser C, Sillerud LO Differentiation of human tumours from non-malignant tissue by natural-abundance ^{13}C NMR spectroscopy Magn Reson Med 7, 384 - 411, 1988
12 Fowler AH, Pappas AA, Holder JC, Finkbeiner AE, Dalrymple GV, Mullins MS, Sprigg JR, Komoroski RA Differentiation of human prostate cancer from benign hypertrophy by *in vitro* ^{1}H NMR Magn Reson Med 25, 140 - 147, 1992
13 Kurhanewicz J, Dahiya R, McDonald JM, Chang LH, James TL, Narayan P Citrate alterations in primary and metastatic human prostatic adenocarcinomas ^{1}H magnetic resonance spectroscopy and biochemical study Magn Reson Med 29, 149 - 157, 1993
14 Schiebler MR, Miyamoto KK, White M, Maygarden SJ, Mohler JL *In vitro* high resolution ^{1}H spectroscopy of the human prostate benign prostatic hyperplasia, normal peripheral zone and adenocarcinoma Magn Reson Med 29, 285 - 291, 1993
15 Cornel FB, Smits GAHJ, Oosterhof GON, Karthaus HFM, Debruyne FMJ, Schalken JA, Heerschap A Characterization of human prostate cancer, benign prostate hyperplasia and normal prostate by *in vitro* ^{1}H and ^{31}P magnetic resonance spectroscopy J Urol 150, 2019 - 2024, 1993
16 Kurhanewicz J, Vigneron DB, Nelson SJ, Hricak HJ, McDonald JM, Konetv B, Narayan P Citrate as an *in vivo* marker to discriminate prostate cancer from benign hyperplasia and normal prostate peripheral zone detection via localized proton spectroscopy Urology 45, 459 - 466, 1995
17 Ordidge RJ, Bendall MR, Gordon RA, Connelly A Volume selection for in-vivo biological spectroscopy *In* "Magnetic Resonance in Biology and Medicine" (Govil G, Khetrapal CL, Saran A, Eds), New Delhi, Tata McGraw-Hill, 1985, pp 386-397
18 Bottomley PA Spatial localization in NMR spectroscopy *in vivo* Ann NY Acad Sci 508, 333 - 348, 1987
19 Brown TR, Kincaid BM, Ugurbil K. NMR chemical shift imaging in three dimensions Proc Natl Acad Sci USA 79, 3523 - 3526, 1982
20 Den Hollander JA, van der Veen, JWC, Luyten, PR Practical aspects of localized in vivo ^{1}H NMR spectroscopy and spectroscopy imaging of the human brain In MR spectroscopy, clinical applications and techniques (Young IR and Charles HC, eds) London, Martin Dunitz Ltd, 1996, pp 161 - 173
21 Barentsz JO, Boetes C, Verstraete KL, Jager GJ, Mus RDM, Ruijs SH Dynamic Gadolinium-enhanced MR imaging of the body Clin MRI 5, 88 - 93, 1995
22 Jager GJ, Barentsz JO, de la Rosette JJMCH, Peters H, Hanselaar A, Oosterhof GON Value of dynamic subtraction turboFlash MR imaging in prostate cancer (abstr) Radiology 193, 316, 1994
23 Heerschap A, Jager G, van der Graaf M, Barentsz JO, Ruijs SHJ Proton MR spectroscopy of the normal human prostate with an endorectal coil and a double spin-echo pulse sequence Magn Reson Med , in press (1996)
24 Kurhanewicz J, Vigneron DB, Hricak H, Narayan P, Carroll P, Nelson SJ Three-dimensional H-1 MR spectroscopic imaging of the in situ human prostate with high (0 24-0 7 cm3) spatial resolution Radiology 198, 795 - 805 , 1996
25 Negendank W Studies of human tumors by MRS a review NMR in Biomed 5, 303-324, 1992

8 The Current Role of MR Imaging in the Local Staging of Prostate Cancer, Future Research and Future Prospects

G. Jager

Introduction

Before advocating the widespread use of MR imaging for selecting patients with prostate cancer for curative therapy, a thorough review and evaluation of the literature should be made, with particular emphasis on: 1) the true clinical need for MR; 2) whether implementation of MR will improve patient outcome; and 3) wether there is a real cost/risk/benefit justification. In the last decade an exponential rise in the number of patients diagnosed with prostate cancer was seen. In the Netherlands, incidence and mortality of prostate cancer are exceeded only by those of lung cancer. In 1989, 4,112 incident cases and 2,079 deaths from cancer of the prostate were recorded in a male population of 7.5 million; this type of cancer caused 3% of total mortality among men and 10% of male mortality from cancer [1,2]. In most western countries the incidence increases with increasing age of the population, and public awareness of the disease. In the USA, prostate cancer incidence rate increased by 6.4% per year between 1983 and 1989 [3].

Prostate cancer is a relatively slow-growing malignancy, with the potential for local and distant spread. The prognosis is highly related to pathological stage, (gleason grade) and volume of the tumor at the time it becomes apparent. Although the tumor is slowly growing, a patient with prostate cancer will develop metastases and die of the disease if he lives long enough [4].

Ideally, clinical staging stratifies patients into comparable groups for definitive therapy and allows comparison of the effectiveness of different therapies, whereas pathological staging is important to predict prognosis and the need for additional therapy.

Current opinion is that clinically localized prostate cancer can be treated successfully by radical prostatectomy in the patient group with life expectancy of 10 to 15 years or more. Nevertheless, benefits of aggressive treatment over watchful waiting in terms of quality-adjusted life expectancy are often small, leading to controversies about the best treatment [3,5-8] .

Among men with prostate cancer, 60% have tumors apparently confined to the prostate [9,10]. However, clinical staging appeared to be unreliable. Understaging occurs in approximately 40% of the cases, and overstaging in about 20% [11]. Transrectal ultrasound did not improve clinically staging satisfactorily. Therefore we conclude that there is a clinical need for better staging of prostate cancer. The question we pose is if this has to be done by MR imaging.

Local staging of prostate cancer

Since 1984 MR imaging has been used as staging modality for prostate cancer. The result are diverse and conflicting [12-14]. In the radiological literature the role of MR imaging in local staging is still under debate. At the moment, urologists in general do not advocate MR imaging for staging prostate cancer since they rely on transrectal ultrasound (TRUS) [15].

MR may be a substitute for TRUS if it is better and cheaper. If MR is better but more expensive (or cheaper but worse!) the relative merits have to be weighted.

MR imaging versus TRUS

To our knowledge two studies addressed the issue of comparing the staging efficacy of the two current imaging modalities [16,17]. In the largest study published to date, by Rifkin et al. [18] (219 patients), body coil MR imaging was more sensitive than TRUS for staging prostate cancer (77% vs 66%, respectively). However, this difference was not statistically significant. Another study reported a significant higher sensitivity of 91% for capsular penetration with MR imaging compared to 48% for TRUS [17]

At the moment TRUS is cheaper and better available than MR and there is too little evidence that staging results are better compared with MR. Even if staging accuracy with MR is significantly better than with TRUS, it is very unlikely for MR to replace TRUS. In general TRUS is also used to establish the diagnosis of prostate cancer by image guided transrectal biopsies. The results of the biopsies add important information about stage, grade, multifocality, tumor volume and seminal vesicle involvement. This is called biopsy-based staging [19,20]. Transrectal MR guided biopsy devices are not expected to be available in short time.

Conclusion: MR will be a complement to rather than a substitute for other staging modalities. The diagnostic impact of MR in prostate cancer staging may be to increase the clinical staging accuracy and to reduce the diagnostic uncertainty. Therefore the question is: "Is there evidence that implementation of MR in staging prostate cancer is efficacious"

Evidence based medicine

Decision making in healthcare is a complex process, often strongly influenced by intuition and unsystematic clinical experience. In this example the decision to recommend MR in the local staging of patients who are a candidate for a radical prostatectomy. It has been emphasized that decisions should be made evidence based [21]. Guidelines and recommendations should be developed, based on strong evidence derived from literature. Evidence-based medicine requires new skills of doctors including efficient literature searching, critical appraisal of the literature, and the capability to assess the strength of evidence, guidelines and recommendations [21].

A randomized control trial (RCT) is considered the most powerful method for

assessing the effect of healthcare interventions. However, the use of RCT is limited in the evaluation of MR in prostate cancer. A rigorous randomized control trial requires a meticulous study design, a large number of patients (approximately 1000), and a long follow-up time (15 years). Even differences in outcomes between different treatment options are difficult to prove [22]. Due to rapid technical evolution with respect to coil design and pulse sequences the imaging method will be obsolete at the time the results become available.

Also evidence may become available from observational studies such as case control studies and cohort studies. But none are available with respect to MR imaging of the prostate. Evidences of the weakest sort may come from expert panels [22]. For example in 1992 "the consensus workshop on screening and global strategy for prostate cancer", did not recommended MR as a staging tool [15]. However there are no estimates on what data the recommendations were based and no radiologists were involved in the development of this guideline.

Decision analysis

Another approach to define the role of MR imaging in prostate cancer is decision analysis. Decision analysis involves choosing an action after weighting the risks and benefits of the alternatives. A decision analysis should include information about pretest probabilities, test accuracy, treatment effectiveness, patient outcome and about costs data with respect to diagnosis treatment and complications. Meta-analysis of the literature should provide data related to the natural history of disease, life-expectancy with and without therapy, complications of diagnosis, complications of therapy, progression of the disease (local, distant) and so on. With these data costs and QALY (Quality-Adjusted Life-Years, see later) saved by introducing MR can be calculated and a cost/benefit analysis can be made.

Modelling a decision tree always involves a compromise between simplicity and reality. A simplified decision tree, to evaluate patient's gain if MR is used to determine the indication for surgery, is helpful to unveil the complexity and pitfalls of such an approach. (fig 1).

Setting up a tree with a binary change node leads to eight outcomes. The relative frequency of each outcome can be calculated from sensitivity and specificity of MR for extra-prostatic disease and the prevalence of extra-prostatic disease in the patient population. In the cases A,B,G,H outcomes are not affected by the use of MR. The additional cost are of the MR examination and the benefits are more diagnostic certainty for doctor and patient. The advantage of latter is difficult to express in money [23].

In the other branches of this tree the decision is supposed to be affected by the results of MR.

We assume positive effects in D and E;

- No surgery because MR depicted a true-positive T3
- Surgery because MR depicted a true-positive T2

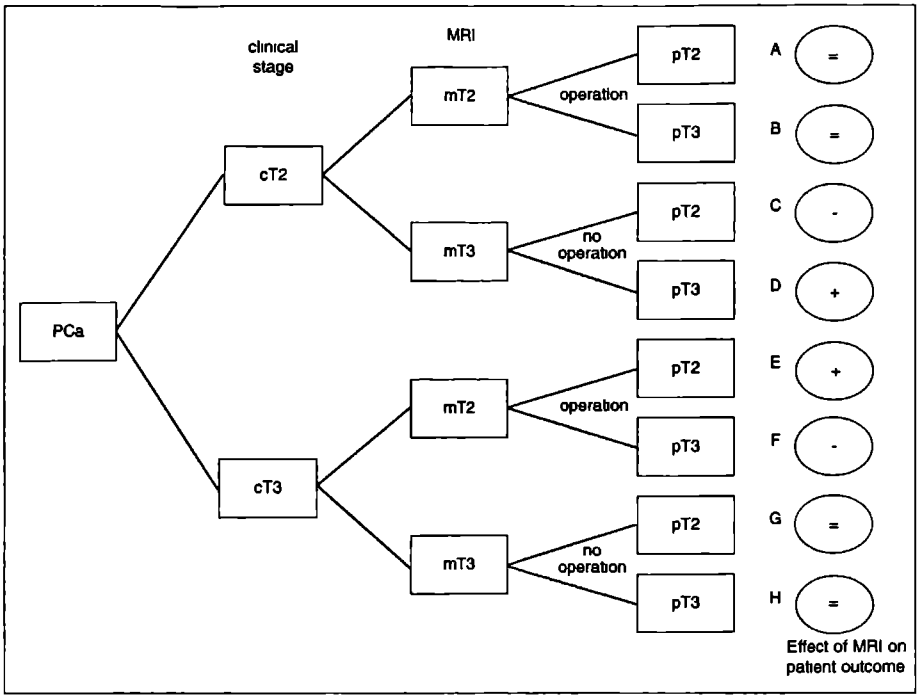

Fig 1. Decision tree for two alternatives. Starting from the decision node far left The treatment decision is supposed to be determined by MR. See text for explanation.

We assume negative effects in C and F;

– No surgery because MR falsely predicted a T3 tumor

– Surgery because MR falsely predicted a T2 tumor

Values can be expressed in money and life years saved. This latter is measured by quality-adjusted life-years, (QALY's). A QALY is an expression of patients value of being in an ill state of health. This is quantified by the period in full time of health which for the patient, is equivalent to a year with illness. For example one year with impotence for one patient equals 6 months of full potency, for another patient this equals 9 months. If these patients live both 10 years after the radical prostatectomy the QALY's are respectively 5 and 7.5 years. Also the quality of life may change during the course of the disease, for example due to the development of metastases. These effects are calculated with Markov modelling. With help of QALY's a patient can better chose between different treatment and allow health care providers to calculate the cost of a particularly procedure for every QALY saved. Many efforts have been made to measure and document life expectancy [24], quality of life outcome [25], treatment costs [26], patients and doctors preference [10], complication rates for different treatment options [27,28]. Still little is known how the quality of life is affected by therapy [29].

Also, reality demands a more complex decision tree because;

– Treatment decisions are dependent on patients and doctors preferences.

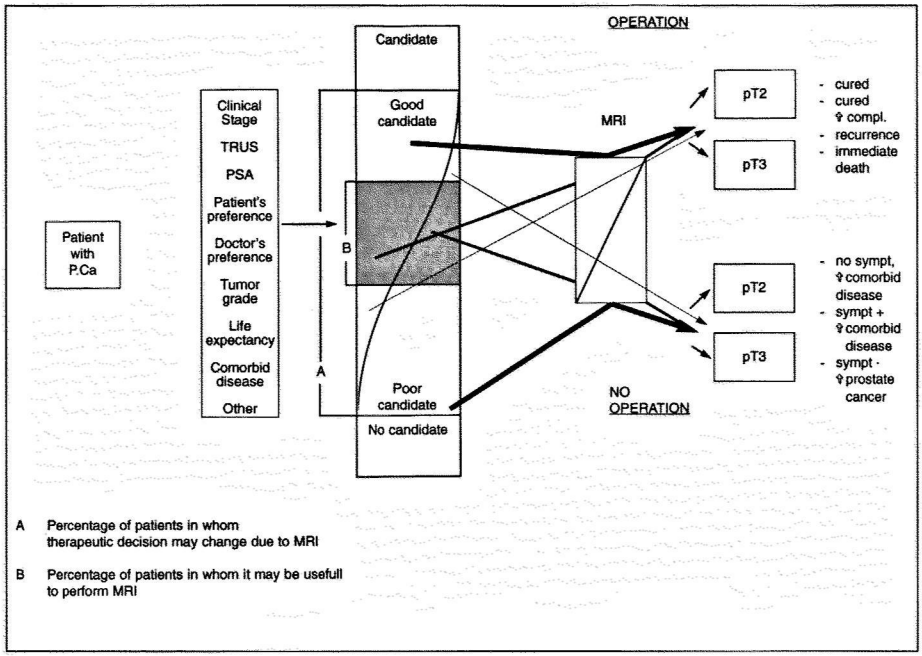

Fig 2. Starting from the decision node far left. A patient with prostate cancer. After initial screening the patient may be a good or a poor candidate for radical prostatectomy, depending on age, patients preference tumor grade and so on. There will be subtle gradations between these extremes. In some of these patients the results of MR will not affect treatment. In other patients the results may seldom affect treatment. MR should not be recommended for these group, although for some individuals the results may be decisive for treatment. For patients in the central (B) part of the node. MR may be decisive. Future research has to determine this group. Value associated with the outcome of the two alternatives, operation or no operation, are not yet determined.

– Patient population is diverse and patients have different pro-test probabilities of having high or low stage disease.
– The results of the MR images will not equally affect therapy. This may vary from no influence to being decisive for treatment.
– In practice the results of MR images are not expressed as a simple yes or no but given on a gradual scale varying from "without doubt" to "cannot be excluded".
– Outcome is not solely dependent on clinical stage but also on other prognostic factors like grade, PSA, tumor volume, nuclear polymorph diploidisn, neovascularity and molecular factors like ϵ-cadherin expression [30-33].
– Patients with a limited T3 disease may still be a candidate for curative surgery

A more realistic decision tree is shown in figure 2. Although much data are lacking, this figure suggests that MR may be useful in a subgroup of patients. One study addressed the question for which subgroup of patients MR may provide additional information concerning patients outcome following radical prostatectomy [34]. This was the case in patients with a intermediate risk of seminal vesicle invasion or extracapsular extension (PSA $\leq$ 20 ng/ml and Gleason sum 5–7, or the PSA level $\leq$ 20 $\geq$ 10, Gleason sum 2–4 predicted).

Medical technology assessment (MTA)

Another approach to analyze the question if local staging with MR is appropriate is medical technology assessment (MTA).

Ideally a diagnostic test should be adequately evaluated before widespread introduction in the medical society. Medical technology assessment (MTA) defines the clinical efficacy of a new diagnostic test. The basic definition of efficacy is "the probability of benefit to individuals in a defined population from a medical technology applied for a given medical problem under ideal conditions of use" [35]. Efficacy overlaps partly with effectiveness, which reflects the use of a medical technology in ordinary clinical practice, rather than ideal conditions. Fryback and Thornbury advocate a hierarchical model to study the efficacy of a diagnostic (imaging) method (tabel 1) [36].

Fryback's and Thornbury's Hierarchical Model of Efficacy

Level 1 Technical efficacy
Level 2 Diagnostic accuracy efficacy
Level 3 Diagnostic thinking efficacy
Level 4 Therapeutic efficacy
Level 5 Patient outcome efficacy
Level 6 Societal efficacy

The first two levels describe efficacy in terms of physical image quality and diagnostic accuracy. Level 3 and 4 assess the impact of diagnostic information on the clinician's thinking and acting; the clinical efficacy. Level 5 and 6 consider patient outcome and impact on the society. The levels are interconnected. Efficacy at lower level is, to a certain extent necessary, to ensure efficacy at a higher level.

For technical efficacy case series with sample sizes ranging from 3 to 10 observations that correlate final diagnosis with MR images are sufficient to demonstrate diagnostic capability. Many studies have demonstrated that MR imaging can provide high-quality images of the prostate.

High-quality studies should have sufficient patients (from 35 to several hundreds) and an independent determination of disease state (gold standard) are necessary to determine diagnostic accuracy efficacy.

It appeared to be difficult to differentiate between benign and malignant lesions especially for lesions located in the central zone of the prostate, nor was it possible to demonstrate a correlation between the tumor volume assessed on the MR images and histopathology [37]. Most reported MR studies have been focused on the differentiation between T2 and T3 tumours. There is a wide range of reported accuracy rates varying from 50% to 90%.

However one should consider that most diagnostic tests are still inadequately appraised [38]. Results of staging studies were difficult to interpret and to compare because there is a large variation in patient selection, technical aspects (pulse sequences, coil design), diagnostic criteria and pathological examination. Also the confidence intervals for the obtained sensitivity and specificity are

seldom reported and correction for work-up bias or verification bias is seldom provided. Test reproducibility is low, due at least to some extent, to a considerable interobserver variation [12,39]. Also there is learning curve [40].

The efficacy on a higher level (diagnostic thinking efficacy, therapeutic efficacy, patient outcome efficacy and society outcome level) have yet not been tested.

Therefore, there are not enough data to date that indicate that the introduction of MR imaging in prostate cancer will improve patient outcome and will be cost-effective. However, at the moment there is strong evidence that patients with gross capsular penetration or seminal vesicle invasion are no candidates for radical prostatectomy [9]. Excluding these patients from operation may be worthwhile. The all-in price for a radical prostatectomy in our hospital is about $ 10.000 and for MRI of the prostate $ 666. If we make a simple calculation, neglecting additional costs, then 1 or more patients out of 15 should be prevented an operation by the use of MR imaging for the method to be cost-effective. Cost-effectiveness is at an intermediate level at short time.

Recommendations for future studies and future prospects

Patients with clinically localized prostate cancer can be divided in three subgroups on basis of PSA and Gleason's grade; Patients with low-risk, intermediate risk and high risk for capsular penetration or seminal vesicle invasion. Staging with MR may be only efficious in one of these subgroup of patients. Sensitivity is dependent on the prevalence of capsular penetration and seminal vesicle invasion. Therefore, it is important that studies evaluating the diagnostic performance of MR should provide data about the spectrum of evaluated patients and provide test indices for reported clinical subgroup.

Also studies that determine the influence of MR imaging on patient management have to be performed next. Due to increasing life expectancy, awareness of doctors and patient for the disease and effective screening methods, the number of patients with early stage localized prostate cancer will rapidly increase the next years. A number of these patients will probably not benefit from surgical or radiation therapy. Also more patients may prefer conservative therapy. This may create a need for a non-invasive monitoring of patients who are treated conservatively. Therefore MR studies should focus on the definition and detection of prognostic factors. MR spectroscopy and dynamic imaging following contrast may have potentials for this purpose.

General conclusion

Because MR imaging still is in an experimental phase we do not advocate MR as a routine staging procedure. MR imaging of the prostate should be performed under the following conditions.

- There should be an investigative setting.
- Due to the learning curve a large number of patients, arbitrary 25 or 50 per year, is warranted.

– The results should be carefully compared with histopathology, preferable whole-mount sections
– The effects on clinical thinking and patient outcome should be analyzed
– studies should provide data about the spectrum of evaluated patients and provide test results for clinical subgroups
– Data should be gathered from multiple institutions in a reasonable time to obtain sound evidences for standard protocols. Imaging strategies and guidelines should be developed by expert panels.

References

1 Gulden van der JWJ, Kiemenev L,A,L,M , Verbeek A,L,M , Straatman H Mortality trend from prostate cancer in the Netherlands (1950-1989) *Prostate* **1994**,24 33-38
2 CBS *Overledenen naar doodsooorzaak, leeftijd en geslacht in het jaar 1989* Voorburg CBS, **1990**
3 Lu-Yao GL, Greenberg ER Changes in prostate cancer incidence and treatment in USA *Lancet* **1994**,343 251-254
4 Hugosson J, Aus G, Bergdahl C, Bergdahl S Prostate cancer mortality in patients surviving more than 10 years after diagnosis *J Urol* **1995**,154 2115-2117
5 Flemming C, Wasson JH, Albertsen PC, Barry MJ, Wennberg JH A decision analysis of alternative treatment strategies for clinically loacalized prostate cancer *JAMA* **1994**,269 2650-2658
6 Walsh PC Prostate cancer kills strategy to reduce deaths *Urology* **1994**,44 463-464
7 Wasson JH, Cushman CC, Bruskewitz RC, Littenberg B, Mulley AG, Wennberg JE A structured literature review of treatment for localized prostate cancer *Arch Fam Med* **1993**,2 487-493
8 Menon M, Parulkar BG, Baker S Should we treat localized prostate cancer? An opinion *Urology* **1995**,46 607-616
9 Rosen MA Impact of proste-specific antigen screening on the natural history of prostate cancer *Urology* **1995**,46 757-768
10 Barry MJ, Flemming C, Coley CM, Wasson JH, Fahs MC, Oesterling JE Should medicare provide reimbursement for prostate-specific antigen testing for early detection of prostate cancer? Part I framing the debate *Urology* **1995**,46 2 13
11 Perrotti M, Kaufman Jr,R P , Jennings TA, et al Endo-rectal coil magnetic resonance imaging in clinically localized prostate cancer is it accurate? *J Urol* **1996**,156 106-109
12 Tempany CMC, Zhou X, Zerhouni EA, et al Staging of prostate cancer results of radiology diagnostic oncology group project comparison of three MR imaging techniques *Radiology* **1994**,192 47-54
13 Langlotz CP, Schnall MD, Pollack H Staging of prostatic cancer Accuracy of MR imaging *Radiology* **1995**,194 645-646
14 Tempany CMC, Gatsonis CA, McNeil BJ Reply *Radiology* **1995**,194 647-648
15 Denis I J, Murphy GP, Schroeder FH Report of the consensus workshop on screening and global strategy for prostate cancer *Cancer* **1995**,75 1187-1207
16 Rifkin MD, Zerhouni EA, Gatsonis CA, et al Comparison of magnetic resonance imaging and ultrasonography in staging early prostate cancer Results of a multi-institutional cooperative trial *N Engl J Med* **1990** 323 621-626
17 Presti JC, Hricak H, Narayan P, Shinohara K, White S, Carroll PR Local staging of prostatic carcinoma comparison of transrectal sonography and endorectal MR imaging *AJR* **1996**,166 109-108
18 McSherry SA, Levy F, Schiebler MI , Keefe B, Dent GA, Mohler JL Preoperative prediction of pathological tumor volume and stage in clinically localized prostate cancer comparison of digital rectal examination, transrectal ultrasonography and magnetic resonance imaging *J Urol* **1991**,146 85-89

19 Bostwick DG, Qian J, Bergstralh EJ, et al Prediction of capsular perforation and seminal vesicle invasion in prostate cancer *J Urol* **1996**,155 1361-1367
20 Narayan P, Gajendran V, Taylor SP, et al The role of transrectal ultrasound-guided biopsy-based staging preoperative serum prostate-specific antigen, and biopsy gleason score in predicting of final diagnosis in prostate cancer *Urology* **1995**,46 205-212
21 Evidence-Based Medicin Working Group Evidence-based medicine – A new approach to teaching the practice of medicine *JAMA* **1992** 268 2420-2425
22 Black N Why we need observational studies to evaluate the effectiveness of health care *BMJ* **1996**,312 1215-1218
23 Evens RG Making difficult health policy decisions most choices are not simply life or death *AJR* **1995**,165 1329-1330
24 Aus G, Pilebad E, Hugosson J Impact of competing mortality on the cancer-related mortality in localized prostate cancer *Urology* **1995**,46 672 675
25 Litwin MS, Hays RD, Fink A, et al Quality-of-live outcomes in men treated for localized prostate cancer *JAMA* **1995**,273 129 135
26 Kramolowsky EV, Wood NL, Rollins KL, Glasheen WP, Nelson CMK. Impact of physician awareness on hospital charges for radical retropubic prostatectomy *J Urol* **1995**,15439 139-142
27 Lerner SE, Blute ML, Zincke H Extended experience with radical prostatectomy for clinical stage T3 prostate cancer outcome and contemporary morbidity *J Urol* **1995** 154 1447-1452
28 Barry MJ Flemming C, Coley CM, Wasson JH, Fahns M, Oesterling JE Should medicare provide reimbursement for prostate-specific antigen testing for early detection of prostate cancer? Part III Managment strategies and outcomes *Urology* **1995**,46 277-289
29 Perez CA Carcinoma of the prostate A model for management under impending health care system reform *Radiology* **1995**,196 309 322
30 Mohler JI , Figlesthaler WM, Zhang X Z, Partin AW, Maygarden SJ Nuclear shape ananlysis for the assessment of local invasion and metastases in clinically localized prostate carcinoma *Cancer* **1994**,74 2996-3001
31 Fujikawa K, Sasaki M, Aoyama T, Itoh T, Yoshida O Prognostic criteria in patients with prostatic cancer correlation with volume weighted mean nuclear volume *J Urol* **1995**,154 2123-2127
32 Stricker HJ, Kay JK, Linden MD, Iamboli P, Amin MB Determing prognosis of clinically localized prostate cancer by immunohistochemical detection of mutant p53 *Urology* **1996**,47 366-369
33 Narayan P, Fournier G, Gajendran V, et al Utility of preoperative serum prostate-specific antigen concentration and biopsy gleason score in predicting risk of pelvic lymph node metastases in prostate cancer *Urology* **1994**,44 519 524
34 d Amico AV, Whittington R, Malkowicz JB, et al A multivariate analysis of clinical and pathological factors that predict for prostate specific antigen failure after radical prostatectomy for prostate cancer *J Urol* **1995**,154 131-138
35 Brook RH, Lohr K. Efficacy, effectiveness, variations and quality boundary crossing research *Med Care* **1985**,23 710-722
36 Thornbury JR, Fryback DG Technology assessment an American view *Eur J Radiol* **1992**,14 147 156
37 Jager GJ, Ruijter ETG, van de Kaa CA, et al Local staging of prostate cancer with endorectal MR imaging correlation with histopathology *AJR* **1996**,166 845-852
38 Reid CM, Lachs MS, Feinstein AR Use of methodological standards in diagnostic test research – Getting better but still not good *JAMA* **1995**,274 645-651
39 Schiebler ML, Yankaskas BC, Tempany CMC, et al MR Imaging in adenocarcinoma of the prostate Interobserver variation and efficacy for determing stage C disease *AJR* **1992**,158 559 562
40 Harris RD, Schned AR, Heaney JA Staging of prostate cancer with endorectal MR imaging Lessons from a learning curve *RadioGraphics* **1995**,15 813-829

9 Summary and Conclusions Samenvatting en conclusies

Summary

Prostate Cancer represents a significant health problem in most western countries. Consequently the prostate is increasingly being studied by MR imaging.

The first goal of this study was to define whether MR imaging with an ERC technique is able to correctly predict the local stage of patients with prostate cancer. The second goal was whether a 3D imaging technique could correctly predict the presence of lymph node metastases in patients with prostate cancer. The third goal was to determine whether new MR techniques such as spectroscopy and dynamic imaging may help to define the presence and spatial extent of prostate cancer. Furthermore to assess if these methods have potential in the characterization of the tumor.

The objective, value and controversies of local staging are discussed in **chapter 2**. Staging is performed according to the revised TNM classification system. Generally spoken, a patient with prostate cancer may be cured of the disease if the tumor does not extend beyond the capsule of the prostate and if there are no distant metastases. However, with respect to the treatment of prostate carcinoma we are facing some controversies. Cure may be possible when there is microscopic capsular penetration while on the other hand, radical prostatectomy may not be the best treatment options for all patients with localized prostate cancer. Some patients with locally confined disease may better be "treated" by conservative management.

Furthermore, pathological stage appeared not to be the sole predictor of outcome in patients with prostate cancer. It is concluded that other prognostic factors such as PSA, histologic grade (Gleason), tumor volume, and neo-vascularity should be incorporated in a staging algorithm.

In **chapter 3** the results of local staging with an ERC technique in 34 patients are described. The results are comparable with those from the literature. In our study, MR could correctly predict pathological stage in 68% of the patients. Because in 70% of the cases capsular penetration not detected on MR images was less than 1 mm and probably did not affect the prognosis of these patients it was concluded that the technique may be helpful in selecting patients for curative therapy. Furthermore it was not possible to predict tumor volume correctly. Also the pitfalls of MR imaging with an ERC-technique were discussed.

One of the pitfalls of MR imaging with an ERC is discussed in an **interlude**. This is a report of a case of a patient with prostate cancer who had also senile amyloidosis of the seminal vesicles, mimicking seminal vesicle invasion by prostate cancer on ERC-MR images.

Chapter 4 reports the results of a 3-dimensional (3D) MR imaging technique in the evaluation of pelvic lymph nodes in 134 patients with prostate or bladder cancer. The sensitivity in patients with prostate cancer was 60%. This is high compared to other MR studies. The results of MR-guided FNAB biopsies were hopeful.

The second **interlude** is a comment on an article in which is suggested that there is no role for imaging in lymph node staging of patients who are a candidate for a radical prostatectomy. It is concluded that imaging is still worthwhile in a select group of patients who are at high risk for nodal metastases to spare them an operation. However, the criteria of what we call a lymph node metastasis should be changed. The upper limit of a normal sized lymph node should be lower than the generally accepted limits of 1 or 1.5 cm.

In **chapter 5** we evaluated the potential of a dynamic MR imaging technique after bolus injection of contrast material. The imaging results of 57 patients were compared to histopathology with respect to tumor location and capsular penetration. Sixty-three contrast-enhanced MR images were obtained at intervals of 1.2 or 2.4 seconds at one level. Lesions that enhanced early or demonstrated a steep slope of enhancement were regarded as malignant. We demonstrated that prostate cancer can be discerned due to earlier and faster enhancement than benign prostatic tissue. With this technique capsular penetration and tumor location could be demonstrated better than with T2-weighted FSE images. Although these differences were not statistically significant, we conclude that the methods have potentials for clinical use.

Chapter 6 Reports the results of proton spectroscopy in healthy volunteers. The presence of various metabolites such as choline, citrate and creatine could be observed. With a PRESS sequence it was possible to obtain high resolution single volume spectroscopy of the prostate. It was also possible to perform spectroscopy in a preselected slice of the prostate with a nominal resolution of 1 cc. Differences in citrate-choline ratio's associated with normal zonal anatomy could be demonstrated.

In **chapter 7** the results of MRS in patients with benign prostatic hypertrophy and prostate cancer are presented. We demonstrated that prostate cancer often may be discerned by a lower citrate level in combination with a significant increase of the choline peak. The citrate-choline ratio's in malignant prostate tissue was significant lower than in benign tissue.

Chapter 8 is a discussion about the role of MR in the local staging of patients with prostate cancer who are a candidate for radical prostatectomy and contains recommendations for future studies.

Conclusions

MR Imaging is playing an important role in the imaging of prostate cancer. Despite initial optimism the accuracy of MR imaging in the detection of capsular penetration is low. A prospective study is however needed, to evaluate if patients with only a microscopic amount of tumor penetration have a worse prognosis compared to patients in whom the tumor is confined to the prostate.

With a 3D MR imaging technique lymph nodes can be detected. However, the incidence of lymph node metastases is low and therefore the yield of lymph node staging is low. On the basis of clinical stage PSA and Gleason grade it can be estimated which patients are at risk for having lymph node metastases and consequently will benefit from imaging.

Prostate cancer shows early and rapid enhancement following bolus injection of contrast. With fast MR imaging and the use of a subtraction technique tumor assessment can be improved.

It is possible to obtain high resolution MR spectra from single volume as from selected slices of the prostate. With MR spectroscopy it is possible to discriminate prostate cancer from non-malignant prostatic tissue on the basis of metabolite levels, specifically citrate and choline.

Presently prostate cancer is detected at a lower grade of malignancy and a lower tumor volume in more and more patients patients. They will probably not benefit from an operation. Furthermore patients today are more involved in treatment decisions. Therefore information about all prognostic factor should be available. Preferable this information should be obtained the less invasive as possible.

With the use of MR techniques such as fast dynamic imaging and spectroscopy more information about the biological behaviour of the tumor may be obtained. At present a study on the correlation of dynamic enhancement and spectroscopy is ongoing. At this moment comparison between enhancement, spectroscopy and pathology is only possible on a single slice. However in the near future it will be possible to perform dynamic imaging and spectroscopy in a multislice manner.

Samenvatting

Het doel van deze studie was drieledig. Ten eerste, de betrouwbaarheid vaststellen van kernspin tomografie, beter bekend als MRI, in combinatie met een endorectale spoel, voor de lokale stadiëring van prostaatkanker. Ten tweede, onderzoeken of met behulp van een 3-dimensionale (3D) MRI techniek lymfkliermetastasen opgespoord kunnen worden bij patiënten die voor een radicale prostatectomie in aanmerking komen. Ten slotte, vaststellen of een tweetal nieuwe MR technieken, n.l. de dynamische opnametechniek na een bolusinjectie met contrast en MR spectroscopie, van waarde kunnen zijn om de aanwezigheid en uitbreiding van prostaatkanker aan te tonen en om de tumor te karakteriseren.

Het doel, de waarde en controverses van het lokaal stadiëren van prostaatkanker worden in **hoofdstuk 2** besproken. Stadiëring gebeurt volgens het TNM classificatiesysteem. In zijn algemeenheid geldt dat een patiënt met prostaatkanker genezen kan worden als de tumor binnen het kapsel van de prostaat beperkt blijft en er geen metastasen op afstand zijn ($\leq$ T2,N0). Opvattingen over de behandeling van prostaatkanker zijn echter niet eenduidig. Zo kan enerzijds genezing ook mogelijk zijn als er slechts sprake is van microscopische kapselpenetratie en anderzijds hoeft een radicale prostatectomie niet de beste behandeling te zijn voor alle patiënten met een klinisch beperkt prostaatcarcinoom. Sommige patiënten met een lokaal beperkte tumor kunnen beter met radiotherapie of een afwachtend beleid behandeld worden.

Verder blijkt dat het pathologische stadium niet alleen de prognose van de patiënt bepaalt. Andere factoren zoals PSA, histologische graad (Gleason), tumorvolume en neovascularisatie bepalen eveneens de prognose en zouden daarom in een stadiërings algorithme moeten worden opgenomen.

In **hoofdstuk 3** worden de resultaten van lokale stadiëring met een endo-rectale spoel beschreven. De resultaten zijn vergelijkbaar met die uit de literatuur. Met behulp van MR kan het pathologische stadium in 68% van de patiënten correct bepaald worden. Omdat 70% van de op MR beelden gemiste kapselpenetraties microscopisch was ($\leq$ 1 mm), werd geconcludeerd dat de MR techniek behulpzaam kan zijn bij het selecteren van patiënten voor curatieve therapie. Het is met deze techniek niet mogelijk het volume van de tumor betrouwbaar te voorspellen. Verder worden de valkuilen van MR beeldvorming met behulp van een endo-rectale spoel besproken.

Eén van die valkuilen wordt besproken in een **interludum**. Dit is een casusbespreking van een patiënt met prostaatkanker die eveneens seniele amyloidosis van de vesicula seminalis had. Dit werd op de MR afbeeldingen met een endorectale spoel ten onrechte genterpreteerd als invasie van tumor in de vesicula seminalis.

Hoofdstuk 4 doet verslag van de resultaten van een drie-dimensionele MR opnametechniek ten behoeve van de evaluatie van pelviene lymfklieren bij 134 patiënten met prostaat-of blaaskanker. Bij patiënten met prostaatkanker was de sensitiviteit 60%. Dit is hoog vergeleken met andere MR studies. In dit hoofdstuk worden ook de eerste resultaten besproken van MR geleide biopsiën van verdachte klieren. Deze eerste resultaten zijn hoopvol en vergelijkbaar met de resultaten van de gangbare CT techniek.

Het tweede **interludum** is een commentaar op een artikel waarin werd gesuggereerd dat er geen rol is voor lymfklierstadiëring met beeldvormende technieken bij patiënten die kandidaat zijn voor een radicale prostatectomie. Geconcludeerd wordt dat beeldvormende technieken waardevol zijn bij een selecte groep van patiënten die een groot risico hebben op lymfkliermetastase. Bij een aantal van hen kan een onnodige operatie worden voorkomen. Het criterium voor de grootte van een lymfkliermetastase moet lager zijn dan de nu geaccepteerde limieten van 1 of 1,5 cm.

Hoofdstuk 5 bevat het verslag van de evaluatie van één dynamische opnametechniek na bolusinjectie van contrast. De resultaten van de MR opname werden vergeleken met de histo-pathologische bevindingen vooral ten aanzien van tumorlokatie en kapselpenetratie. Drie en zestig opnamen op een niveau werden verkregen met een tijdsinterval van 1.2 of 2.4 seconden tijdens een intraveneuze bolusinjectie met contrast. Afwijkingen die een vroege en/of snelle aankleuring lieten zien werden als maligne beschouwd. Wij toonden aan dat prostaatkanker kan worden onderscheiden van benigne weefsel door de vroege en snelle aankleuring. Met deze techniek was kapselpenetratie en tumorlokalisatie beter aantoonbaar dan met de gangbare T2-gewogen opname. Hoewel de verschillen statistisch niet significant waren, concluderen wij dat de methode mogelijkheden heeft voor klinisch gebruik.

Hoofdstuk 6 doet verslag van de resultaten van protonspectroscopie bij gezonde proefpersonen. De aanwezigheid van verschillende metabolieten zoals choline, citraat en kreatine kon worden waargenomen. Met een PRESS-sequentie was het mogelijk om spectroscopische metingen met een hoge resolutie van de prostaat te verkrijgen. Ook was het mogelijk om spectroscopische opnamen van één vlak te vervaardigen met een spatiële resolutie van 1 cc. Verschillen in citraat-choline ratio's, geassocieerd met de normale anatomie konden worden aangetoond.

In **hoofdstuk 7** worden de resultaten van MR spectroscopie bij patiënten met BPH en met prostaatkanker gepresenteerd. Wij toonden aan dat prostaatkanker in het algemeen gekarakteriseerd wordt door een lager citraat gehalte gecombineerd met een verhoogd cholinegehalte. In vergelijking met het weefsel van de normale prostaat en de prostaat met BPH is de citraat-choline ratio significant lager in tumorweefsel.

Hoofdstuk 8 is een discussie over de rol van MR bij het stadiëren van prostaatkanker. Met behulp van een beslisboom en principes uit de "MTA" (Medical Technology Assessment) wordt met gegevens uit de literatuur bekeken of er genoeg reden is om algemene toepassing van MR bij de stadiëring te propageren. De conclusie is dat deze techniek, ondanks veelvuldig gebruik, zich nog steeds in een experimenteel stadium bevindt. Wel zijn er sterke aanwijzingen dat met deze techniek bij patiënten met een beperkt risico op lokale uitbreiding(matig gedifferentieerde tumor met een PSA $\leq$ 10, en goed gedifferentieerde tumor met een PSA $\geq$ 10, $\leq$ 20) een verbetering van de klinische stadiëring wordt verkregen.

Conclusies

Afbeelding met MR speelt in toenemende mate een belangrijke rol bij de diagnostiek van prostaatkanker. De nauwkeurigheid van MR voor microscopische kapselpenetratie is laag. Patiënten met evidente kapsel penetratie hebben een slechtere prognose dan patiënten bij wie de tumor tot de prostaat beperkt blijft. Een prospectieve studie is nodig om te onderzoeken of de prognose van patiënten met slechts microscopische tumorpenetratie ook slechter is dan die van patiënten met een beperkte tumor.

De onderzochte drie-dimensionele MR afbeeldingstechniek is gevoelig bij het opsporen van lymfkliermetastasen. Omdat de incidentie van lymfkliermetastasen laag is, is de opbrengst van routine stadiëring ook laag. Op basis van klinisch stadium, PSA, en histologische graad (Gleason) moeten patenten geselecteerd worden bij wie beeldvorming zinvol is.

Prostaatkanker vertoont een snelle en vroege aankleuring na bolusinjectie van contrast. Met een snelle opnametechniek en het gebruik van subtractie kan de tumor beter worden beoordeeld.

Het is mogelijk om een spectroscopische opname met een hoge resolutie van een enkel volume, of een geselecteerde snede van de prostaat te verkrijgen. Met spectroscopie is het mogelijk om onderscheid te maken tussen kanker en benigne weefsel op basis van de citraat/choline verhouding.

Momenteel wordt prostaatkanker bij meer patiënten in een vroege fase geconstateerd. Deze tumoren zijn vaak goed gedifferentieerd en hebben een klein volume. Deze patiënten hebben mogelijk geen baat bij een operatie. Omdat patiënten vandaag de dag meer betrokken willen worden bij de besluitvorming rond de behandeling zal zo veel mogelijk prognostische informatie beschikbaar moeten zijn. Bij voorkeur dient deze informatie op een zo min mogelijke invasieve manier verkregen te worden.

Met behulp van MR technieken zoals snelle dynamische opnames en spectroscopie kan meer informatie over het biologische gedrag van de tumor worden verkregen. Op dit moment is een studie gaande naar de correlatie tussen snelle aankleuring en spectroscopie. Thans is vergelijking tussen aankleuring, spectroscopie en histopathologie slechts mogelijk in één vlak. In de toekomst zullen echter de dynamische opnamen en de spectroscopie techniek op meerdere snedes tegelijk toegepast kunnen worden.

Curriculum Vitae

De auteur werd geboren op 13 november 1954 te Heerlen. Na het behalen van het VWO diploma aan het Sintermeerten College te Heerlen in 1975 werd in datzelfde jaar begonnen met de studie Geneeskunde aan de Katholieke Universiteit te Nijmegen. Op 28 januari 1983 behaalde hij zijn artsexamen. Van april tot en met december van dat jaar was hij werkzaam op de afdeling algemeen interne geneeskunde van het St Jozef Ziekenhuis te Kerkrade. Op 1 januari 1984 begon hij zijn opleiding radiodiagnostiek in het De Wever Ziekenhuis te Heerlen (opleider en hoofd: dr J.J.H. Lamers). Op 1 januari 1988 werd hij ingeschreven in het specialistenregister. Sinds 1 december 1988 is hij als staflid verbonden aan het Instituut voor Radiodiagnostiek van het Academische Ziekenhuis Nijmegen St Radboud (hoofd prof. dr S.H.J. Ruijs. Tot zijn deel-vakgebied behoren alle aspecten van de abdominale radiologie. Hij is gehuwd met Tineke Rijsemus en zij hebben twee zonen, Koos (1993) en Hans (1995).

Chapters Originally Published in

2 Primary Staging of Prostate Cancer
Eur Radiol 6,129-133(1996)

3 Local Staging of Prostate Cancer with Endorectal MR Imaging: Correlation with Histopathology
AJR 1996;166,845-852

Interlude I
Amyloidosis of the Seminal Vesicles Simulating Tumor Invasion of Prostatic Carcinoma on Endorectal MR Images
Eur Radiol 1996; 6 (in press)

4 Pelvic Adenopathy in Prostate and Bladder Carcinoma: MR Imaging with a Three-dimensional T1-weighted Magnetization Prepared-Rapid Gradient-Echo Sequence
AJR 1996; 167 (in press)

Interlude II
Sensitivity of Frozen Section Examination of Pelvic Lymph Nodes for Metastatic Prostate Carcinoma
Cancer 1996; 77:1003-1005

5 Dynamic Turbo-FLASH Subtraction Technique for Contrast-enhanced MR Images of the Prostate: Correlation with Histopathology
submitted

6 Proton MR Spectroscopy of the Normal Human Prostate with an Endorectal Coil and a Double Spin-echo Puls Sequence
Accepted for publication in Magn Res in Med

7 In-vivo Proton MR Spectroscopy Reveals Altered Metabolite Content in Malignant Prostate Tissue
Accepted for publication in Anticancer Res

Stellingen

behorende bij het proefschrift:

Magnetic Resonance in Prostate Cancer: Clinical Potentials

1. Gebruik van een 3D-opnametechniek is het meest betrouwbaar voor het opsporen van lymfkliermetastasen in het kleine bekken (dit proefschrift).

2. MR opnamen van de prostaat met contrast hebben alleen zin indien van een snelle dynamische opnametechniek gebruik gemaakt wordt (dit proefschrift).

3. Beeldvorming van lymfklieren heeft alleen zin wanneer bij verdenking op een metastase, bevestiging van de diagnose middels een dunne naaldbiopsie plaatsvindt (dit proefschrift).

4. Bij proton MR spectroscopie kenmerkt prostaatcarcinoom zich door een verlaagd citraat- en een verhoogd cholinegehalte (dit proefschrift).

5. Omdat prostaatcarcinoom in een steeds vroeger stadium wordt ontdekt, is het nodig patiënten die waarschijnlijk nooit last van het carcinoom zullen krijgen te onderscheiden van hen die behandeling behoeven (dit proefschrift).

6. **Het stellen van een diagnose mag nooit een doel op zichzelf zijn.**

7. **Het laagdrempelig karakter van echografie voor de diagnose diepe veneuze trombose leidt tot een paradoxale stijging van het aantal flebografieen.**

8. **Subcutaan emphyseem van het bovenbeen wijst meestal op een ernstige intra-abdominale aandoening en vereist direct nader onderzoek middels een abdominale CT.**

9. **Door de enorme toename van nieuwe en vaak duurdere diagnostische technieken is het wenselijk dat het vak medische besliskunde onderricht en geexamineerd wordt tijdens de opleiding tot basisarts.**

10. **Voor een radiodiagnost is een analytisch denkvermogen en een goede visus essentieel. Het is daarom tegennatuurlijk dat hij voor het voltooien van een proefschrift vaak het verstand op nul en de blik op oneindig moet zetten.**

11. **Een onderzoek met goede resultaten wordt vaak verward met een goed onderzoek.**

12. **De beschrijving "De echo-specialist heeft twee enorme flaporen en in elk oor steekt een gehoorapparaat" * toont nogmaals aan dat echo meer om te kijken dan om te luisteren is.**

* *Lidy Nicolasen, de Volkskrant 16 september 1995*

13. **Wanneer een tennisspeler die omwille van het belasting-klimaat in Monaco is gaan wonen een lintje ontvangt, dient hij zelf en niet de nederlandse belastingbetaler de produktie-kosten te betalen.**

14. **Wanneer boeren doorgaan met ongecontroleerd injiciëren van mest in de bodem, kunnen zij vanzelf binnenkort niet meer de kop in het zand steken voor de gevolgen van dit beleid.**

15. **Kamerleden die menen dat het voor een beter contact met de samenleving nodig is om een commissariaat te vervullen, hebben inderdaad een beter contact met de samenleving nodig.**

16. **Het niet opnemen van een dankwoord in een proefschrift wil zeggen dat woorden tekort schieten.**

Gerrit Jan Jager

Nijmegen, 11 december 1996.